

General Disclaimer

One or more of the Following Statements may affect this Document

- This document has been reproduced from the best copy furnished by the organizational source. It is being released in the interest of making available as much information as possible.
- This document may contain data, which exceeds the sheet parameters. It was furnished in this condition by the organizational source and is the best copy available.
- This document may contain tone-on-tone or color graphs, charts and/or pictures, which have been reproduced in black and white.
- This document is paginated as submitted by the original source.
- Portions of this document are not fully legible due to the historical nature of some of the material. However, it is the best reproduction available from the original submission.

CR 151365

MCR-77-107
NAS9-14767 Exhibit B

Final Report

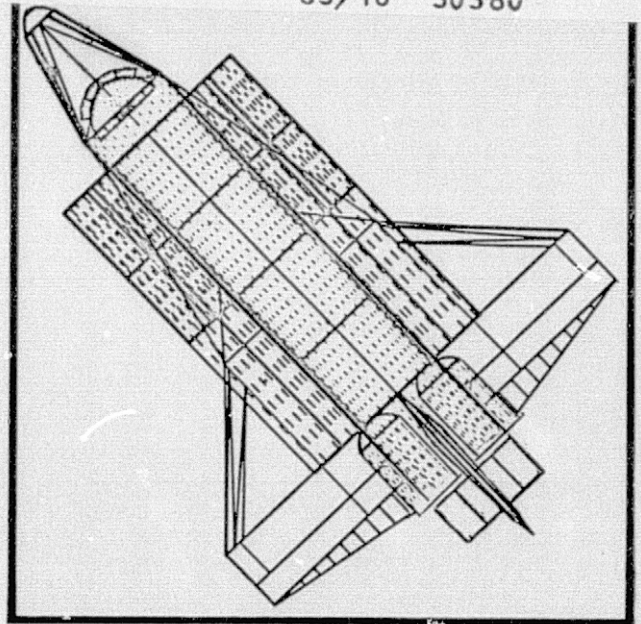
April 1977

Orbiter/Payload Contamination Control Assessment Support

(NASA-CR-151365) ORBITER/PAYLOAD
CONTAMINATION CONTROL ASSESSMENT SUPPORT
Final Report (Martin Marietta Aerospace,
Denver, Colo.) 134 p HC A07/MF A01 CSCL 22A

N77-25225

Unclas
G3/16 30380



MARTIN MARIETTA

MCR-77-107
April 29, 1977

Technical Report

ORBITER/PAYLOAD CONTAMINATION CONTROL
ASSESSMENT SUPPORT

Final Report

Contract NAS9-14767 Exhibit B

Author

R. O. Rantanen
D. A. Strange Jensen

Prepared for

Lyndon B. Johnson Space Center
Houston, Texas 77058

MARTIN MARIETTA AEROSPACE
Denver Division
P. O. Box 179
Denver, Colorado 80201

TABLE OF CONTENTS

	<u>Page</u>
1.0 INTRODUCTION	1-1
1.1 Purpose	1-1
1.2 Scope	1-1
1.3 Summary	1-1
2.0 APPLICABLE DOCUMENTS	2-1
2.1 Program Documents	2-1
3.0 STUDY RESULTS	3-1
3.1 Shuttle Orbiter Contamination Model	3-1
3.1.1 Model Description	3-1
3.1.1.1 Contaminant Source Functions	3-2
3.1.1.2 Contaminant Transport Functions	3-10
3.1.1.3 Contamination Degradation Effects	3-30
3.1.2 Orbiter Surface Description	3-32
3.1.3 Source Characteristics	3-65
3.1.4 Lines-of-Sight	3-77
3.1.5 Sample Output Format	3-78
3.1.6 Model Delivery and Checkout	3-78
3.2 Induced Environment Predictions	3-86
3.3 Trade Studies	3-111
3.3.1 Evaporator Location Influence	3-111
3.3.2 Surface Resolution Influence on Reflected Effluents	3-113
3.3.3 Canted Elevon Influence on Evaporator Effluents	3-119
4.0 CONCLUSIONS AND RECOMMENDATIONS	4-1
4.1 Conclusions	4-1
4.2 Recommendations	4-2
5.0 NOTES	5-1
5.1 Abbreviations	5-1

Figures

1	Geometry for Viewfactor Between Finite Areas	3-3
2	Temperature Dependence of Outgassing Rate Upon Activation Energy	3-5
3	Elemental Volume Definition	3-15
4	Elemental Volume Geometry (Line-of-Sight Location)	3-16
5	Critical Surface, Location, Orientation and Field-of-View	3-16
6	High Density and Low Density Ambient Atmosphere Variation From Medium Density Values	3-21

Figures (cont'd)

		<u>Page</u>
7	Molecular Density of Ambient Atmosphere Versus Altitude for the Three Densities Input to the Model	3-22
8	Comparison of Model Sticking Coefficient Prediction to Testing	3-29
9	New Wing Configuration Compared to Previous Wing	3-33
10	Updated Nose/Cabin Configuration	3-34
11	Updated Tail Configuration	3-36
12	Updated and Previous Configuration of the Shuttle Orbiter (Top View)	3-37
13	Updated and Previous Configuration of the Shuttle Orbiter (Side View)	3-38
14	Location of Surface Types Modeled on Shuttle Orbiter	3-66
15	Location of Surface Groups Modeled on Shuttle Orbiter	3-70
16	RCS Engine Location Using the Rockwell Numbering System	3-76
17	Baseline Column Density Output of Contamination Model	3-79
18	Baseline Return Flux Output of Contamination Model	3-80
19	Molecular Number Column Density From Evaporator Effluents for the Zero Degree Line-of-Sight as a Function of Z Location With X Location Constant and Equal to 1504	3-112
20	Top and Side View of Original Orbiter Wing Configuration and Flash Evaporator at X = 1504 and Z = 291	3-114
21	Further Subdivisions of Wing Trailing Edge for Investigation of Surface Resolution Requirements	3-115
22	Variation of Molecular Number Column Density and Reflected Mass as a Function of Surface Resolution	3-116
23	Elevon/Fuselage - Evaporator Geometry	3-120
24	Evaporator Induced Molecular Number Column Density for Elevon Canted up 35 Degrees	3-122

Tables

I	Shuttle Orbiter Geometry Breakdown	3-39
II	Orbiter TRASYS Input Listing	3-51
III	Major Surface Source Characteristics	3-72
IV	VCS Engine Location Data	3-73
V	Major Point Source Parameters	3-74
VI	User Output Options	3-81
VII	Integrated Contamination Model Similarities and Differences to Previous Independent Subroutines	3-83
VIII	Outgassing, Early Desorption Predictions	3-87
IX	Detailed Outgassing, Early Desorption Predictions in Computer Format	3-88
X	VCS/RCS Induced Environment Predictions	3-109
XI	Evaporator Predictions	3-110

TABLE OF CONTENTS (cont'd)

	<u>Page</u>
<u>Tables (cont'd)</u>	
XII Variation in Column Density and Reflected Mass for VCS and RCS Engines	3-118
XIII NCD for Evaporator at $X = 1507$, $Z = 305$	3-120
XIV Number Column Density Due to Evaporator Flow Between Elevon and Fuselage	3-121

1.0 SCOPE

1.1 Purpose

The purpose of this report is to present the results achieved in performing the Orbiter/Payload Contamination Control Assessment Support study. The intent of this activity was to develop, check-out and deliver a contamination model of the Shuttle Orbiter and perform support trade studies of Orbiter sources. In conjunction with the contamination model a User's Manual was prepared to facilitate model operation by Johnson Spacecraft Center (JSC) personnel. Additionally, an updated prediction of the Shuttle Orbiter induced environment is included. The predictions are based on the best available data to date in the model as delivered to JSC at the end of this contract period.

1.2 Scope

This report describes the development and use of a contamination math model of the Shuttle Orbiter which incorporates specific Shuttle Orbiter configurations and contamination sources. These configurations and sources represent the latest design of the Shuttle Orbiter and its sources. The results of model predictions for many lines-of-sight and individual and grouped sources are presented in a summary table. In addition, support trade studies primarily concerned with the supplemental flash evaporator location and operation are presented as part of this report for completeness and as a record of activities conducted.

1.3 Summary

An integrated Shuttle Orbiter contamination math model has been established. The model is a result of previous contamination modeling contracts reported in MCR-74-93, MCR-74-474, MCR-75-202 and MCR-75-13. The contamination math model has an updated configuration of the Shuttle Orbiter and source changes over those presented in the above mentioned documents. The sources include different surface group types, location areas and point sources. The area sources considered are:

- a) Radiator Doors
- b) Fuselage
- c) OMS Pod
- d) Wing Minus Elevon
- e) Elevon
- f) Crew Cabin Area

- g) Tail
- h) Payload Bay
- i) Windows

The material types assigned to these areas consist of a combination of the following materials for each area.

- a) FRSI (NOMEX)
- b) LRSI (Tile)
- c) HRSI (Tile)
- d) Bulkhead
- e) Payload Bay Liner
- f) RCC (Carbon Leading Edges)
- g) Teflon (Radiators)
- h) Leakage

The point sources modeled are the VCS and RCS engines and the supplemental flash evaporator.

The modeling approach and philosophy used throughout this study had the eventual goal of becoming an integrated mission profile model. The methodology employed and subroutines developed were directed toward this goal. Additionally, the model was maintained in a form during its development, that allowed timely trade studies to be performed for specific sources.

Extensive trade studies were performed for the supplemental flash evaporator by locating it at various positions on the exterior of the Shuttle Orbiter vehicle. The impact of these locations on the induced contaminant environment was assessed in conjunction with thrust considerations resulting from the evaporator impingement upon Shuttle surfaces and the evaporator orientation. The final location was selected as $X = 1505$, $Y = 126$ and $Z = 305$. This location was decided as the best choice after considering acceptable penetration areas, plumbing limitations, contamination levels, forces generated at various locations, wing geometry and weight restrictions. All of these parameters had to be considered thus the decision on location was not based on contamination predictions alone.

The effects of canting the elevon on the evaporator effluents for an evaporator location near $X = 1507$ and $Z = 305$ was also investigated to minimize contamination levels to acceptable values for as much of the payload viewing volume as possible. As part of this analysis, the surface resolution required for a surface near a point source was also determined. The surface resolution had a major influence on the resulting fraction of a vent plume that can be reflected for unique situations.

2.0 APPLICABLE DOCUMENTS

2.1 Program Documents

The following documents form a part of this report in the extent that they were used for related program information relevant to this study.

PROGRAM DOCUMENTS

- | | |
|--------------------------|--|
| MCR-73-105
Revision 1 | "Thermal Radiation Analysis System", (TRASYS), NAS9-14318, May 1975, Martin Marietta Aerospace, Denver Division. |
| MCR-74-93 | "Payload/Orbiter Contamination Control Requirement Study" NAS8-30755 Exhibit A, December 1974, Martin Marietta Aerospace, Denver Division. |
| MCR-74-474 | "Payload Orbiter Contamination Control Requirement Study" NAS8-30755 Exhibit A, December 1974, Martin Marietta Aerospace, Denver Division. |
| MCR-75-13 | Final Report, "Payload/Orbiter Contamination Control Assessment Support", NAS9-14212, June 1975, Martin Marietta Aerospace, Denver Division. |
| MCR-75-202 | "Payload/Orbiter Contamination Control Requirement Study" NAS8-30755 Exhibit B, June 1975, Martin Marietta Aerospace, Denver Division. |

3.0 STUDY RESULTS

3.1 Shuttle Orbiter Contamination Model

The intent of this section is to summarize the work performed in developing, checking out and delivering the model. The model was first delivered at the end of the initial twelve month period of the contract as two separate subroutines. These routines were the surface source program including outgassing, offgassing and leakage and the point-source program which included VCS and RCS engines and the supplemental flash evaporator. Finally, at the end of the 3 month extension an integrated form of the above mentioned programs was delivered along with a user's manual for its operation.

3.1.1 Model Description - The modeling of spacecraft contamination involves many phases of ground handling, the launch environment and the orbital conditions. The modeling described herein deals only with the on-orbit environment experienced by the spacecraft.

Contamination is said to exist if spacecraft or launch vehicle produced material interferes with the intended performance of a surface or a sensor. The contamination can deposit on a surface and thus alter the absorptivity, emissivity, transmittance, reflectance or conductivity characteristics. The contamination can also intercept the field-of-view of a sensor or experiment and either scatter, emit or absorb electromagnetic radiation.

The deposition on a surface is usually expressed in terms of mass per unit area or thickness if a density and uniformity of the contaminant is known. The material within an experiment or instrument field-of-view is normally expressed as mass column density (MCD) in units of g/cm^2 , molecular number column density (NCD) in units of mol/cm^2 or particles/ cm^2 of a specific size range.

The sources of the molecular species are mass loss from nonmetallic materials, venting of confined spacecraft or experiment volumes, attitude control systems exhaust and operational venting or purging of systems such as fuel cells and sublimators. Manned spacecraft have in addition leakage of cabin atmosphere and Extra Vehicular Activity (EVA) by the flight crew. Anomalous sources such as leaks in coolant lines, propellant tanks and hydraulic systems also contribute to the molecular induced environment. The major sources of particulates are sloughing off of particles acquired during ground handling and assembly, attitude control exhausts, overboard vents, leaks or purges capable of condensing into particles upon vacuum exposure, abrasion of moveable surfaces and micrometeorite impacts.

A complete contamination model must thus consist of 3 major elements which are source kinetics, transport mechanisms and degradation effects. Major elements contained in the model are described in the following sections.

3.1.1.1 Contaminant Source Functions

Geometric Considerations - All the contaminant source functions are basically dependent upon the geometrical parameters of distance from the source (r) and the angle off of the centerline of the specific contaminant source plume (θ) where a region of investigation is located. In the case of surface sources, the "plume" centerline is the normal vector to the emitting surface. These "configuration factors" $f(r, \theta)$ are essentially the backbone of the contamination modeling methodology. Because surface sources such as outgassing, early desorption and cabin leakage are characteristically Lambertian*, line-of-sight transport for these sources can be considered analogous to black body thermal radiation. Therefore, for such sources, the geometric viewfactor is determined to establish the percentage of mass emitted by a Lambertian source that is capable of impinging upon another surface of interest or a point in space. Referring to Figure 1 the viewfactor between two finite areas can be determined from

$$VF_{i-j} = \frac{1}{A_i} \int_{A_i} \int_{A_j} \frac{\cos \theta_i \cos \theta_j}{\pi r^2} dA_j dA_i \quad (1)$$

The reciprocity relationship for a cosine distribution can be utilized to show that

$$VF_{i-j} A_i = VF_{j-i} A_j \quad (2)$$

The viewfactor in conjunction with the appropriate Lambertian contaminant source function,

$$\psi_j \cdot VF_{j-i} \frac{A_j}{A_i} = \psi_j VF_{i-j} \quad (3)$$

*The Lambertian distribution assumption for surface sources has been verified by experimental data obtained through numerous ground test programs.

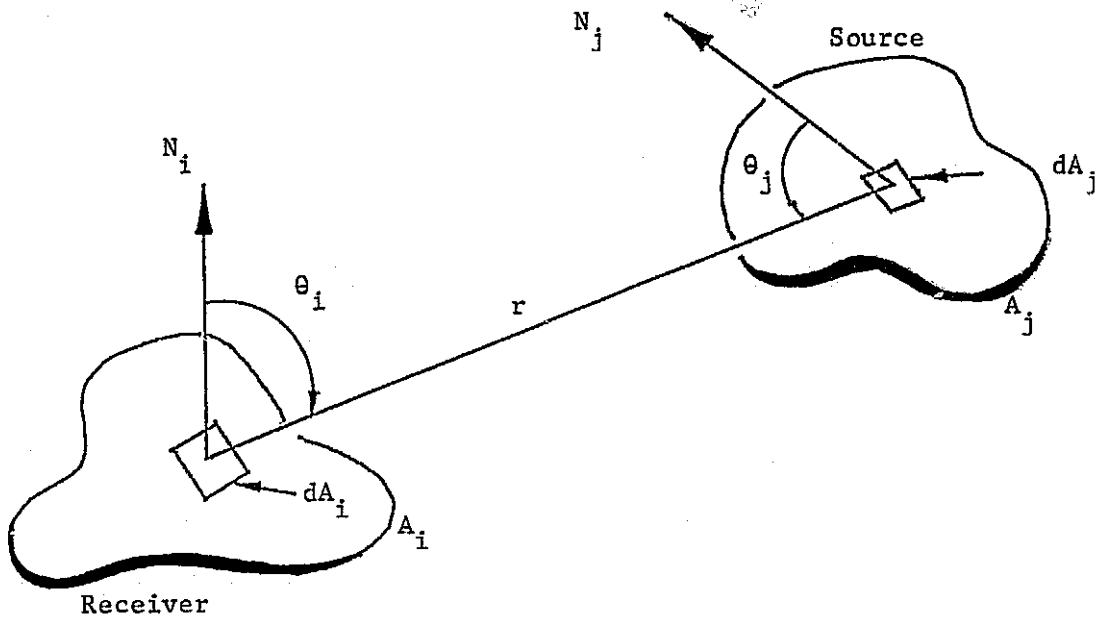


Figure 1. Geometry for Viewfactor Between Finite Areas

Outgassing Source Kinetics - One of the most difficult sources to characterize is the mass loss behavior of nonmetallic materials such as paints, adhesives, insulation, etc. under vacuum exposure. Other sources such as attitude control systems and vents are more classical in their characterizations because their mass flow is usually well known.

During Skylab, an initial approach used to determine source rates was based on kinetic theory which employed molecular weight and vapor pressure. This approach used the Langmuir-Knudsen relationship equating mass loss rate to vapor pressure, molecular weight, temperature and desorption coefficient. This relationship could be used on generic substances such as water, but for polymeric spacecraft materials where the abundance of each molecular weight varies with temperature and time the problem was intractable. A more practical macroscopic approach was used for Skylab involving a direct measurement of mass loss characteristics. Although these measurements were limited, they formed the beginning of the current approach. The mass loss rate as a function of temperature is expressed as

$$\dot{m} = M_0 e^{(T-100)/29},$$

where;

M_o^o = initial steady state outgassing rate at 100°C and
T = surface temperature °C.

This exponential function form when compared to the Arrhenius expression $k = A_o e^{-E/RT}$ (rate constant variation with temperature) has the characteristics of an activation energy near 10 to 12 Kcal/mole. Similar values have been observed during limited testing of nonmetallics at MSFC.

Figure 2 shows curves normalized to 100°C for outgassing rate as a function of temperature for several activation energies of desorption (curves A, C and D for 8, 10, and 15 Kcal/mole respectively) and the relation derived from Skylab flight data (curve B).

At the lower temperatures, the Skylab derived equation appears to follow an equivalent activation energy near 8 Kcal/mole. While at higher temperatures, the equation falls between 10 and 15 Kcal/mole. The use of an equation of the form $e^{-E/RT}$ is only good for a narrow temperature range because of the many activation energies involved in a complex nonmetallic surface. The temperature relation of the form $e^{-E/RT}$ is good for substances whose behavior is more thoroughly understood by appropriate testing.

The mass loss rate time dependency in the model is expressed as $e^{-t/\tau}$ where τ is the decay time which is the time for the mass loss rate to fall to 1/e of its original value. The value of τ depends strongly on the percent sunlight exposure of the vehicle. On Skylab, it was determined to be 4100 hours and 1000 hours has been observed on other satellite systems.

Therefore, primarily due to the lack of good, comprehensive test data, the outgassing mass loss rate is currently expressed as

$$\dot{m}_j = M_o^o e^{(T_j - 100)/29} e^{-t/\tau}.$$

However, this expression has been found to fit the only extensive spacecraft flight data from monitors on board Skylab.

The constituents of early desorption as opposed to those of outgassing are basically simple gases (H₂O, N₂, etc.) and can be assumed to exhibit zero order source kinetics. Their mass loss rates as a function of surface temperature can therefore be expressed by the classical relationship

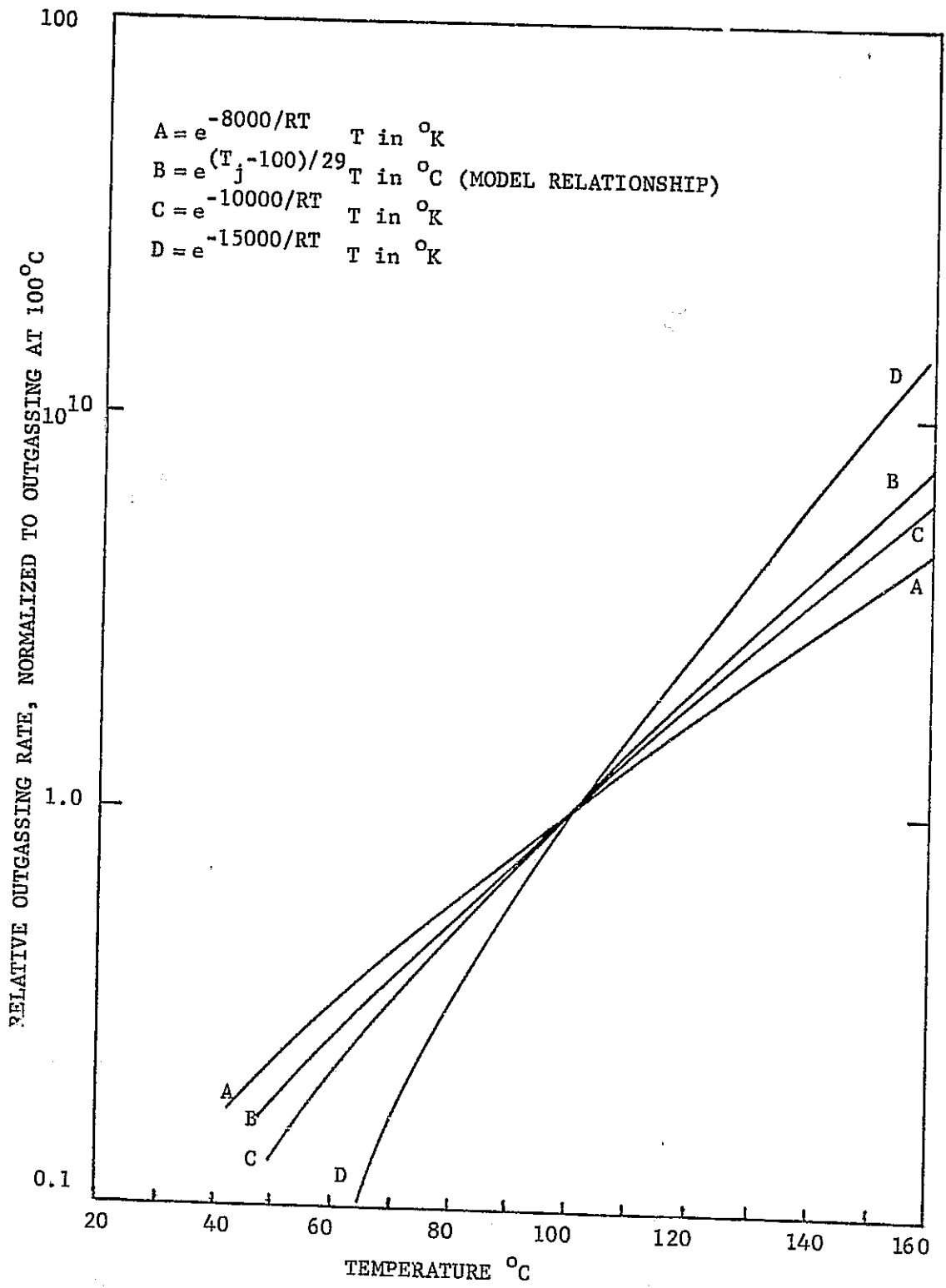


Figure 2. Temperature Dependence of Outgassing Rate Upon Activation Energy

$$\dot{m} = A_0 e^{-E/RT},$$

where E can be obtained from published literature for most simple gases (e.g., E = 12.2 Kcal/mole for H₂O) and T is in °K. A₀ which is a constant characteristic of the early desorbing material can be cancelled out by knowing the \dot{m} at a given T. For example, if from materials testing a certain nonmetallic material demonstrates an initial mass loss rate of 1.24×10^{-8} g/cm²/s at 100°C, then by assuming that the emitted mass is primarily simple gases with an activation energy of desorption E, Kcal/mole, the rate at any other temperature can be determined from

$$\frac{\dot{m}_T}{\dot{m}_{100^\circ\text{C}}} = \frac{A_0 e^{-E/RT}}{A_0 e^{-E/R373}} = e^{\frac{E}{R} \left(\frac{1}{373} - \frac{1}{T} \right)}.$$

The value of A₀ can also be determined directly by plotting the log of \dot{m} versus $\frac{1}{T}$. The intercept on the log scale would be A₀. Evalu-

ation of limited ground test data for the initial high mass loss rates of early desorption indicates a τ of approximately 18 hours. It must be realized that this value is actually the result of the superposition of the decay rates of the individual molecular components of early desorption. To account for this, the model has been configured to accept varying values for τ for each specie. However, this data is also limited and a τ of 18 hours is currently assumed for all early desorption species.

Ideally, tests should be performed that will determine those parameters required to model this complex process of outgassing and early desorption as a function of temperature and time. Source mass loss rate theory founded on thermochemical rate processes can result in simple, concise source equations. The rate theory applied to polymeric source kinetics results in the following expression for mass loss rate:

$$\dot{m}(t, T) = k(T) (a_0 - X)^n = k(T) m^n, \quad (4)$$

where;

- \dot{m} = mass loss rate,
- $k(T)$ = rate constant,
- X = active mass outgassed,

m = active mass remaining,
 n = order of the reaction and
 a_0 = initial amount of active mass available.

The rate constant can be expressed as a function of temperature by

$$k(T) = A_0 e^{-E/RT}, \quad (5)$$

where;

A_0 = constant,
 E = activation energy of the process,
 R = molar gas constant and
 T = absolute temperature.

The values of A , E , a_0 , m , m and n can be determined from a test procedure known as thermogravimetric analysis (TGA). The degree of testing depends on the configuration of the nonmetallic material, whether it is a uniform film such as a paint or a composite of several materials in a layered formation. Additionally, the quantity of each active component may require several tests with different mass samples so the required resolution can be obtained.

Many investigators assume zero order ($n = 0$) and first order ($n = 1$) kinetics when determining the activation energy, E . However, it is relatively easy to determine the order of reaction, n from the TGA data.

Integration of equation (4) yields

$$\int \frac{dm}{(a_0 - x)^n} = \int -k(T) dt, \text{ or}$$

$$\frac{(a_0 - x)^{1-n}}{(1-n)} = -k(T) t + C, \quad n \neq 1, \quad (6)$$

For a zero order reaction,

$$M = -kt$$

and for a first order reaction the integrated form of equation (4) becomes

$$M = -e^{-kt},$$

where M = the total mass lost after time t at temperature T .

At $t = 0$, $m = 0$ and C in equation (7) is

$$C = \frac{a_0^{1-n}}{1-n}$$

so that equation (6) becomes

$$\frac{m^{1-n}}{(1-n)} = k(T) + \frac{a_0^{1-n}}{1-n},$$

where a_0 = the initial amount of active mass of a given component and m is the active mass remaining.

The majority of nonmetallic materials used on the STS exhibit 2 or more components available for outgassing. The mass loss rate for such a case would be expressed for each surface coating in the form of

$$\dot{m} = \dot{m}_1 + \dot{m}_2 + \dot{m}_3 + \dots = \sum_{i=1}^K \dot{m}_i, \text{ or}$$

$$\dot{m} = \sum_{i=1}^K A_i \left(e^{-E_i/RT} \right) m_i^{n_i}. \quad (7)$$

Therefore, to determine the mass loss characteristics of an outgassing surface, the temperature history versus time must be known. The above expressions appear to be one way a closed form analytical treatment can be made for a material mass loss where the emitted components change with time and temperature.

Many spacecraft materials behave in a manner that is dictated by diffusion limited mass loss rates. Therefore, in materials testing, one must determine if the mass loss rate is limited by surface desorption rates or diffusion rates from the material.

Fick's first law of diffusion is expressed as

$$F = -D \left(\frac{\partial c}{\partial x} \right)$$

where;

F = mass loss rate from a surface,
D = diffusion constant and
C = concentration of diffusing species.

The diffusion coefficient can be expressed as a function of temperature by

$$D = D_0 e^{-E/RT},$$

where D_0 and E are constants. Substituting for D in the first law of diffusion above yields

$$F = D_0 e^{-E/RT} \frac{\partial c}{\partial x},$$

which has the same form as equation 7 for a first order reaction. That is, both forms have a dependency on the amount of mass remaining and the exponential dependency on the activation energy of the process and the temperature at which it is taking place.

It appears that both dynamic and isothermal testing of nonmetallic materials is necessary to determine the type of mass loss process. Ideally, the as applied configuration should be tested since a composite of materials will behave much differently than the pure materials themselves.

Leakage Source Kinetics - Leakage from the crew compartments of the Shuttle Orbiter will continuously emerge from structural seams, hatches, microscopic cracks and seals around support hardware such as instrumentation feed-throughs. The crew compartments are pressurized to 14.7 psia (one atmos.) with O_2 and N_2 the predominant species. Leakage contaminants from these compartments will consist primarily of; 1) normal atmospheric gases, 2) internal materials and black box outgassing products, 3) astronaut byproducts,

4) frictional erosion creating particles from materials subject to abrasion and 5) evaporation from liquid sources.

Presently, the modeling approach is to allow the specification leak rate to be emitted uniformly from the forward bulkhead area. The leak rate is continuous because of the constant pressure maintained in the habitation area. The components of the modeled gas leakage are the main components of the pressurized atmosphere which includes O₂, N₂, CO₂ and H₂O.

Point Source Kinetics - Point sources considered in the model are the supplemental flash evaporator and the VCS and RCS attitude control engines. These point sources are expressed as an analytical function describing the mass flow as a function of distance and angle off of the central axis of the source.

The flow field of the engines is expressed by an analytical function developed by Simons*. For given engine physical dimensions, injector pressures and chamber pressure; the flow field is expressed as a function of these parameters. For example, the expression for a region of the VCS engine flowfield is expressed as

$$\dot{m} = \frac{k}{r^2} \cos \left(\frac{\pi}{2} \cdot \frac{\theta}{\theta_i} \right)^{8.65} \quad \text{for } 0^\circ \leq \theta \leq 40^\circ, \quad (9)$$

where k is a constant and θ_i is a function of the engine design. Beyond the limiting angle from the centerline axis where the Simons approach is valid, another approach by Chiravella[†] is utilized. This data shows that the flux beyond the limiting angle is a constant and has been incorporated into the model for all engine backflow regions.

The flash evaporator plume distribution was measured in testing at JSC. The analytical function was supplied by JSC analysis personnel and has the same general Simons' approach format as the engine expressions.

3.1.1.2 Contaminant Transport Functions - Included in the following subsections are the analytical approaches currently employed to describe the transport of emitted contaminant molecules to locations of interest. These transport functions in conjunction with the appropriate contaminant source functions comprise the basic expressions necessary to evaluate the induced environment of

*Simons, G. A.; "Effect of Nozzle Boundary Layers on Rocket Exhaust Plumes", AIAA Journal, Vol. IV, No. 11, 1972.

[†]Chiravella, J. E. and Simon, E., "Molecular Flux Measurements in the Back Flow Region of a Nozzle Plume", JANNAF 7th Plume Technology Meeting, April 19, 1973.

a space vehicle.

Source to Surface or Point Transport - The mass flux on a surface (i) from another surface (j) can be expressed as

$$\dot{m}_i = \dot{m}_j VF_{j-i} \frac{A_j}{A_i}, \quad (10)$$

where;

\dot{m}_i = mass flux on i,

A_i = surface area of i,

A_j = surface area of j and

VF_{j-i} = viewfactor or the fraction of mass leaving j that impinges on i.

Because of the reciprocity theorem for a cosine emitter,

$$VF_{j-i} \frac{A_j}{A_i} = VF_{i-j}$$

and does simplify the above equation for mass flux on a surface so that $\dot{m}_i = \dot{m}_j VF_{i-j}$. It is this equation that is actually used in the model calculations.

For determination of densities in space around the STS system, a viewfactor is calculated between each surface node and the point of interest. The flux at the point is expressed in the same manner as for a surface except the reciprocity theorem does not hold for a point. The flux at a point is given by

$$\dot{m}_p = \dot{m}_j VF_{j-p}, \quad (11)$$

where;

\dot{m}_p = flux at a point p,

\dot{m}_j = mass loss rate of source j and

VF_{j-p} = viewfactor between a surface and a mathematical point.

The viewfactor VF_{j-p} from a surface to a point is defined as

$$\frac{A_j \cos \theta_j}{\pi r^2},$$

where;

A_j = area of surface,

θ_j = angle between normal to A_j and line connecting A_j and point and

r = distance between point and center of A_j .

If the flux is integrated over the entire hemisphere above the active side of A_j , the total mass flux over the hemisphere has to equal $\dot{m}_j A_j$ where \dot{m}_j is the mass loss rate per unit area. The integral becomes,

$$\begin{aligned} & \int_{\phi=0}^{2\pi} \int_{\theta=0}^{\pi/2} \frac{\dot{m}_j A_j r^2 \sin \theta_j \cos \theta_j d\theta_j d\phi}{\pi r^2} \\ &= \frac{\dot{m}_j A_j 2\pi}{\pi} \int_0^{\pi/2} \sin \theta_j \cos \theta_j d\theta_j \\ &= \dot{m}_j A_j. \end{aligned}$$

Therefore, mass is conserved since $\dot{m}_j A_j$ is the total amount leaving A_j and the flux at a point is correct.

In the modified TRASYS II program, the viewfactor between a point and a surface A_j is calculated by determining the solid angle subtended by A_j , and then dividing by 4π steradians so that the viewfactor is the ratio of the mass striking A_j that is emitted by a point. For this case, the viewfactor is

$$\frac{A \cos \theta_j}{4\pi r^2}.$$

This is a factor of 4 too small than the viewfactor presented above. It is correct for thermal analysis of a point as an emitter but is too small when using the point as a receiver. Therefore, the viewfactor currently calculated for a point emitting into 4π steradians by the TRASYS II Program should be multiplied by a factor of 4 before being used in the model.

For simple geometries, it is important to remember some definitions. These are:

$$d\Omega = \text{solid angle} = \frac{A_j \cos \theta_j}{r^2},$$

$$\text{viewfactor} = \frac{d\Omega}{\pi} = \frac{A_j \cos \theta_j}{\pi r^2} \quad \text{and}$$

$$\text{viewfactor for a point as an emitter} = \frac{A_j \cos \theta_j}{4\pi r^2}.$$

Mass and Molecular Number Column Density - The density at a point is expressed as

$$d_p = \frac{\dot{m}_p}{V_j} = \frac{\dot{m}_j \text{VF}_{j-p}}{V_j},$$

where;

d_p = the density at p from source j and

V_j = the velocity of the source j molecules.

By determining the density at many points along a line-of-sight, the mass column density (g/cm^2) can be determined by integration where

$$\text{MCD} = \int_{r=0}^{r_{\text{max}}} d_p \, dr \quad (12)$$

and

r = distance along the line-of-sight.

Knowledge of the molecular constituents of each jth source allows conversion of the mass column density into molecular number column density (molecules/cm²).

Molecules are assumed to leave a surface and arrive at another surface or point in space without experiencing a collision with another molecule during transit. The model has the option of reducing the flux of molecules at a point by considering the interaction of the contaminant molecules and the subsequent scattering of the contaminant before it intercepts the line-of-sight. For this case, the density can be expressed as

$$d_p = \frac{\sum_j \dot{m}_j V_{F_{j-p}} e^{-R/\lambda}}{V_j}, \quad (13)$$

where;

- R = the distance from j to point p and
- λ = mean free path of the j molecules.

It should be cautioned that this is a least case determination of the mass column density since other molecules are scattered into the line-of-sight while others are scattered out. To determine what numbers are scattered into versus those scattered out of a line-of-sight, a great deal of effort is required. It is a complicated process involving knowledge of all mass densities around the vehicle and the orientation of the velocity vectors and requires costly, extensive Monte Carlo techniques. Preliminary estimates have indicated that the amount scattered into a field-of-view from adjacent fields-of-view is approximately equal to those scattered out for many situations. Therefore, the decision was made to baseline the density calculations without considering the mean free path. At high altitudes, the mean free path becomes large enough so that the influence is negligible or non-existent. For orientations where the Shuttle Orbiter essentially blocks the ambient from interacting with the contaminant molecules, the model approach is also accurate. This would occur, for example, when the Orbiter is flying belly first and the ambient impinges on its underside and thus does not interact with many of the contaminant molecules on the payload bay side.

Return Flux Transport Determination - Return flux is a term applied to contaminant molecules that are scattered back to the vehicle through gas-gas collisions with the ambient atmosphere. Due to the geometries of the Orbiter and the payloads, the primary

transport mechanism of contaminant species between sources and receivers is the phenomena of return flux.

The approach for modeling the return flux (RF) to a surface of interest divides the hemispherical space above the Orbiter/Spacelab into a matrix of volume elements that have midpoints strategically located along given (up to 25) lines-of-sight (see Figures 3 and 4). The origin of this matrix is located at station $X_0 = 1107$, $Y_0 = 0$ and $Z_0 = 507$ with respect to the Shuttle Orbiter.

This particular origin in no way limits the return flux or column density calculation capability to a surface located at $X_0 = 1107$. A point select subroutine was developed for the model that will select the proper points for interpolating along any selected line-of-sight originating at any desired location as shown in Figure 5.

The amount of mass leaving each outgassing surface or other source that can enter the volume element centered around point P (Figure 4) can be computed by accessing precalculated "form factors" (or mass transport factors) between point P and each of the outgassing surfaces or vent and engine sources. As a result, the contaminant cloud density at any point above the vehicle can be defined knowing the particular source emission characteristics.

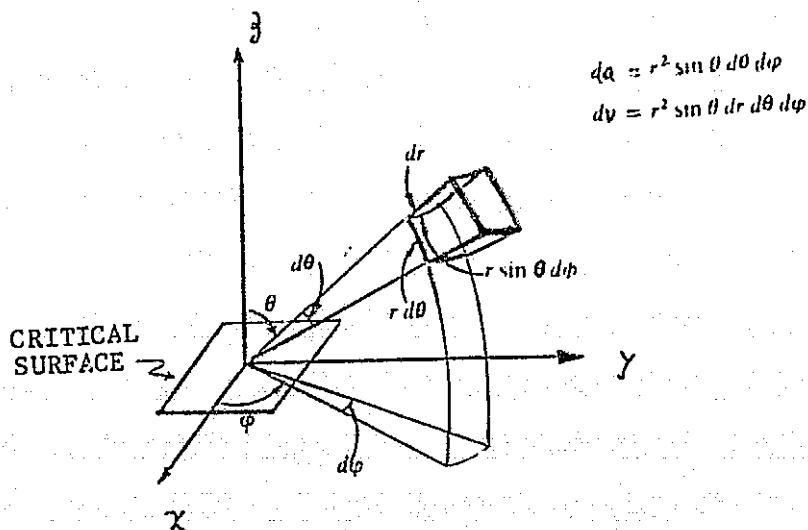


Figure 3. Elemental Volume Definition

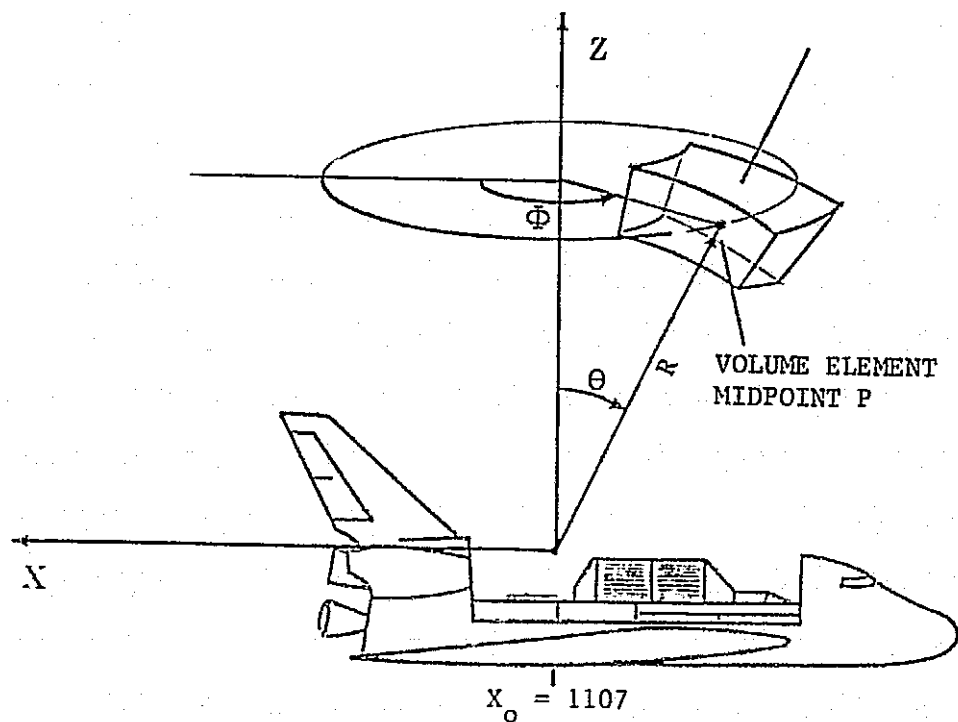


Figure 4. Elemental Volume Geometry (Line-of-Sight Location)

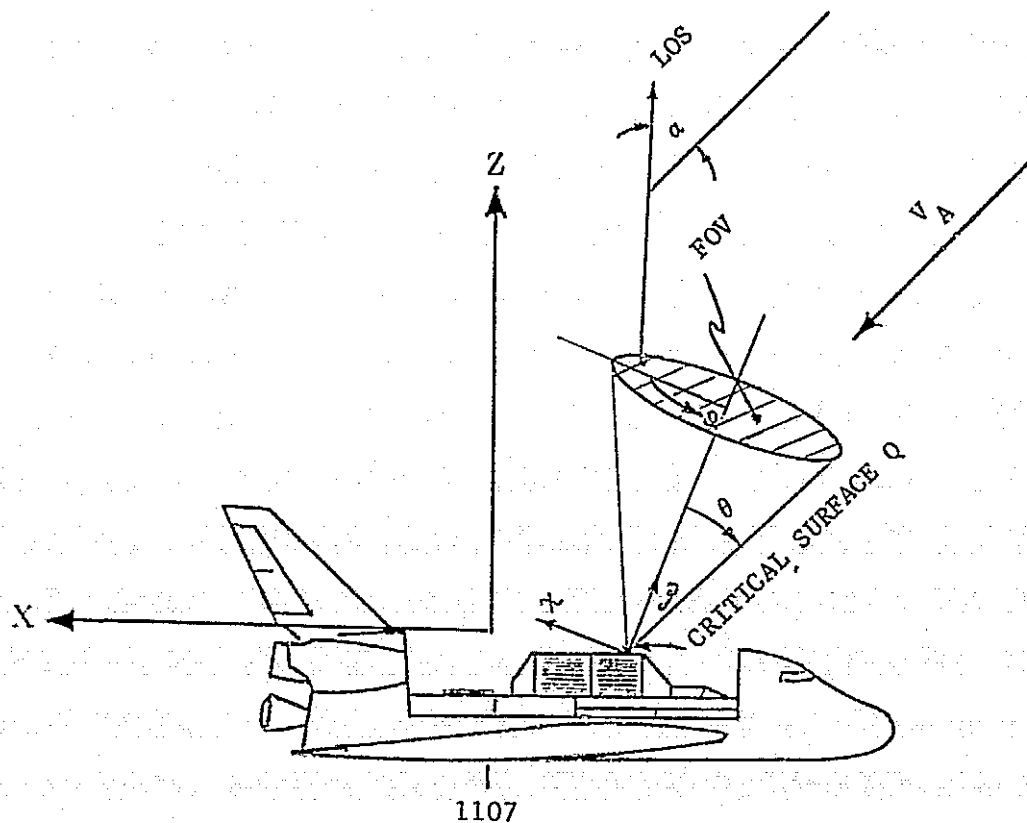


Figure 5. Critical Surface Location, Orientation and Field-of-View

To calculate the return flux to a surface, the location and orientation of the critical surface Q (Figure 5) is defined. In addition, the field-of-view (FOV) for this surface in terms of θ and ϕ and the direction of the incoming ambient flux vector, V_A , with respect to the line-of-sight (LOS) in terms of α must be defined. The return flux to the surface is then computed by performing a volume integration over the defined region of space within the surface field-of-view. (Note: abnormal fields-of-view such as rectangles can also be considered through special analytical manipulation).

The return flux per unit volume of space centered at point P is a direct function of the collision rate of the contaminant and ambient species within that volume. The collision rate can be defined by knowing the number density of both the contaminants ($N_C(P)$) and the ambient species (N_A) within that volume. This together with the relative velocity (V_A) and the effective cross section of the collision process (σ_{AC}) is used to determine the collision rate within the volume element

$$\dot{n}(P) = N_A N_C(P) V_A \sigma_{AC} \quad (14)$$

It is assumed that there is no attenuation in the ambient density due to the perturbation by the contaminant environment and that the impact of the ambient flux upon the contaminant density is negligible at all altitudes above approximately 250 km. It is also assumed that densities induced by surface sources such as outgassing and leakage can be defined knowing the mass loss characteristics and utilizing a Lambertian distribution from each surface.

A scattering model is assumed which defines the number of collisions given in equation (14) that deflect molecules toward the critical surface. The scattering model currently used by most analysts (hard sphere) reduces to a cosine or Lambertian distribution from the scattering center. By integrating over all space within the geometric acceptance angle of the FOV of a critical surface, the total return flux ($g/cm^2/s$) to the surface can be determined. Using the hard sphere scattering model, the return flux can be expressed as

$$RF = \int_{\theta} \int_{\phi} \int_0^{r_{max}} \frac{r^2 \dot{n} \cos \alpha \cos \theta \sin \theta dr d\phi d\theta}{r^2}, \quad (15)$$

or

$$RF = N_A V_A \frac{\pi}{4} \left[\mu (\delta_C + \delta_A) \right]^2 \iint_{\theta \emptyset} \frac{\cos \alpha}{\pi} \int_0^{r_{\max}} \quad (16)$$

$$\frac{N_C dr}{NCD} \sin \theta \cos \theta d\theta d\emptyset.$$

In performing the volume integration, observe that for a given θ and \emptyset that a line-of-sight (LOS) has been defined emanating from a critical surface (Figure 5). Since the scattering angle, α , is a constant along each LOS, integration is first performed over the variable r (along the LOS) to obtain the number column density (The NCD is often a useful piece of information if the surface is a viewing optic and there is concern with not only the return flux deposition but also field-of-view interference through scattering, emission and/or absorption). The return flux is, therefore

$$RF = N_A V_A \frac{\pi}{4} \left[\mu (\delta_C + \delta_A) \right]^2 \sum_N \frac{\cos \alpha_N}{\pi r^2} NCD_N r^2 \sin \theta_N \cos \theta_N \Delta \theta \Delta \emptyset, \quad (17)$$

and the volume integration has reduced to LOS integration followed by summation of a series of lines-of-sight that encompass the desired field-of-view.

Note that if equation (17) is further modified, the return flux becomes

$$RF = N_A V_A \frac{\pi}{4} \left[\mu (\delta_C + \delta_A) \right]^2 \sum_N \cos \alpha_N NCD_N \frac{\cos \theta_N}{\pi r^2} r^2 \sin \theta_N \Delta \theta \Delta \emptyset. \quad (18)$$

Now,

$$\frac{\cos \theta_N}{\pi r^2} \cdot r^2 \sin \theta_N \Delta \theta \Delta \emptyset = \Delta \frac{A_N \cos \theta_N}{\pi r^2} = VF_{I-N}$$

Therefore,

$$RF = N_A V_A \frac{\pi}{4} \left[\mu (\Delta_C + \delta_A) \right]^2 \sum_N \cos \alpha_N NCD_N VF_{I-N} \quad (19)$$

where;

NCD_N = molecular column density along line-of-sight N,
(mol/cm²),

α_N = angle the incoming ambient species subtend with
LOS N, degrees,

N_A = ambient density, (mol/cm³),

V_A = ambient velocity, (cm/s),

δ_A = ambient diameter, (cm),

μ = velocity factor (3.0 assumed) and

VF_{I-N} = form factor from volume element coincident with
line-of-sight N to surface of interest I.

This is the basic relationship currently being used to define the contaminant return flux.

An important factor in the calculation of the return flux of contaminant molecules through collisions with the ambient atmosphere is the collision cross section σ_A and the ambient density. Where possible, experimental data has been used in determining an effective collision cross section. As a result, the velocity factor μ , is included in the scattering cross-section expressions to account for the average differences between measured molecular diameters and their "effective" diameters during high speed collision processes.* The return flux expression is based on the assumption the scattered molecules are scattered in a cosine distribution with respect to the velocity vector. The assumption has also been made that the vehicle induced contaminant molecules are at rest with respect to the ambient molecules in the vehicle

* Kydd, P. H.: "Total Scattering Cross Sections of H₂O and NH₃", Journal of Chemical Physics, Vol. 37, Number 5, September 1962.

Snow, W. R. et al: "Molecular Beam Measurements of Total Collision Cross Sections of H₂O", Journal of Chemical Physics, Vol. 58, Number 6, March 1973.

frame of reference.

The ambient density can currently be requested in the model as high density daytime near sunspot maximum, low density (nighttime near sunspot minimum) and what is referred to as medium density.* Figure 6 shows the variation between the high and low case and the medium density value, Figure 7 shows the values of the 3 cases input to the model as a function of altitude. Therefore, for a complete mission profile, the variation between day time and night portions of the orbit and the influence and degree of sunspot activity must be determined. The extremes can be obtained in Figure 7.

Second Surface Transport - Impingement on a surface by a source can result in possible deposition and reemission of contaminants that do not adhere. In addition, some of the deposited material can desorb with time under the influence of temperature variations of the surface deposited on. In most instances, the effluents from the RCS engines and flash evaporator will not deposit on surfaces because of their temperature and the relatively high vapor pressure of the effluents. For this case, the reflection rate is equal to the impingement rate on a surface. The emission distribution of the reflected components is considered to be a $\cos \theta/r^2$ distribution with respect to the normal of the surface. The re-emission velocities are assumed to be the most probable velocity based upon the temperature of the emitting surface and the molecular weight of the impinging effluents.

The treatment of surface reflected species was arrived at following a survey of experimental work and contacts with investigators in this field. The following observations are pertinent to the decision to model the scattered molecules as described above:

a) Molecules with large dipole moments (H_2O , CO_2 , etc.) have long interaction times (i.e., a few milliseconds) with a surface, thus allowing for more complete thermal accommodation with a surface. That is, one or more vibrations occur before being re-emitted. The result is diffuse emission patterns.

b) Molecules with incident energies less than 1 to 2 eV exhibit diffuse scattering with surfaces.† These energies correspond to velocities of 1000 to 3000 m/s for the molecules of interest. The engine molecular exhaust products are near 3500 m/s and the evaporator exhaust near 1000 m/s and thus fall close to this energy range.

*F. S. Johnson, "Satellite Environment Handbook", second edition, Stanford University Press, 1965.

†Private communication, Dr. T. Dickinson, Washington State University.

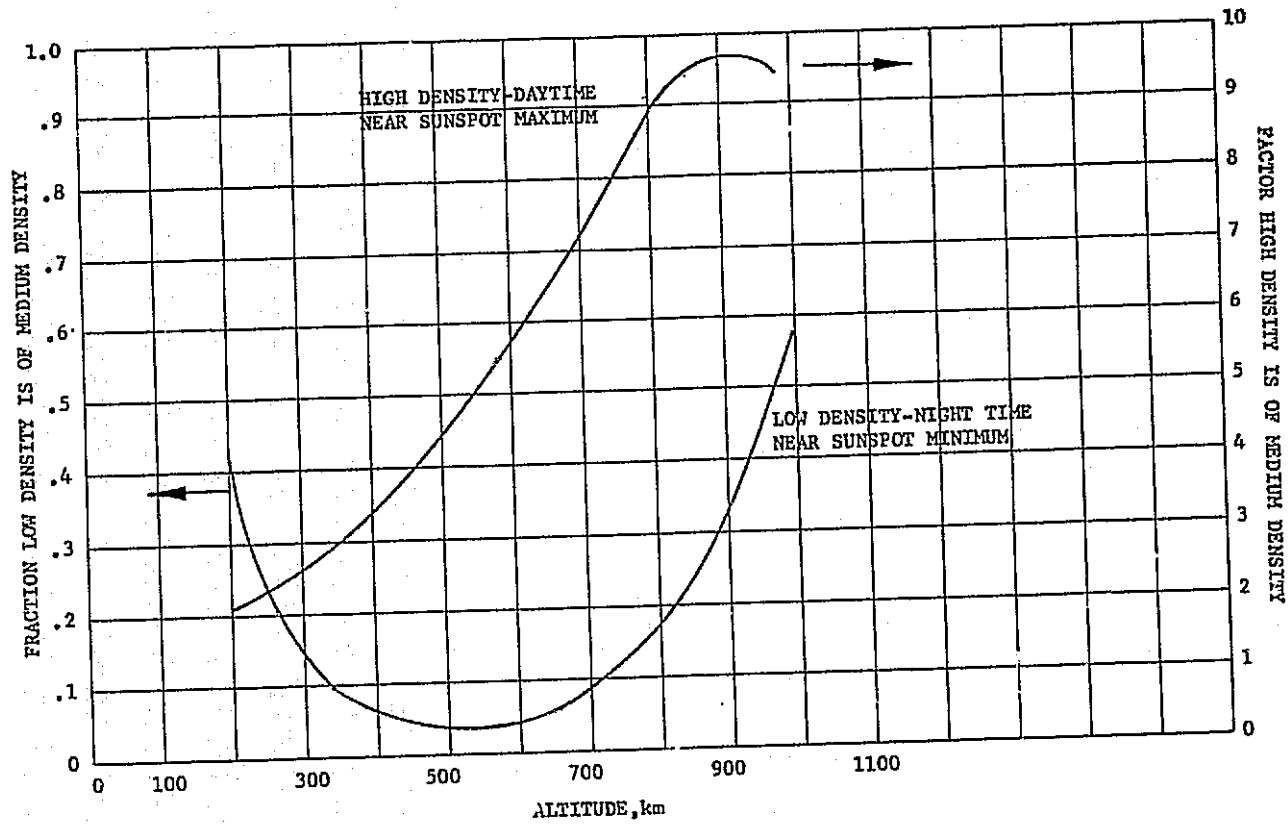


Figure 6. High Density and Low Density Ambient Atmosphere Variation From Medium Density Values

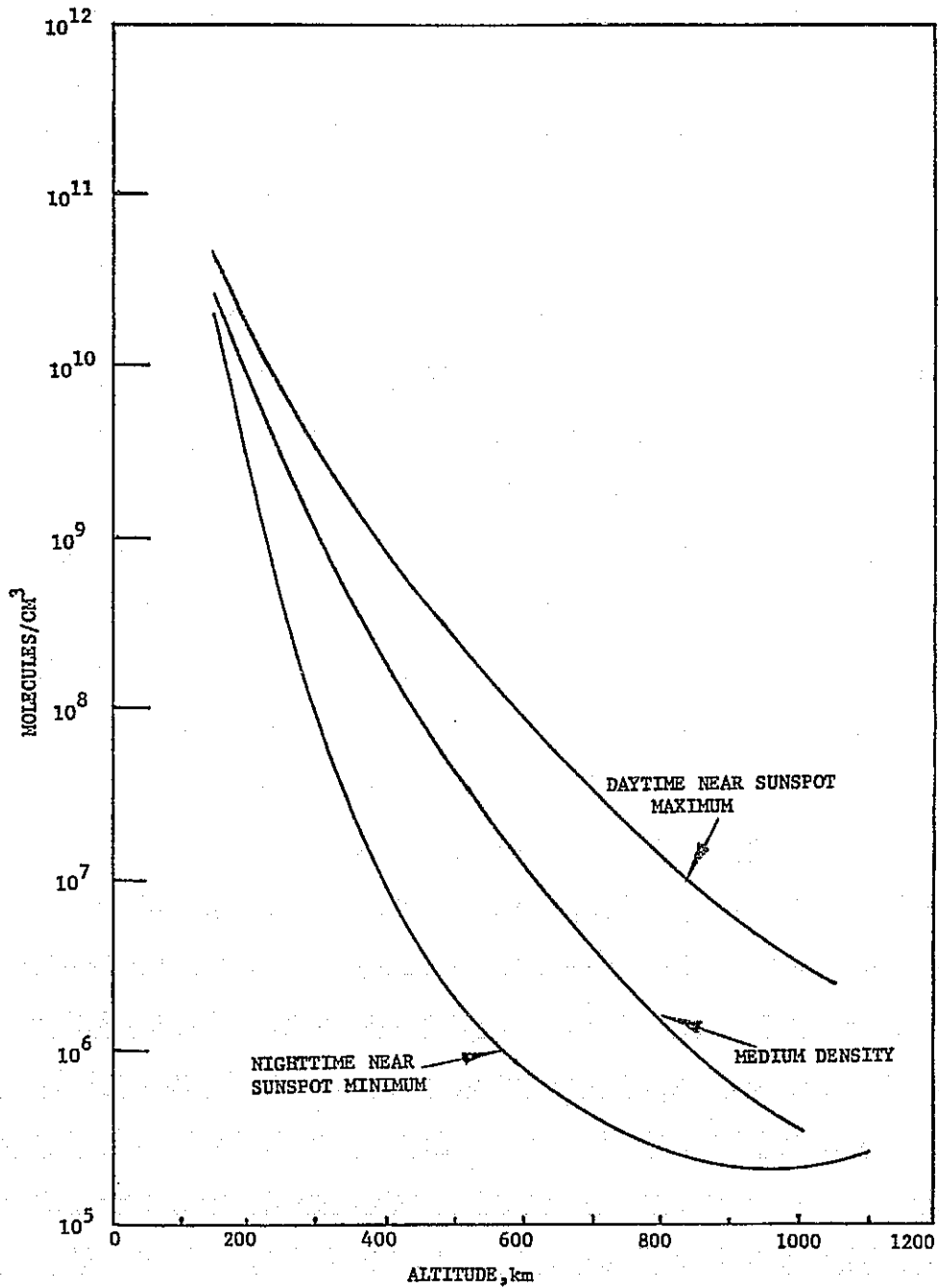


Figure 7. Molecular Density of Ambient Atmosphere Versus Altitude for the Three Densities Input to the Model

c) A rough surface causes diffuse scattering of impinging molecules. A rough surface can be categorized as one having any irregularities such as the seams, penetrations and tile cracks such as those on the Orbiter wings.

d) Contamination on a surface (even fractions of a monolayer) tends to drive specular scattering to diffuse scattering due to the nonuniformity of contaminant deposits. Significant contamination results in total diffuse scattering.

e) For the previous conditions, the scattered molecules have velocities indicative of the surface temperature impinged upon which implies complete thermal accommodation.

f) Low incident impingement angles can introduce lobular scattering (approaching specular) for a very clean surface with none of the above conditions.

g) Specular scattering of molecules is very hard to obtain and requires ultra-high vacuum conditions, atomically smooth, well characterized surfaces, no contamination, and a unique gas and surface combination.

h) The portion of the plumes impinging on the wing surfaces that can contribute to the lines-of-sight are in the near molecular and free molecular flow regime, thus approximating experimental conditions from which the results were obtained for the decision making process.

i) For regions of the plume that are viscous (continuum) or in the transition flow region from viscous to molecular and are impinging on the Shuttle Orbiter wing surfaces, the angle of incidence is near perpendicular, significant plume interference will occur.* However, once the engine/vent has been turned off, the reemission from those surfaces impinged upon will be diffuse.

Therefore, the available data appears to strongly support a cosine (diffuse) scattering from the Orbiter Surfaces (in particular the wings) for the conditions anticipated on orbit.

For materials that do deposit and are subsequently desorbed, the desorption rate can be expressed by

*Robertson, S. J.: "Molecular Scattering of Vernier and Flash Evaporator Plumes from Space Shuttle Orbiter Wings", LMSC-HREC TMD496810, April 1976, Lockheed Missiles and Space Company, In.

$$\dot{m}_j = 5.83 \times 10^{-2} P_v \left(\frac{M}{T} \right)^{1/2}, \quad (20)$$

where;

- \dot{m}_j = mass loss, g/cm²/s,
- P_v = vapor pressure, Torr,
- M = molecular weight and
- T = temperature °K.

The emission pattern of desorbed gases is known to be cosine dependent also. Therefore, if the vapor pressure and molecular weight of a gas is known (i.e., water), the desorption rate can be determined as a function of temperature and treated in a manner analogous to outgassing sources which utilizes viewfactors to a point or a surface in determining flux. This can be expressed as

$$\dot{m}_p = 5.83 \times 10^{-2} P_{vj} \left(\frac{M_j}{T_j} \right)^{1/2} V_{j-p}, \quad (21)$$

where;

- \dot{m}_p = mass flux at a point p,
- P_{vj} = vapor pressure of source j at temperature T_j ,
- T_j = source j temperature,
- M_j = molecular weight of source j and
- V_{j-p} = viewfactor between source j and point p.

Alternatively, an expression $\dot{m}_j = A_j e^{-E/RT}$ can be used such as for early desorption. Some pure material mass loss rates can be expressed in this manner.

Contaminant Self-Scattering - This situation occurs when the density of contaminant gases allows significant collisions among like molecules or combinations of spacecraft induced molecules. In most instances, this effect is secondary in nature when compared to other mechanisms already cited above. Unique situations involving confined volumes and high source rates may require consideration of self-scattering. Self-scattering of a contaminant species uses an approach similar to return flux as proposed by Robertson.*

*Robertson, S. J.: "Spacecraft Self-Contamination Due to Back-Scattering of Outgas Products", LMSC-HREC TR D496676, January 1976, Lockheed Missiles and Space Company, Inc.

For the case of self scattering, equation 14 is replaced by

$$\dot{n}_{ss} (P) = \frac{N_{C1}}{2} \cdot \frac{N_{C2}}{2} (P) (V_{C1} + V_{C2}) \cdot \frac{\pi}{4} \left[\mu (\delta_{C1} + \delta_{C2}) \right]^2 \quad (22)$$

$$\frac{N_C^2 (P) V_C \pi \mu^2 \delta_C^2}{2} \text{ (for like contaminants),}$$

where;

C1 and C2 denote contaminant species 1 and 2, respectively.

Using the assumption that the self scattered molecules emerge from the volume element with an equal probability in all directions and integrating over the hemispherical space above the vehicle, the self-scattering return flux becomes

$$RF_{ss} = \iiint_{\theta \phi r} \frac{\dot{n}_{ss} \cos \theta r^2 dr d\theta d\phi}{4\pi r^2}, \text{ or}$$

$$RF_{ss} = \frac{(V_{C1} + V_{C2}) \left[\mu (\delta_1 + \delta_2) \right]^2}{64} \pi \iint_{\theta \phi} \left[\int_0^{r_{max}} \underbrace{N_1 \cdot N_2}_{N_{ss}} dr \right] \cdot \frac{\sin \theta \cos \theta r^2 d\theta d\phi}{r^2} \quad (23)$$

Although the volume integration is performed over the variable r first (in brackets), the result is not the NCD as found for return flux. This term is easily integrated in the model with the final relationship determined using the same procedure as was used in the equation (19) determination.

Therefore, the self scattering return flux is

$$RF_{ss} = (V_{C1} + V_{C2}) \frac{\pi}{64} \left[\mu (\delta_1 + \delta_2) \right]^2 \sum_N N_{ssN} \cdot VF_{I-N} \quad (24)$$

Plume Intermolecular Interference - Situations can occur where the effluent reflected off of a surface can interfere with the incoming effluents. This occurs for large sources such as the flash evaporators or the attitude control engines. This, in effect, would reduce some of the surface reflection rates during operation of the source. However, once the source ceases, there could be a larger burst of effluents from a surface that were held there (viscous layer) by the action of the incoming effluent plume. Because of the uncertainties in determining both these phenomena and their cancellation effect on each other with time it is generally accurate to allow the impingement rate from a high volume source to be the reflected rate. For experiments that cannot tolerate unusually high pulses over a short period of time, this effect should be investigated further.

Ambient Impingement - The model currently assumes no impingement of the ambient atmosphere on surfaces parallel to the ambient gas flow as it streams by the Orbiter at orbital velocities (near 8 km/s). As said another way, the potential of return flux does not exist when the ambient velocity vector is greater than 90 degrees with a surface or receptor normal. However, there does exist an ambient molecule flux perpendicular to the velocity vector and is a function of the ambient gas internal thermal temperature. This can be expressed as:

$$\dot{m}_i = \frac{N_A \bar{V}_A}{4},$$

where;

\dot{m}_i = flux of ambient on surface i parallel to orbital velocity vector,

N_A = ambient density and

\bar{V}_A = average thermal velocities of ambient gas.

This expression is analogous to the expression for a surface in a static vacuum chamber under laboratory conditions and does hold for the case presented above. The actual impact of this phenomena for return flux should be less when considering orbital velocities (approximately 8 km/s) and thermal velocities (approximately 1 km/s) for momentum exchange with contaminant molecules and subsequent scattering. However, once again this may be of importance for unique systems or situations.

Surface Deposition Determination - The direct source-to-surface outgassing sticking coefficient term

$$\frac{T_j - T_i}{200}, = 0 \text{ for } T_i > T_j,$$

where;

T_j = source temperature, °C and

T_i = surface temperature of receiver, °C,

was estimated from percent weight loss and percent VCM comparisons from materials testing.* The value of 200 in the denominator is the worst case for the materials observed. The option exists to replace this value with other values for different materials so that the general value of 200 may be substituted as data is available. For lack of good test data, this approach is currently baselined in the model.

The relation also encompassed limited data† observed at other source temperatures. The deposits observed during these tests is of a permanent nature and of long duration. It was decided during the Skylab Program that a desorption equation based on $e^{-E/RT}$ for the deposit would not suffice. This type of phenomena was also apparent in the TPS tests conducted at MSFC where heating the QCM did not remove the deposit even though it should have if the 15 Kcal/mole ascertained at lower temperatures for the source was applied to the deposit.

The problem is that the source activation energies cannot be applied to VCM deposits on a surface because repolymerization or other chemical reactions can occur. In the presence of sunlight, photopolymerization can also occur thus changing the nature of the deposit. It was for these reasons that a simplified sticking coefficient based on a limited temperature range of materials testing was applied for the Skylab outgassing contaminants.

*Miraca, R. F. and Whittick, J. S.: "Polymers for Spacecraft Applications", N67 40270, Stanford Research Institute, September 15, 1967.
Campbell, W. A., et al: "A Compilation of Outgassing Data for Spacecraft Materials", NASA TND 7362.

†Poehlman, H. C.: "Vacuum Weight-Loss and Contamination Tests of Some Materials for Space Application", Proc. of the Fourth INTERNL. Vacuum Congress 1968.

Figure 8 shows the comparison of the $\frac{T_j - T_i}{200}$ expression to test data of RTV-602 outgassing onto a gold substrate. The upper curve corresponds to the $\frac{T_j - T_i}{150}$ expression while the lower predicted curve corresponds to $\frac{T_j - T_i}{200}$ which was preliminarily determined from testing of DC-92007 white paint at JSC.

Ideally, the condensation or sticking coefficient should be determined experimentally using the expression

$$\dot{m}_i = \dot{m}_j S_{j-i} VF_{i-j} - \dot{m}_{ej} \quad (26)$$

where;

- \dot{m}_i = the condensation rate on surface i,
- \dot{m}_j = mass loss rate of source j,
- S_{j-i} = fraction of j condensing on i at the temperature T_i ,
- VF_{i-j} = viewfactor and
- \dot{m}_{ej} = reevaporation rate of j deposit from i at temperature T_i .

This test should be performed with and without vacuum ultraviolet radiation of the deposit during deposition to determine the change in \dot{m}_{ej} and any possible influence on S_{j-i} , the condensation coefficient. Until adequate testing has been performed, the previous temperature difference expression for outgassing deposition is used in the model. Material testing currently being conducted at MMA has as a primary goal the determination of values of \dot{m}_j , S_{j-i} and \dot{m}_{ej} for accurate modeling in the future.

The condensation coefficient for return flux (either from self-scattering or ambient collisions) could be calculated in a way similar to equation (25). However, one must consider the molecular kinetic energy gained during the collision processes and its ultimate impact on the ability of a contaminant molecule to adhere to a surface. Existing ground test data of this phenomena is inadequate to establish a general condensation coefficient relationship. It is, therefore, necessary to select a value for this parameter based upon engineering judgement of the analysis being conducted.

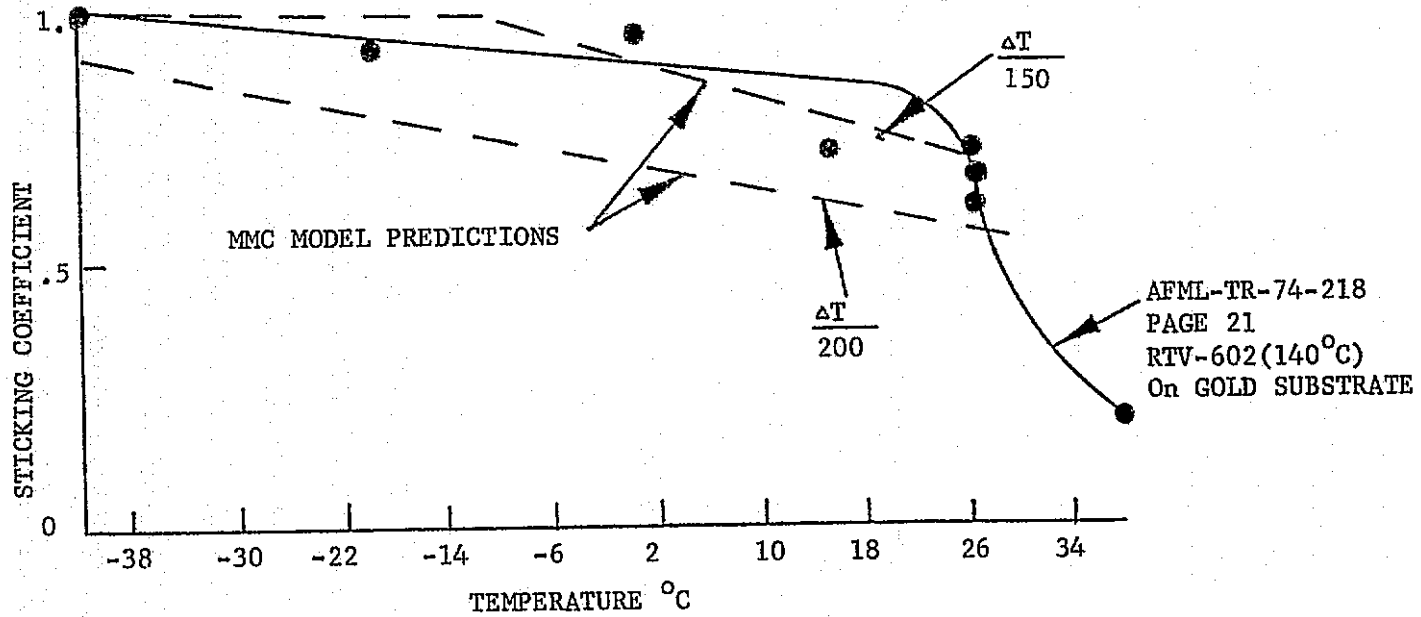


Figure 8. Comparison of Model Sticking Coefficient Prediction to Testing

This value could be estimated by averaging the temperatures of the deposition sensitive surface, T_1 . Additional items which should also be considered include:

a) If the deposition sensitive surface operates at cryogenic temperatures, the sticking coefficient for return flux will be near 1;

b) If the deposition sensitive surface operates at warm temperatures ($>50^{\circ}\text{C}$), the sticking coefficient will probably be relatively low (i.e., < 0.1) (dependent upon source temperatures); and

c) If the deposition sensitive surface operates at nominal temperatures (approximately 25°C), the sticking coefficient averaged over a typical orbit (60 to 70% sunlite exposure) will probably fall within the range of 0.25 to 0.30 (dependent upon source temperatures).

Each situation requires individual evaluation, and therefore, the model has been configured to accept user input of the return flux sticking coefficient for surface deposition analysis. When, and if the influence of this phenomena is accurately determined through ground testing or flight experimentation, the methodology can and should be refined.

For MMH/ N_2O_4 bi-propellant engines, the condensation coefficient has been determined through limited engine testing at Lewis Research Center to be 0.002 of the total engine flux. This value was established during engine testing with deposition collectors held near 0°C and was reverified by onboard deposition detectors of Skylab operating at an average temperature near 10°C . The deposits observed during the engine testing were determined to be MMH-Nitrate which is a small fraction of the total engine effluents. For the simple gases which comprise the majority of engine exhausts (H_2O , H_2 , etc.), the desorption rate on a surface is compared to the corresponding engine flux rate to determine if a net deposit could result. Surface desorption rates are calculated utilizing the vapor pressure equation (20) knowing the temperature of the given surface.

3.1.1.3 Contamination Degradation Effects - Once the amount of a material on a surface or in a field-of-view is determined; the effect on experiments, sensors or thermal control surfaces must be ascertained. This type of analysis is not currently a part of the contamination math model. Initially, the model was developed for design and trade studies. The predicted values were then compared

to established contamination criteria established for the STS. However, as mission analyses becomes important and the effects upon given payloads must be better understood, these effects will become important considerations for the model.

Deposited Films - Associated with each contaminant species, or a known combination, a series of coefficients can be developed that relate the change in transmission of a particular wavelength through the deposited film; relate the change in reflectance of a particular wavelength that interacts with the deposited film; relate the change in conductivity of the surface or relate changes in solar absorptivity and emissivity. The net effect of a contaminant deposit is to reduce transmitted signal strength, change the reflectivity of a surface, change its electrical properties or discolor a thermal control surface. For integrated responses such as solar cells or eye response, the attenuation must be applied to all wavelengths of the detector response curve. The deposit characteristics can change significantly in the presence of ultraviolet, electron or proton radiation through chemical changes of the deposited film.

Normally, the shorter wavelengths (UV) are affected the most, even by relatively small levels of contaminant. The visible and infrared wavelengths are affected to a lesser degree.

It was noted that on Skylab the white thermal control surfaces experienced a solar absorptivity change from 0.18 to 0.25 due to surface deposits and their subsequent interaction with solar ultraviolet radiation.

By changing the electrical conductivity of surfaces, the deposit could cause a conductor to become a semiconductor thus changing the charge characteristics of the surface. This could lead to serious voltage breakdown problems for differentially charged areas and could also enhance the deposition of ionized molecules or charged particles.

Cloud Degradation - Particular experiments or instruments are sensitive to specific molecular or particulate species in their field-of-view. The degradation mechanisms are molecular scattering, absorption or emission and particulate scattering or emission. The net effect is an addition to or reduction of a signal for a particular wavelength of interest. Computer programs are in existence that can predict the above mentioned degradation effects.

Other Effects - Other degradation phenomena that can occur and cause irreparable damage or unsatisfactory operation are corona and multipacting. Corona occurs when the induced contaminant gas density in the vicinity of high voltages is sufficient to cause electrical breakdown through the gas cloud. This is likely to occur in poorly vented areas and/or where contaminant effluent levels are high.

Multipacting occurs when the gas density in the vicinity of an antenna is high enough to allow ionized contaminants (by photoionization) to impinge on the antenna thus releasing secondary electrons which develop into an interference cloud around the antenna rendering it inoperable for periods.

3.1.2 Orbiter Surface Description - This section lists all of the Orbiter surfaces modeled and schematically shows the numbering scheme of the surfaces. The groupings by surface type and surface sections are also identified and pictorially presented. The Orbiter has undergone physical changes during this contract to the nose/cabin area, tail, radiators, wings and elevon. These areas of the Shuttle Orbiter were updated for geometry fidelity and resolution.

The Orbiter wing underwent a series of final modifications because of the extremely high fidelity required for analyzing the effects from the evaporator located when near the proposed $X = 1507$ and $Z = 305 \pm 15$ site. Figure 9 shows the new wing shape and the previous wing shape. There were 4 areas of modification for the Orbiter wing. The first was positioning the high point of the wing (along Z) at exactly $X = 1024$ and was extended along Y at this point another 16 inches. The second area was the slope of the trailing edge of the wing from the high point to the trailing edge of the elevon. The third area was the six inch gap between the elevon and the Orbiter fuselage. The fourth area of modification was the increased resolution of the trailing edge from a one node triangle to a 10 node triangle. These modifications reflect the latest Rockwell data.

Figure 10 shows the updated nose/cabin configuration. A series of planar surfaces plus an end cap were used for defining the nose shape instead of surfaces of revolution used previously. This allowed for more accurate simulation of the "drop nose" feature of

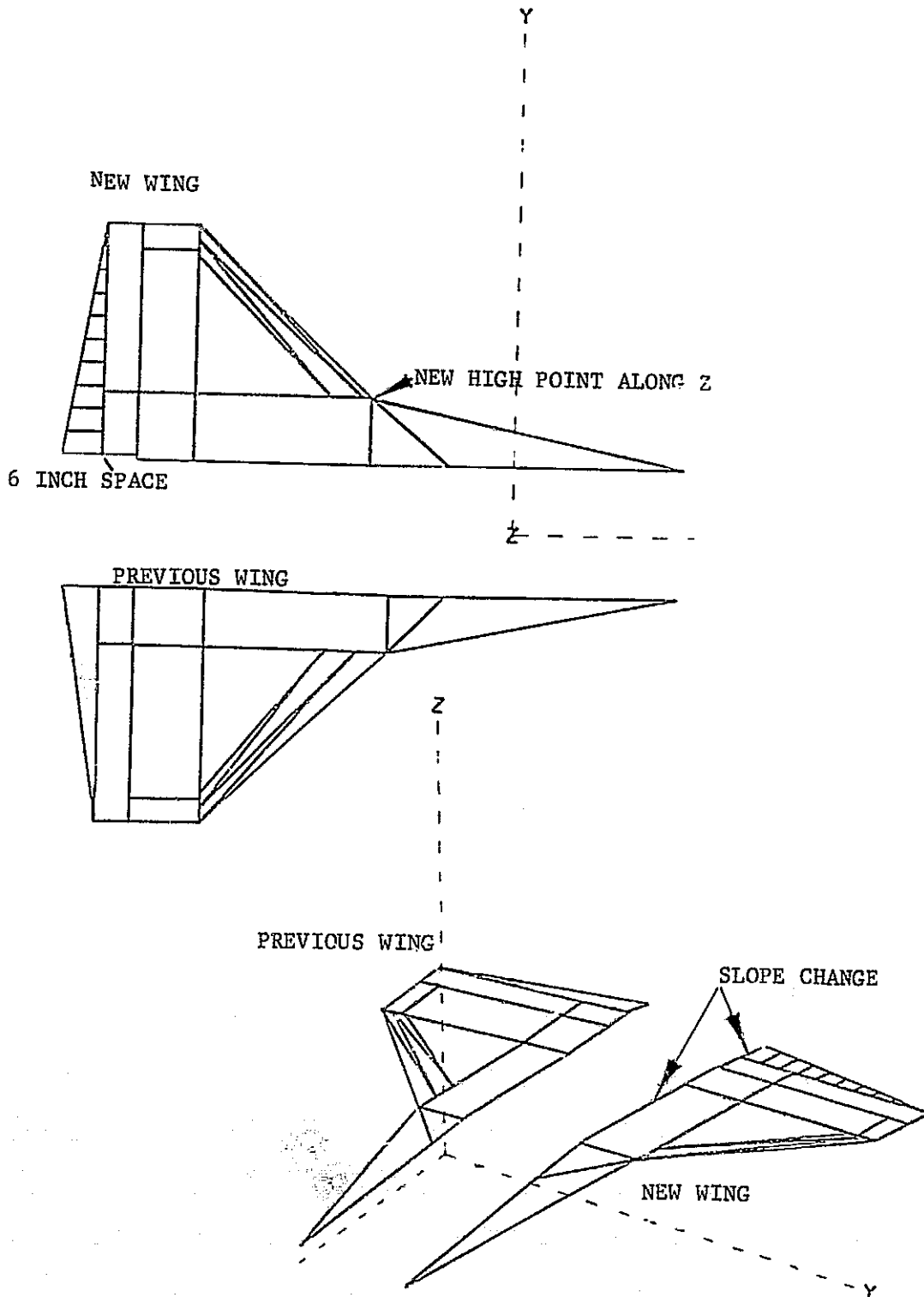
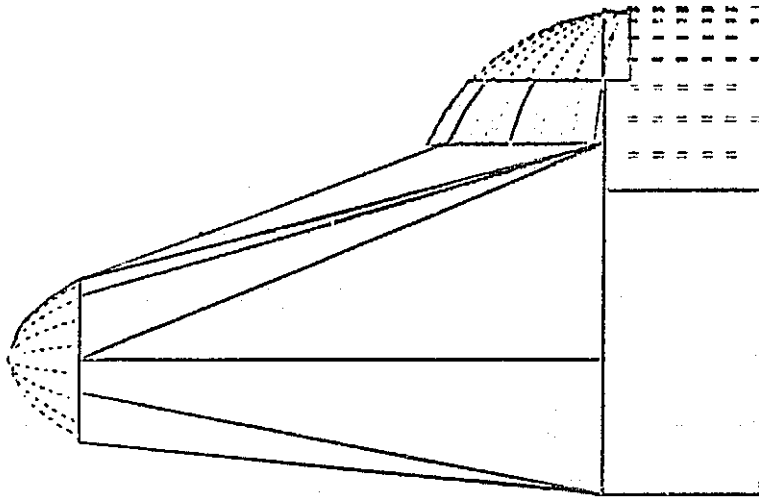
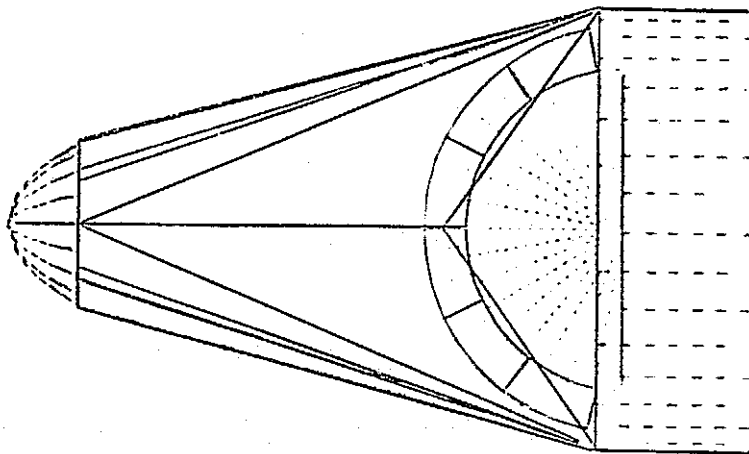


Figure 9. New Wing Configuration Compared to Previous Wing



Side View



Top View

Figure 10. Updated Nose/Cabin Configuration

the Orbiter and evaluation of engine impingement and flowfield evaluation. Figure 11 shows isolated views of the tail section. The major feature of importance from a contamination viewpoint is the angle of the tail sides. This will allow a small fraction of either outgassed material or reflected engine exhausts to impinge on the door radiators and the payload bay opening. This slope is best visualized in the top view of the tail in Figure 11. Figures 12 and 13 show the overall configuration of the new Orbiter when compared to the previous configuration. The new configuration shown in Figures 12 and 13 represent the configuration used in the present model.

The surface data input for the Thermal Radiation Analysis System (TRASYS)* includes a descriptive name, type of surface, its assigned number, the number of nodes that it is divided into and the actual coordinate input data to the TRASYS system for determination of the geometric relationships. Table I is a list of all but the detailed coordinate input data for the Shuttle Orbiter surfaces, Table II lists the actual input surface data to TRASYS for geometry relationship determination.

From the specific TRASYS input parameters; the user can determine the exact shape, location, orientation, size and shadowing properties of individual surfaces. All input parameters are in units of inches from a selected coordinate system origin. The surface input data to TRASYS presented here is based upon a coordinate system compatible with the standard NASA STS axis/station number identification system. To facilitate programming, two differences exist. The differences involve transformation of the coordinate system origin to NASA station $X_o = 800$, $Y_o = 0$, $Z_o = 400$ and reversing the right-handed system from +X aft to +X forward. This was done solely to allow for proper sizing and maximum visibility of the TRASYS generated graphic displays of the Orbiter configuration and is unique to the TRASYS input. To convert NASA station numbers to those used in the model the following transformation must be used,

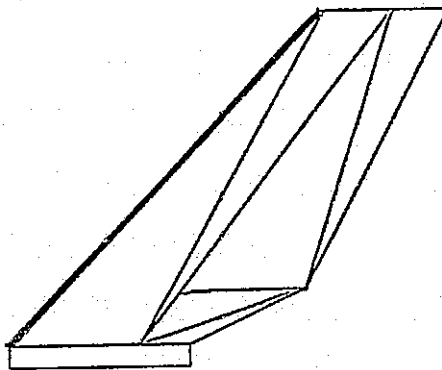
$$\begin{aligned} X_m &= X_o - 800 \\ Y_m &= -Y_o \\ Z_m &= Z_o - 400 \end{aligned}$$

where the subscript m refers to the TRASYS model input and the subscript o refers to NASA STS station numbers.

*"Thermal Radiation Analysis System (TRASYS II) User's Manual", MCR-73-105 (Revision 1), contract NAS9-14318, Martin Marietta Aerospace, Denver Division, May 1975.

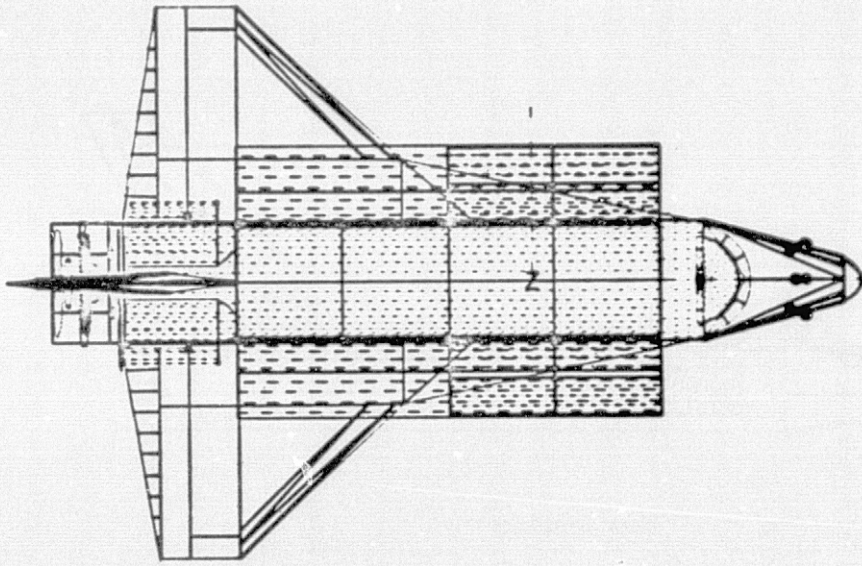


Top View

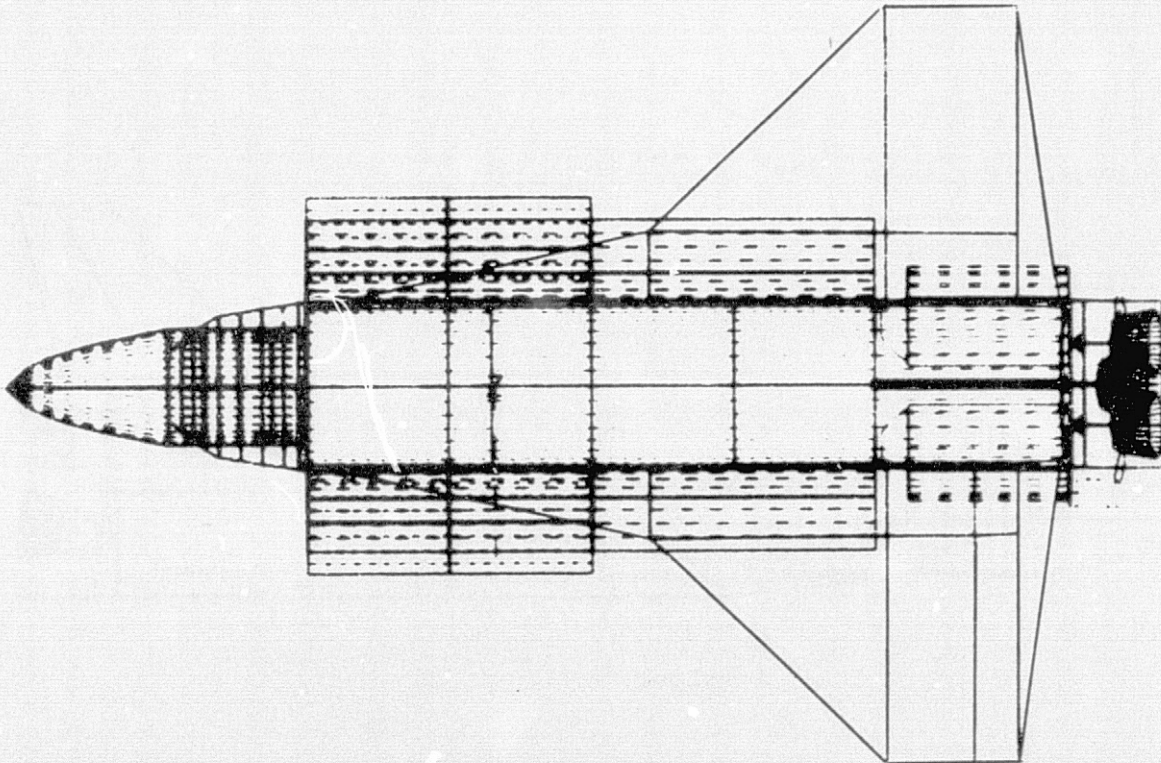


Side View

Figure 11. Updated Tail Configuration

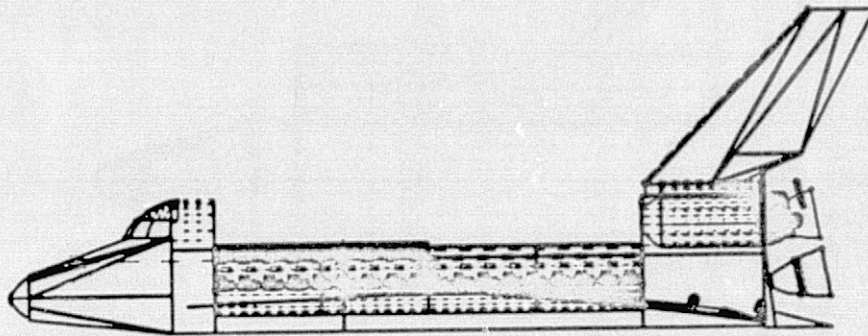


New Update

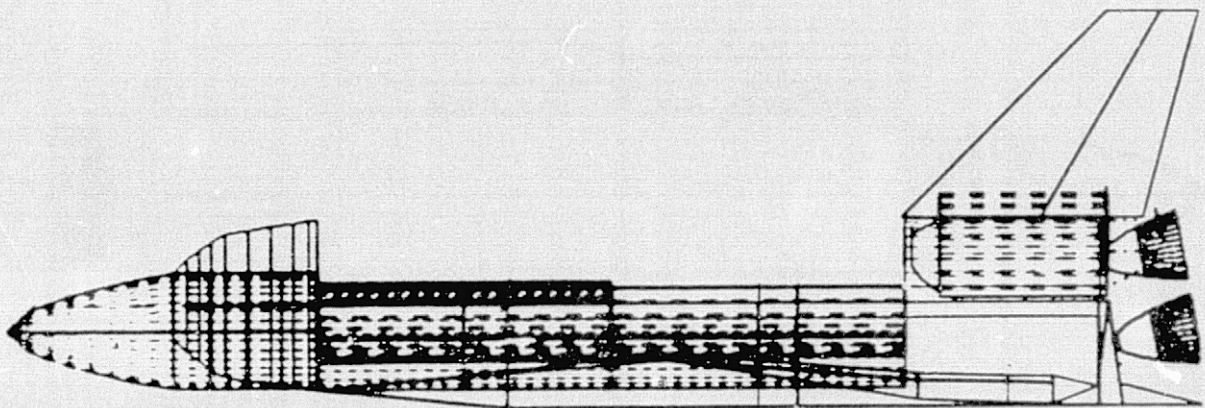


Previous

Figure 12. Updated and Previous Configuration of the Shuttle Orbiter (Top View)



New Update



Previous

Figure 13. Updated and Previous Configuration of the Shuttle Orbiter (Side View)

TABLE I. SHUTTLE ORBITER GEOMETRY BREAKDOWN

<u>GENERAL AREA</u>	<u>NAME</u>	<u>TYPE</u>	<u>SURFACE NUMBER</u>	<u>NUMBER OF NODES</u>	<u>NODE NUMBERS</u>
BODY	BAY AREA BOTTOM CYLINDER	CYLINDER	1	8	1, 2, 3, 4, 5, 6, 7, 8
	INSIDE -Y LINER STRIP	RECTANGLE	440	4	440, 441, 442, 443
	INSIDE +Y LINER STRIP	RECTANGLE	445	4	445, 446, 447, 448
	FRONT BAY AREA DISK	DISK	13	1	13
	END BAY AREA DISK	DISK	11	1	11
	-Y RADIATOR	CYLINDER	20	8	20, 21, 22, 23, 24, 25, 26, 27
	+Y RADIATOR	CYLINDER	30	8	30, 31, 32, 33, 34, 35, 36, 37
	-Y SIDE DOOR	CYLINDER	40	8	40, 41, 42, 43, 44, 45, 46, 47
	+Y SIDE DOOR	CYLINDER	50	8	50, 51, 52, 53, 54, 55, 56, 57
	BACK BODY TOP	CYLINDER	202	2	202, 203
	BACK RECTANGLE @ 7.35 DEGREES	RECTANGLE	230	1	230

TABLE I. SHUTTLE ORBITER GEOMETRY BREAKDOWN (cont'd)

<u>GENERAL AREA</u>	<u>NAME</u>	<u>TYPE</u>	<u>SURFACE NUMBER</u>	<u>NUMBER OF NODES</u>	<u>NODE NUMBERS</u>
BODY	REAR FLAT PLATE OUT BACK	RECTANGLE	250	1	250
	SLOPING REAR FLAT PLATE	RECTANGLE	260	1	260
	-Y SIDE FRONT TRAPEZOID	RECTANGLE	301	1	301
	+Y SIDE FRONT TRAPEZOID	RECTANGLE	311	1	311
	-Y SIDE PANEL	RECTANGLE	305	2	305, 306
	+Y SIDE PANEL	RECTANGLE	315	2	315, 316
	REAR PORT BACK, SIDE	RECTANGLE	307	1	307
	REAR STARBOARD BACK, SIDE	RECTANGLE	317	1	317
	-Y REAR SIDE TAPER	TRAPEZOID	420	1	420
	+Y REAR SIDE TAPER	TRAPEZOID	425	1	425
BODY:	TOTAL SURFACES = 21		TOTAL NODES = 65		
CREW	NOSE	PARABOLOID	160	1	160

TABLE I. SHUTTLE ORBITER GEOMETRY BREAKDOWN (cont'd)

<u>GENERAL AREA</u>	<u>NAME</u>	<u>TYPE</u>	<u>SURFACE NUMBER</u>	<u>NUMBER OF NODES</u>	<u>NODE NUMBERS</u>
CREW	+Y TOP NOSE TRIANGLE	POLYGON	162	1	162
	-Y TOP NOSE TRIANGLE	POLYGON	161	1	161
	FIRST -Y SIDE NOSE TRIANGLE	POLYGON	163	1	163
	FIRST +Y SIDE NOSE TRIANGLE	POLYGON	164	1	164
	SECOND -Y SIDE NOSE TRIANGLE	POLYGON	165	1	165
	SECOND +Y SIDE NOSE TRIANGLE	POLYGON	166	1	166
	THIRD -Y SIDE NOSE TRIANGLE	POLYGON	167	1	167
	THIRD +Y SIDE NOSE TRIANGLE	POLYGON	168	1	168
	-Y SIDE NOSE TRAPEZOID	TRAPEZOID	169	1	169
	+Y SIDE NOSE TRAPEZOID	TRAPEZOID	170	1	170
	-Y SIDE BOTTOM NOSE TRIANGLE	POLYGON	171	1	171
	+Y SIDE BOTTOM NOSE TRIANGLE	POLYGON	172	1	172

TABLE I. SHUTTLE ORBITER GEOMETRY BREAKDOWN (cont'd)

<u>GENERAL AREA</u>	<u>NAME</u>	<u>TYPE</u>	<u>SURFACE NUMBER</u>	<u>NUMBER OF NODES</u>	<u>NODE NUMBER</u>
CREW	NOSE CYLINDER HOOD	CYLINDER	174	1	174
	-Y RECTANGLE BELOW SURFACE 174 NOSE HOOD	RECTANGLE	175	1	175
	+Y RECTANGLE BELOW SURFACE 174 NOSE HOOD	RECTANGLE	177	1	177
	WINDOW SPHERE SECTION	SPHERE	180	6	180, 181, 182, 183, 184, 185
	DOME SPHERE SECTION ABOVE WINDOW	SPHERE	190	1	190
CREW:	TOTAL SURFACES = 18		TOTAL NODES = 23		
TAIL	LEADING EDGE TAIL FIN	CYLINDER	399	1	399
	FIRST POLYGON -Y SIDE	POLYGON	380	1	380
	SECOND POLYGON -Y SIDE	POLYGON	382	1	382
	THIRD POLYGON -Y SIDE	POLYGON	384	1	384
	FOURTH POLYGON -Y SIDE	POLYGON	386	1	386

TABLE I. SHUTTLE ORBITER GEOMETRY BREAKDOWN (cont'd)

<u>GENERAL AREA</u>	<u>NAME</u>	<u>TYPE</u>	<u>SURFACE NUMBER</u>	<u>NUMBER OF NODES</u>	<u>NODE NUMBER</u>
TAIL	FIFTH POLYGON BENEATH SURFACE 386 (-Y)	POLYGON	388	1	388
	SIXTH POLYGON BENEATH SURFACE 388 (-Y)	POLYGON	390	1	390
	BOTTOM TAIL RECTANGLE	RECTANGLE	392	2	392, 393
	FIRST POLYGON +Y SIDE	POLYGON	381	1	381
	SECOND POLYGON +Y SIDE	POLYGON	383	1	383
	THIRD POLYGON +Y SIDE	POLYGON	385	1	385
	FOURTH POLYGON +Y SIDE	POLYGON	387	1	387
	FIFTH POLYGON BENEATH SURFACE 387 (+Y)	POLYGON	389	1	389
SIXTH POLYGON BENEATH SURFACE 389 (+Y)	POLYGON	391	1	391	

TAIL: TOTAL SURFACES = 14 TOTAL NODES = 15

TABLE I. SHUTTLE ORBITER GEOMETRY BREAKDOWN (cont'd)

<u>GENERAL AREA</u>	<u>NAME</u>	<u>TYPE</u>	<u>SURFACE NUMBER</u>	<u>NUMBER OF NODES</u>	<u>NODE NUMBER</u>
WING	FIRST TRIANGLE NOMEX WING (-Y)	TRAPEZOID	100	1	100
	FIRST RECTANGLE NOMEX WING (-Y)	RECTANGLE	102	1	102
	SECOND RECTANGLE (TOWARD X) NOMEX WING (-Y)	RECTANGLE	104	1	104
	TRIANGLE ABOVE SURFACE 102 NOMEX WING (-Y)	TRAPEZOID	110	1	110
	INSERT IN WING TILE WING (-Y)	POLYGON	117	1	117
	OUTER WING STRIP CARBON WING (-Y)	POLYGON	121	1	121
	LONG BACK RECTANGLE NOMEX WING (-Y)	RECTANGLE	112	1	112
	SHORT BACK RECTANGLE ON BOTTOM OF 112 TILE WING (-Y)	RECTANGLE	119	1	119
	FORWARD TRIANGLE TILE WING (-Y)	TRAPEZOID	115	1	115

TABLE I. SHUTTLE ORBITER GEOMETRY BREAKDOWN (cont'd)

<u>GENERAL AREA</u>	<u>NAME</u>	<u>TYPE</u>	<u>SURFACE NUMBER</u>	<u>NUMBER OF NODES</u>	<u>NODE NUMBER</u>
WING	FIRST TRIANGLE NOMEX WING (+Y)	TRAPEZOID	130	1	130
	FIRST RECTANGLE NOMEX WING (+Y)	RECTANGLE	132	1	132
	SECOND RECTANGLE (TOWARD X) NOMEX WING (+Y)	RECTANGLE	134	1	134
	TRIANGLE ABOVE SURFACE 132 NOMEX WING (+Y)	TRAPEZOID	140	1	140
	INSERT IN WING TILE WING (+Y)	POLYGON	147	1	147
	OUTER WING STRIP CARBON WING (+Y)	POLYGON	151	1	151
	LONG BACK RECTANGLE NOMEX WING (+Y)	RECTANGLE	142	1	142
	SHORT BACK RECTANGLE ON TOP OF 142 TILE WING (+Y)	RECTANGLE	149	1	149
	FORWARD TRIANGLE TILE WING (+Y)	TRAPEZOID	145	1	145

WING:

TOTAL SURFACES = 18 TOTAL NODES = 18

3-45

TABLE I. SHUTTLE ORBITER GEOMETRY BREAKDOWN (cont'd)

<u>GENERAL AREA</u>	<u>NAME</u>	<u>TYPE</u>	<u>SURFACE NUMBER</u>	<u>NUMBER OF NODES</u>	<u>NODE NUMBER</u>
ELEVON	THIRD RECTANGLE (INNER AILERON) NOMEX WING (-Y)	RECTANGLE	106	1	106
	THIRD RECTANGLE (OUTER AILERON) NOMEX WING (-Y)	RECTANGLE	107	1	107
	TAIL EDGE NOMEX WING (-Y)	POLYGON	450	10	450, 451, 452, 453, 454, 455, 456, 457, 458, 459
	THIRD RECTANGLE (INNER AILERON) NOMEX WING (+Y)	RECTANGLE	136	1	136
	THIRD RECTANGLE (OUTER AILERON) NOMEX WING (+Y)	RECTANGLE	137	1	137
	TAIL EDGE NOMEX WING (+Y)	POLYGON	460	10	460, 461, 462, 463, 464, 465, 466, 467, 468, 469
ELEVON:	TOTAL SURFACES = 6		TOTAL NODES = 24		
OMS	+Y OMS SEALER	DISK	60	1	60
	FIRST PARABOLOID +Y OMS	PARABOLOID	62	1	62
	OMS END CYLINDER RADIUS = 65	CYLINDER	64	1	64

TABLE I. SHUTTLE ORBITER GEOMETRY BREAKDOWN (cont'd)

<u>GENERAL AREA</u>	<u>NAME</u>	<u>TYPE</u>	<u>SURFACE NUMBER</u>	<u>NUMBER OF NODES</u>	<u>NODE NUMBER</u>
OMS	TRAPEZOID BOTTOM OF OMS END SEALER (+Y)	POLYGON	66	1	66
	FIRST TRIANGLE LEFT SIDE LOOKING BACK (+Y)	DISK	68	1	68
	LAST TRIANGLE RIGHT SIDE +Y OMS	DISK	70	1	70
	SECOND TRIANGLE LEFT SIDE	DISK	72	1	72
	THIRD TRIANGLE MIDDLE RIGHT SIDE +Y OMS	DISK	74	1	74
	TOP INSIDE TRAPEZOID +Y OMS	POLYGON	76	1	76
	-Y OMS SEALER	DISK	79	1	79
	FIRST PARABOLOID -Y OMS	PARABOLOID	82	1	82
	-Y OMS END CYLINDER	CYLINDER	84	1	84
	TRAPEZOID BOTTOM OMS END SEALER	POLYGON	86	1	86

TABLE I. SHUTTLE ORBITER GEOMETRY BREAKDOWN (cont'd)

<u>GENERAL AREA</u>	<u>NAME</u>	<u>TYPE</u>	<u>SURFACE NUMBER</u>	<u>NUMBER OF NODES</u>	<u>NODE NUMBER</u>
OMS	FIRST TRIANGLE LEFT SIDE LOOKING BACK -Y OMS	DISK	88	1	88
	LAST TRIANGLE RIGHT SIDE -Y OMS	DISK	90	1	90
	SECOND TRIANGLE LEFT SIDE -Y OMS	DISK	92	1	92
	THIRD TRIANGLE MIDDLE RIGHT SIDE -Y OMS	DISK	94	1	94
	TOP INSIDE TRAPEZOID	POLYGON	96	1	96
OMS:	TOTAL SURFACES = 18		TOTAL NODES = 18		
EVAP	REAR SONIC EVAPORATOR	DISK	879	1	879
EVAP:	TOTAL SURFACES = 1		TOTAL NODES = 1		
ENGINES	AFT RCS (-Z) 712 - FFLOW 713 - BFLOW	DISK	712	2	712, 713

TABLE I. SHUTTLE ORBITER GEOMETRY BREAKDOWN (cont'd)

<u>GENERAL AREA</u>	<u>NAME</u>	<u>TYPE</u>	<u>SURFACE NUMBER</u>	<u>NUMBER OF NODES</u>	<u>NODE NUMBER</u>
ENGINES	AFT RCS (-Y) 722 - FFLOW 723 - BFLOW	DISK	722	2	722, 723
	AFT RCS (+Z) 732 - FFLOW 733 - BFLOW	DISK	732	2	732, 733
	FRONT SCARFED RCS LOOKING 45° OFF -Z → -Y 737 - FFLOW 736 - BFLOW	DISK	736	2	736, 737
	FRONT RCS LOOKING +Z 740 - FFLOW 741 - BFLOW	DISK	740	2	740, 741
	FRONT RCS LOOKING -X 742 - FFLOW 743 - BFLOW	DISK	742	2	742, 743
	FRONT RCS LOOKING -Y 745 - FFLOW 744 - BFLOW	DISK	744	2	744, 745
	REAR -Y VCS 800 - FFLOW 801 - BFLOW	DISK	800	2	800, 801

TABLE I. SHUTTLE ORBITER GEOMETRY BREAKDOWN (cont'd)

<u>GENERAL AREA</u>	<u>NAME</u>	<u>TYPE</u>	<u>SURFACE NUMBER</u>	<u>NUMBER OF NODES</u>	<u>NODE NUMBER</u>
ENGINES	REAR -Z VCS 805 - FFLOW 806 - BFLOW	DISK	805	2	805, 806
	FRONT SCARFED VCS 837 - FFLOW 836 - BFLOW	DISK	836	2	836, 837
ENGINES:	TOTAL SURFACES = 10		TOTAL NODES = 20		

Table II. Orbiter TRASYS Input Listing

```

BCS      BODY
D        1.
S        SURFN=1, SHADE=BOTH, BSHADE=BOTH, ALPHA=0., EMISS=0.
        TRANS=-0., TRANI=-0., COM=*BAY AREA CYLINDER *
        TYPE=CYLINDER, ACTIVE=INSIDE, ALPH=93.5
        BMIN=0., BMAX=7.25000E+02, GMIN=0.
        GMAX=1.80000E+02, NNX=2, NNY=4, ICSN=-0
        POSITION=-5.07000E+02, 0., 0.
        ROTZ = -0., ROTY = 90.0000, ROTX = 0.
S        SURF=440, TYPE=RECT, ACTIVE=TOP, SHADE=BOTH, BSHADE=BOTH
        P1=218., 93.5, 0.
        P2=218., 93.5, 19.
        P3=-507., 93.5, 19.
        PROP=0., 0.
        NNX=4
        COM=* INSIDE +Y LINER STRIP*
S        SURF=445, TYPE=RECT, ACTIVE=BOTTOM, SHADE=BOTH, BSHADE=BOTH
        P1=218., -93.5, 0.
        P2=218., -93.5, 19.
        P3=-507., -93.5, 19.
        PROP=0., 0.
        NNX=4
        COM=* INSIDE -Y LINER STRIP*
S        SURFN=13, SHADE=BOTH, BSHADE=BOTH, ALPHA=-0., EMISS=-0.
        TRANS=-0., TRANI=-0., COM=* FRONT BAY AREA DISK *
        TYPE=DISC, ACTIVE=TOP, ALPH=0.
        BMIN=0., BMAX=1.02000E+02, GMIN=0.
        GMAX=3.60000E+02, NNX=1, NNY=1, ICSN=-0
        POSITION=2.18000E+02, 0., 0.
        ROTZ = -0., ROTY = -90.0000, ROTX = 0.
S        SURFN=11, SHADE=BOTH, BSHADE=BOTH, ALPHA=-0., EMISS=-0.
        TRANS=-0., TRANI=-0., COM=* END BAY AREA DISK *
        TYPE=DISC, ACTIVE=TOP, ALPH=0.
        BMIN=0., BMAX=1.02000E+02, GMIN=0.
        GMAX=3.60000E+02, NNX=1, NNY=1, ICSN=-0
        POSITION=-507., 0., 0.
        ROTZ = -0., ROTY = 90.0000, ROTX = 0.
S        SURF=20, SHADE=BOTH, BSHADE=BOTH, ALPHA=0., EMISS=0.
        TRANS=0., TRANI=0., COM=* +Y RADIATOR *
        TYPE=CYLINDER, ACTIVE=BOTH, ALPH=101.
        BMIN=0., BMAX=362.5, GMIN=00.00, GMAX=76.38
        NNX=2, NNY=2, ICSN=3
        POSITION=-165.1, 104.2, 570.
        ROTZ=-141.8, ROTY=0., ROTX=0.
S        SURF=30, SHADE=BOTH, BSHADE=BOTH, ALPHA=0., EMISS=0.
        TRANS=0., TRANI=0., COM=* -Y RADIATOR *
        TYPE=CYLINDER, ACTIVE=BOTH, ALPH=101.
        BMIN=0., BMAX=362.5, GMIN=13.62, GMAX=90.
        NNX=2, NNY=2, ICSN=3
        POSITION=165.1, 104.2, 570.
        ROTZ=-128.1, ROTY=0., ROTX=0.
S        SURFN=40, TYPE=CYL, ACTIVE=BOTH, SHADE=BOTH, BSHADE=BOTH
        P1=218., 198.51, 52.00
        P2=218., 102., 19.
        P3=218., 231.51, -44.51
        P4=-507., 231.51, -44.51
        PROP=0., 0.
        NNX=2, NNY=2
        COM=*.....+Y SIDE DOOR.....*

```

ORIGINAL PAGE IS
OF POOR QUALITY

Table II. Orbiter TRASYS Input Listing (cont'd)

```

S   SURFN= 50,TYPE=CYL,ACTIVE=BOTH,SHADE=BOTH,BSHADE=BOTH
    P1=218.,-198.51,52.00
    P2=218.,-231.51,-44.51
    P3=218.,-102.,19.
    P4=-507.,-102.,19.
    PROP=0.0,0.
    NNX=2,NNY=2
    COM=*... -Y SIDE DOOR....*
S   SURF=202,TYPE=CYL,ACTIVE=OUTSIDE,SHADE=BOTH,BSHADE=BOTH
    P1=1307.,0.,0.
    P2=1307.,-102.,0.
    P3=1307.,102.,0.
    P4=1510.,102.,0.
    ICS=34
    NNAX=2,PROP=0.,0.
    COM=* BACK BODY TOP *
S   SURF=230,TYPE=RECT,ACTIVE=BOTTOM,SHADE=BOTH,BSHADE=BOTH
    P1=-728.,-102.,-125.
    P2=-728.,102.,-125.
    P3=-711.,102.,0.0
    PROP=0.,0.
    COM=* BACK RECT 7.35DEG*
S   SURF=240,TYPE=DISC,ACTIVE=BOTH,SHADE=BOTH,BSHADE=BOTH
    DIMENSIONS=0.0,0.0,102.,90.,270.
    PROP=0.,0.
    ICSN=15
    COM=* REAR END HALF DISK*
S   SURF=250,TYPE=RECT,ACTIVE=TOP,SHADE=BOTH,BSHADE=BOTH
    P1=-728.,-102.,-125.
    P2=-728.,102.,-125.
    P3=-824.,102.,-125.
    PROP=0.,0.
    COM=* REAR FLAT PLATE OUT BACK *
S   SURF=260,TYPE=RECT,ACTIVE=TOP,SHADE=BOTH,BSHADE=BOTH
    P1=-728.,-102.,-100.
    P2=-728.,102.,-100.
    P3=-824.,102.,-125.
    PROP=0.,0.
    COM=* SLOPING REAR FLAT PLATE *
S   SURFN= 301,TYPE=RECT,BSHADE=BOTH,SHADE=BOTH,ACTIVE=TOP
    P1=218.,102.,-122.
    P2=0.,102.,-122.
    P3=0.,102.,0.
    COM=* +Y SIDE FRONT TRAPEZOID*
    PROP=0.,0.
S   SURFN= 311,TYPE=RECT,BSHADE=BOTH,SHADE=BOTH,ACTIVE=BOTTOM
    P1=218.,-102.,-122.
    P2=0.,-102.,-122.
    P3=0.,-102.,0.
    COM=* -Y SIDE FRONT TRAPEZOID*
    PROP=0.,0.
S   SURF=305,TYPE=RECT,SHADE=BOTH,BSHADE=BOTH,ACTIVE=BOTTOM
    P1=800.,102.,0.
    P2=1307.,102.,0.
    P3=1307.,102.,-122.
    PROP=0.,0.,ICS=34,NNX=2
    COM=* +Y SIDE PANNEL*
S   SURF=315,TYPE=RECT,SHADE=BOTH,BSHADE=BOTH,ACTIVE=TOP
    P1=800.,-102.,0.
    P2=1307.,-102.,0.
    P3=1307.,-102.,-122.
    PROP=0.,0.,ICS=34,NNX=2
    COM=* -Y SIDE PANNEL*
S   SURF=307,TYPE=RECT,ACTIVE=BOTTOM,SHADE=BOTH,BSHADE=BOTH

```

Table II. Orbiter TRASYS Input Listing (cont'd)

```

P1=1307.,-102.,0.
P2=1510.,-102.,0.
P3=1510.,-102.,-122.
ICSN=34
PROP=0.,0.
COM=* REAR PORT BACK,SIDE*
S   SURF=317,TYPE=RECT,ACTIVE=TOP,SHADE=BOTH,BSHADE=BOTH
    P1=1307.,102.,0.
    P2=1510.,102.,0.
    P3=1510.,102.,-122.
    PROP=0.,0.
    ICSN=34
COM=*REAR STBD BACK,SIDE*
S   SURF=420,TYPE=TRAP,ACTIVE=TOP,SHADE=BOTH,BSHADE=BOTH
    P1=-709.,102.,0.
    P2=-709.,102.,-125.
    P3=-728.,102.,-125.
    P4=-711.,102.,0.
    PROP=0.,0.
COM=** Y REAR TAPER*
S   SURF=425,TYPE=TRAP,ACTIVE=BOTTOM,SHADE=BOTH,BSHADE=BOTH
    P1=-709.,-102.,0.
    P2=-709.,-102.,-125.
    P3=-728.,-102.,-125.
    P4=-711.,-102.,0.
    PROP=0.,0.
COM= * - Y. REAR SIDE TAPER...*
BCS CREW
S   SURF=160,TYPE=PARAB,ACTIVE=OUTSIDE,SHADE=BOTH,BSHADE=BOTH
    P1=269.,0.0,-60.
    P2=269.,0.0,-22.
    P3=269.,0.0,-22.
    P4=235.,0.0,-60. SAPEX OF PARABOLA,MAJOR RADIUS=38IN.
    PROP=0.,0.
    ICSN=34
COM=* NOSE *
S   SURF=162,TYPE=POLY,ACTIVE=TOP,SHADE=BOTH,BSHADE=BOTH
    P1=269.,0.,-22.
    P2=437.0,0.,41.
    P3=510.,-101.,41.
    PROP=0.,0.
    ICSN=34
COM=* -Y TOP TRIANGLE NOSE *
S   SURF=161,TYPE=POLY,ACTIVE=BOTTOM,SHADE=BOTH,BSHADE=BOTH
    P1=269.,0.,-22.
    P2=437.0,0.,41.
    P3=510.,+101.,41.
    PROP=0.,0.
COM=* +Y TOP TRIANGLE NOSE *
S   SURF=163,TYPE=POLY,ACTIVE=TOP,SHADE=BOTH,BSHADE=BOTH
    P1=269.,0.,-22.
    P2=269.,-25.,-30.
    P3=510.,-101.,41.
    PROP=0.,0.
    ICSN=34
COM=* -Y SIDE TRI(1ST) NOSE *
S   SURF=164,TYPE=POLY,ACTIVE=BOTTOM,SHADE=BOTH,BSHADE=BOTH
    P1=269.,0.,-22.
    P2=269.,+25.,-30.
    P3=510.,+101.,41.
    PROP=0.,0.
    ICSN=34
COM=**Y SIDE TRI(1ST) NOSE *

```

Table II. Orbiter TRASYS Input Listing (cont'd)

```

S   SURF=165,TYPE=POLY,ACTIVE=TOP,SHADE=BOTH,BSHADE=BOTH
    P1=269.,-25.,-30.
    P2=269.,-38.,-60.
    P3=510.,-101.,41.
    PROP=0.,0.
    COM=*-Y SIDE TRI(2ND)(DOWN) NOSE *
    ICSN=34
S   SURF=166,TYPE=POLY,ACTIVE=BOTTOM,SHADE=BOTH,BSHADE=BOTH
    P1=269.,+25.,-30.
    P2=269.,+38.,-60.
    P3=510.,+101.,41.
    PROP=0.,0.
    ICSN=34
    COM=* +Y SIDE TRI(2ND) NOSE *
S   SURF=167,TYPE=POLY,ACTIVE=TOP,SHADE=BOTH,BSHADE=BOTH
    P1=269.,-38.,-60.
    P2=510.,-102.,60.
    P3=510.,-102.,41.
    PROP=0.,0.
    ICSN=34
    COM=* -Y SIDE TRI(3RD) NOSE *
S   SURF=168,TYPE=POLY,ACTIVE=BOTTOM,SHADE=BOTH,BSHADE=BOTH
    P1=269.,38.,-60.
    P2=510.,102.,-60.
    P3=510.,101.,41.
    PROP=0.,0.
    ICSN=34
    COM=* +Y SIDE TRI(3RD) NOSE *
S   SURF=169,TYPE=TRAP,ACTIVE=BOTTOM,SHADE=BOTH,BSHADE=BOTH
    P1=269.,-38.,-60.
    P2=510.,-102.,-60.
    P3=510.,-102.,-122.
    P4=269.,-38.,-75.
    PROP=0.,0.
    ICSN=34
    COM=* -Y SIDE TRAP NOSE *
S   SURF=171,TYPE=POLY,ACTIVE=TOP,SHADE=BOTH,BSHADE=BOTH
    P1=510.,-102.,-122.
    P2=269.,-38.,-75.
    P3=269.,-20.,-98.
    PROP=0.,0.
    ICSN=34
    COM=* -Y SIDE TRI NOSE BOTTOM*
S   SURF=170,TYPE=TRAP,ACTIVE=TOP,SHADE=BOTH,BSHADE=BOTH
    P1=269.,38.,-60.
    P2=510.,+102.,-60.
    P3=510.,+102.,-122.
    P4=269.,38.,-75.
    PROP=0.,0.
    ICSN=34
    COM=*+Y SIDE TRAP NOSE *
S   SURF=172,TYPE=POLY,ACTIVE=BOTTOM,SHADE=BOTH,BSHADE=BOTH
    P1=510.,+102.,-122.
    P2=269.,38.,-75.
    P3=269.,20.,-98.
    PROP=0.,0.
    ICSN=34
    COM=*+Y SIDE TRI NOSE BOTTOM *
S   SURF=174,TYPE=CYL,ACTIVE=OUTSIDE,SHADE=BOTH,BSHADE=BOTH
    P1=510.,0.,0.
    P2=510.,-102.,19.
    P3=510.,102.,19.
    P4=582.,102.,19.
    PROP=0.,0.
    ICSN=34
    COM=* CYLINDER HOOD NOSE *

```

Table II. Orbiter TRASYS Input Listing (cont'd)

S SURF=175,TYPE=RECT,ACTIVE=TOP,SHADE=BOTH,BSHADE=BOTH
P1=510.,-102.,19.
P2=510.,-102.,-122.
P3=582.,-102.,-122.
PROP=0.,0.
ICSN=34
COM=* RECT BELOW SURF 174 SIDE(-Y) HOOD NOSE *

S SURF=177,TYPE=RECT,ACTIVE=BOTTOM,SHADE=BOTH,BSHADE=BOTH
P1=510.,102.,19.
P2=510.,102.,-122.
P3=582.,102.,-122.
PROP=0.,0.
ICSN=34
COM=* RECT BELOW SURF 174 SIDE(+Y) HOOD NOSE *

S SURF=180,TYPE=SPHERE,ACTIVE=OUTSIDE,BSHADE=BOTH,SHADE=BOTH
DIMENSIONS=102.,40.,70.,10.,170.
TX=522.2,TY=0.,TZ=0.0
ROTX=0.,ROTY=0.,ROTZ=-270.
PROP=0.,0.
NNAX=6
ICSN=34
COM=* WINDOW SPHERE SECITON ORIGIN=TX,TY,TZ*

S SURF=190,TYPE=SPHERE,ACTIVE=OUTSIDE,BSHADE=BOTH,SHADE=BOTH
DIMENSIONS=102.,70.,102.,0.,180.
ICSN=34
TX=522.2,TY=0.,TZ=0.
ROTX=0.,ROTY=0.,ROTZ=-270.
PROP=0.,0.
COM=* LID SPHERE SECITON ORIGIN=TX,TY,TZ*

BCS
S TAIL
SURF=399,TYPE=CYL,ACTIVE=OUTSIDE,BSHADE=BOTH,SHADE=BOTH
P1=1312.,0.0,121.5
P2=1312.,-3.0,121.5
P3=1312.,3.0,121.5
P4=1591.,3.0,416.0
ICSN=34
PROP=0.,0.
COM=* LEADING EDGE TAIL FIN X=1312,1594,HGT=316*

S SURF=380,TYPE=POLY,ACTIVE=TOP,BSHADE=BOTH,SHADE=BOTH
P1=1594.,00.,416.
P2=1312.,-3.,121.5
P3=1425.,-17.5,121.5
PROP=0.,0.
ICSN=34
COM=* FROM BEG TO REAR 1ST PLOY -Y SIDE*

S SURF=382,TYPE=POLY,ACTIVE=TOP,SHADE=BOTH,BSHADE=BOTH
P1=1594.,0.0,416.
P2=1425.,-17.5,121.5
P3=1653.,-7.5,416.
PROP=0.,0.
ICSN=34
COM=* 2ND POLY -Y SIDE *

S SURF=384,TYPE=POLY,ACTIVE=TOP,BSHADE=BOTH,SHADE=BOTH
P1=1653.,-7.5,416.
P2=1463.,-15.,170.
P3=1575.,0.0,170.
PROP=0.,0.
ICSN=34
COM=* 3RD POLY -Y SIDE TAIL *

Table II. Orbiter TRASYS Input Listing (cont'd)

S SURF=386,TYPE=POLY,ACTIVE=TOP,BSADE=BOTH,SHADE=BOTH
P1=1653.,-7.5,416.
P2=1575.,0.0,170.
P3=1702.,0.0,416.
PROP=0.,0.
ICSN=34
COM=*4TH POLY -Y SIDE TAIL *

S SURF=388,TYPE=POLY,ACTIVE=TOP,BSHADE=BOTH,SHADE=BOTH
P1=1425.,-17.5,121.5
P2=1575.,0.0,170.
P3=1463.,-15.,170.
PROP=0.,0.
ICSN=34
COM=* 5 POLY BENEATH 386 TAIL*

S SURF=390,TYPE=POLY,ACTIVE=TOP,SHADE=BOTH,BSHADE=BOTH
P1=1425.,-17.5,121.5
P2=1470.,-17.5,121.5
P3=1575.,0.0,170.
PROP=0.,0.
ICSN=34
COM=* 6TH POLY BENEATH 388 TAIL*

S SURF=392,TYPE=RECT,ACTIVE=BOTH,SHADE=BOTH,BSHADE=BOTH
P1=1312.,0.0,121.5
P2=1312.,0.0,102.
P3=1470.,0.0,102.
PROP=0.,0.
ICSN=34
COM=* BOTTOM RECT TAIL *

S SURF=381,TYPE=POLY,ACTIVE=BOTTOM,SHADE=BOTH,BSHADE=BOTH
P1=1594.,00.,416.
P2=1312.,+3.,121.5
P3=1425.,+17.5,121.5
PROP=0.,0.
ICSN=34
COM=* FROM BEG TO REAR 1ST POLY -Y SIDE)

S SURF=383,TYPE=POLY,ACTIVE=BOTTOM,SHADE=BOTH,BSHADE=BOTH
P1=1594.,0.0,416.
P2=1425.,+17.5,121.5
P3=1653.,7.5,416.
PROP=0.,0.
ICSN=34
COM=* 2ND POLY -Y SIDE *

S SURF=385,TYPE=POLY,ACTIVE=BOTTOM,BSHADE=BOTH,SHADE=BOTH
P1=1653.,7.5,416.
P2=1463.,+15.,170.
P3=1575.,0.0,170.
PROP=0.,0.
ICSN=34
COM=* 3RD POLY -Y SIDED TAIL *

S SURF=387,TYPE=POLY,ACTIVE=BOTTOM,BSADE=BOTH,SHADE=BOTH
P1=1653.,7.5,416.
P2=1575.,+0.0,170.
P3=1702.,0.0,416.
PROP=0.,0.
ICSN=34
COM=*4TH POLY -Y SIDE TAIL *

S SURF=389,TYPE=POLY,ACTIVE=BOTTOM,SHADE=BOTH,BSHADE=BOTH
P1=1425.,+17.5,121.5
P2=1575.,0.0,170.
P3=1463.,+15.,170.
PROP=0.,0.
ICSN=34
COM=* 5 POLY BENEATH 386 TAIL*

S SURF=391,TYPE=POLY,ACTIVE=BOTTOM,SHADE=BOTH,BSHADE=BOTH
P1=1425.,17.5,121.5
P2=1470.,17.5,121.5

Table II. Orbiter TRASYS Input Listing (cont'd)

```

P3=1575.,0.0,170.
PROP=0.,0.
ICSN=34
COM=* 6TH POLY BENEATH 388 TAIL*
BCS
S EVAP
SURF=877,TYPE=DISC,ACTIVE=BOTTOM,SHADE=BOTH,BSHADE=BOTH
P1=-704.,-103.,-95.
P2=-704.,-103.,-98.
P3=-707.,-103.,-95.
P4=-707.,-103.,-95.
PROP=0.,0.
COM=* SONIC EVAP REAR (LUBERT) + -Y 305 **
S SURF=879,TYPE=DISC,ACTIVE=TOP,SHADE=BOTH,BSHADE=BOTH
P1=-704.,103.,-95.
P2=-704.,103.,-98.
P3=-707.,103.,-95.
P4=-707.,103.,-95.
PROP=0.,0.
COM=* SONIC EVAP REAR (LUBERT) + +Y 305 **
BCS
S WING
SURF=100,TYPE=TRAP,ACTIVE=BOTTOM,SHADE=BOTH,BSHADE=BOTH
P1=-103.,0.,-62.1
P4=-103.,0.,-62.1
P3=-224.,105.,-58.
P2=-224.,0.,-58.0
PROP=0.,0.
ICSN=20
COM=* +Y 1ST TRIANGLE NOMEX WING *
S SURF=102,TYPE=RECT,ACTIVE=BOTTOM,SHADE=BOTH,BSHADE=BOTH
P1=-224.,0.,-58.
P2=-504.,0.,-90.
P3=-504.,105.,-90.
PROP=0.,0.
ICSN=20
COM=* +Y 1ST RECT NOMEX WING *
S SURF=104,TYPE=RECT,ACTIVE=BOTTOM,SHADE=BOTH,BSHADE=BOTH
P1=-590.34,0.,-99.9
P2=-590.34,105.,-99.9
P3=-504.,105.,-90.
PROP=0.,0.
COM=* +Y 2ND RECT(TWRD-X) NOMEX WING *
ICSN=20
C
S SURF=110,TYPE=TRAP,ACTIVE=BOTTOM,SHADE=BOTH,BSHADE=BOTH
P1=-504.,105.,-90.
P4=-504.,105.,-90.
P2=-504.,319.,-90.
P3=-287.,105.,-68.16
PROP=0.,0.
ICSN=20
COM=* +Y TRI ABOVE SURF102 NOMEX WING *
S SURF=117,TYPE=POLY,ACTIVE=TOP,SHADE=BOTH,BSHADE=BOTH
P1=-287.,105.,-68.16
P4=-504.,319.,-90.
P3=-504.,342.,-90.
P2=-239.5,105.,-64.03
PROP=0.,0.
ICSN=20
COM=* +Y INSERT IN WING TILE WING *

```

Table II. Orbiter TRASYS Input Listing (cont'd)

```

S   SURF=121,TYPE=POLY,ACTIVE=TOP,SHADE=BOTH,BSHADE=BOTH
    P1=-239.5,105.,-64.03
    P4=-504.,342.5,-90.
    P3=-504.,366.,-90.
    P2=-224.,105.,-58.
    PROP=0.,0.
    ICSN=20
    COM=* +Y   OUTER WING STRIP CARBON WING *
S   SURF=112,TYPE=RECT,ACTIVE=BOTTOM,SHADE=BOTH,BSHADE=BOTH
    P1=-504.00,105.,-90.
    P2=-590.34,105.,-99.9
    P3=-590.34,328.,-99.9
    ICSN=20
    PROP=0.,0.
    COM=* +Y LONG BACK RECT NOMEX WING *
S   SURF=119,TYPE=RECT,ACTIVE=BOTTOM,SHADE=BOTH,BSHADE=BOTH
    P1=-504.,328.,-90.
    P2=-590.34,328.,-99.9
    P3=-590.34,366.,-99.9
    ICSN=20
    PROP=0.,0.
    COM=**+Y SHORT BACK RECT ON BOTTOM OF 112 TILE WING *
S   SURF=115,TYPE=TRAP,ACTIVE=BOTTOM,SHADE=BOTH,BSHADE=BOTH
    P1=263.9,0.,-78.7
    P4=263.9,0.,-78.7
    P2=-103.,0.,-62.1
    P3=-224.,105.,-58.
    PROP=0.,0.
    ICSN=20
    COM=* +Y FORWARD TRIANGLE TILE WING *
S   SURF=130,TYPE=TRAP,ACTIVE=TOP,SHADE=BOTH,BSHADE=BOTH
    P1=-103.,0.,-62.1
    P4=-103.,0.,-62.1
    P3=-224.,-105.,-58.0
    P2=-224.,0.,-58.0
    PROP=0.,0.
    ICSN=21
    COM=**-Y 1ST TRIANGLE NOMEX WING *
S   SURF=132,TYPE=RECT,ACTIVE=TOP,SHADE=BOTH,BSHADE=BOTH
    P1=-224.,0.,-58.
    P2=-504.,0.,-90.
    P3=-504.,-105.,-90.
    PROP=0.,0.
    ICSN=21
    COM=**-Y 1ST RECT NOMEX WING. *
S   SURF=134,TYPE=RECT,ACTIVE=TOP,SHADE=BOTH,BSHADE=BOTH
    P1=-590.34,0.,-99.9
    P2=-590.34,-105.,-99.9
    P3=-504.,-105.,-90.
    PROP=0.,0.
    COM=* -Y 2ND RECT(TWRD-X) NOMEX WING *
    ICSN=21
S   SURF=140,TYPE=TRAP,ACTIVE=TOP,SHADE=BOTH,BSHADE=BOTH
    P1=-504.,-105.,-90.
    P4=-504.,-105.,-90.
    P2=-504.,-319.,-90.
    P3=-287.,-105.,-68.16
    PROP=0.,0.
    ICSN=21
    COM= * -Y TRI ABOVE SURF 132 NOMEX WING *

```

Table II. Orbiter TRASYS Input Listing (cont'd)

```

S   SURF=147,TYPE=POLY,ACTIVE=BOTTOM,SHADE=BOTH,BSHADE=BOTH
    P1=-287.,-105.,-68.16
    P4=-504.,-319.,-90.
    P3=-504.,-342.,-90.
    P2=-239.5,-105.,-64.03
    PROP=0.,0.
    ICSN=21
    COM=* -Y          INSERT IN WING TILE WING *
S   SURF=151,TYPE=POLY,ACTIVE=BOTTOM,SHADE=BOTH,BSHADE=BOTH
    P1=-239.5,-105.,-64.03
    P4=-504.,-342.5,-90.
    P3=-504.,-366.,-90.
    P2=-224.,-105.,-58.
    PROP=0.,0.
    ICSN=21
    COM=* -Y          OUTER WING STRIP CARBON WING *
S   SURF=142,TYPE=RECT,ACTIVE=TOP,SHADE=BOTH,BSHADE=BOTH
    P1=-504.00,-105.,-90.
    P2=-590.34,-105.,-99.9
    P3=-590.34,-328.,-99.9
    ICSN=21
    PROP=0.,0.
    COM=* -Y LONG BACK RECT NOMEMX WING *
S   SURF=149,TYPE=RECT,ACTIVE=TOP,SHADE=BOTH,BSHADE=BOTH
    P1=-504.,-328.,-90.
    P2=-590.34,-328.,-99.9
    P3=-590.34,-366.,-99.9
    PROP=0.,0.
    ICSN=21
    COM=* -Y SHORT BACK RECT ON TOPE OF 142 TILE WING *
S   SURF=145,TYPE=TRAP,ACTIVE=TOP,SHADE=BOTH,BSHADE=BOTH
    P1=263.9,0.,-78.7
    P4=263.9,0.,-78.7
    P2=-103.,0.,-62.1
    P3=-224.,-105.,-58.
    PROP=0.,0.
    ICSN=21
    COM=* -Y FORWARD TRIANGLE      TILE WING *
C
BCS
S   ELEVON
    SURF=106,TYPE=RECT,ACTIVE=BOTTOM,BSHADE=BOTH,SHADE=BOTH
    P1=-644.,6.,-106.56
    P2=-644.,105.,-106.56
    P3=-590.34,105.,-99.9
    PROP=0.,0.
    ICSN=20
    COM=* +Y 3RD RECT(INNER ALERION) NOMEMX WING *
S   SURF=107,TYPE=RECT,ACTIVE=TOP,BSHADE=BOTH,SHADE=BOTH
    P1=-644.,105.,-106.56
    P2=-590.,105.,-99.9
    P3=-590.34,366.,-99.9
    PROP=0.,0.
    ICSN=20
    COM=* +Y 3RD RECT(OUTER ALERION) NOMEMX WING *
S   SURF=450,TYPE=POLY,ACTIVE=BOTTOM,SHADE=BOTH,BSHADE=BOTH
    P3=-707.,6.,-116.0
    P1=-644.,366.,-106.56
    P2=-644.,6.,-106.56
    PROP=0.,0.,NNY=10
    ICSN=20
    COM=* +Y WING TAIL EDGE NOMEMX WING *

```

Table II. Orbiter TRASYS Input Listing (cont'd)

```

S   SURF=136,TYPE=RECT,ACTIVE=TOP,BSHADE=BOTH,SHADE=BOTH
    P1=-644.,-6.,-106.56
    P2=-644.,-105.,-106.56
    P3=-590.34,-105.,-99.9
    PROP=0.,0.
    ICSN=21
    COM=* -Y 3RD RECT(INNER ALERION) NOMEX WING *
S   SURF=137,TYPE=RECT,ACTIVE=BOTTOM,BSHADE=BOTH,SHADE=BOTH
    P1=-644.,-105.,-106.56
    P2=-590.,-105.,-99.9
    P3=-590.,-366.,-99.9
    PROP=0.,0.
    ICSN=21
    COM=* -Y 3RD RECT(OUTER ALERION) NOMEX WING *
S   SURF=460,TYPE=POLY,ACTIVE=TOP,SHADE=BOTH,BSHADE=BOTH
    P3=-707.,-6.,-116.0
    P1=-644.,-366.,-106.56
    P2=-644.,-6.,-106.56
    PROP=0.,0.,NNY=10
    ICSN=21
BCS OMS
S   SURF=60,TYPE=DISC,ACTIVE=OUT,SHADE=BOTH,BSHADE=BOTH
    DIMENSIONS=0.0,0.0,25.,125.,335.
    PROP=0.,0.
    ICSN=1!
    COM = * ...-Y OWS SEALER ...*
S   SURF=62,TYPE=PARAB,ACTIVE=OUTSIDE,SHADE=BOTH,BSHADE=BOTH
    DIMENSIONS=22.5,7.,40.,25.,238.
    POSITION=-500.,-78.14,65.56
    ROTX=180.,ROTY=-90.,ROTZ=0.
    PROP=0.,0.
    ICS=25
    COM=* 1ST PARAB -Y OMS *
S   SURF=64,TYPE=CYLINDER,ACTIVE=OUTSIDE,SHADE=BOTH,BSHADE=BOTH
    DIMENSIONS=60.,40.,210.,25.,238.
    POSITION=-500.,-78.14,65.56
    ROTX=180.,ROTY=-90.,ROTZ=0.
    PROP=0.,0.
    COM=* OMS END CYLINDER RADIUS=65.*
    ICS=25
S   SURF=66,TYPE=POLY,ACTIVE=TOP,SHADE=BOTH,BSHADE=BOTH
    P1=-710.,-140.,40.
    P2=-710.,-50.,130.
    P3=-710.,-23.75,112.
    P4=-710.,-120.,17.5
    PROP=0.,0.
    COM=*TRAP BOTTOM OMS END SEALER -Y *
    ICSN=25
S   SURF=68,TYPE=DISC,ACTIVE=BOTTOM,SHADE=BOTH,BSHADE=BOTH
    P1=-710.,-111.88,67.5
    P2=-710.,-141.25,95.
    P3=-710.,-150.625,58.75
    P4=-710.,-140.,40.
    PROP=0.,0.
    COM=*1ST TRIANGLE LT SIDE LOOKING BACK -Y *
    ICSN=25
S   SURF=70,TYPE=DISC,ACTIVE=BOTTOM,BSHADE=BOTH,SHADE=BOTH
    P1=-710.,-82.5,71.25
    P2=-710.,-13.75,68.75
    P3=-710.,-50.,131.25
    P4=-710.,-78.75,138.13
    PROP=0.,0.
    COM=*LAST TRI RT SIDE -Y OMS *
    ICS=25

```

Table II. Orbiter TRASYS Input Listing (cont'd)

```

S      SURF=72,TYPE=DISC,ACTIVE=BOTTOM,BSHADE=BOTH,SHADE=BOTH
      P1=-710.,-96.88,68.75
      P2=-710.,-135.,27.
      P3=-710.,-150.,56.88
      P4=-710.,-137.5,105.
      PROP=0.,0.
      ICSN=25
      COM=*2ND TRI LEFT SIDE*
S      SURF=74,TYPE=DISC,ACTIVE=TOP,SHADE=BOTH,BSHADE=BOTH
      P1=-710.,-81.25,84.38
      P2=-710.,-43.13,124.375
      P3=-710.,-76.875,138.75
      P4=-710.,-120.625,121.875
      PROP=0.,0.
      ICSN=25
      COM=*3RD TRI MIDDLE RT SIDE -Y OMS *
S      SURF=76,TYPE=POLY,ACTIVE=TOP,SHADE=BOTH,BSHADE=BOTH
      P1=-710.,-96.88,68.75
      P2=-710.,-140.0,105.
      P3=-710.,-120.625,121.875
      P4=-710.,-81.25,84.38
      PROP=0.,0.
      ICSN=25
      COM=*TOP INSIDE TRAP -Y OMS *
S      SURF=80,TYPE=DISC,ACTIVE=OUT,SHADE=BOTH,BSHADE=BOTH
      DIMENSIONS=0.0,0.0,25.,25.,235.
      PROP=0.,0.
      ICSN=12
      COM=* ..+Y OWS SEALER ...*
S      SURF=82,TYPE=PARAB,ACTIVE=OUTSIDE,SHADE=BOTH,BSHADE=BOTH
      DIMENSIONS=22.5,7.,40.,-56.,156.
      PROP=0.,0.
      POSITION=-500.,78.14,65.56
      ROTX=0.,ROTY=-90.,ROTZ=0.
      ICS=25
      COM=* 1ST PARAB +Y OMS*
S      SURF=84,TYPE=CYLINDER,ACTIVE=OUTSIDE,SHADE=BOTH,BSHADE=BOTH
      DIMENSIONS=60.,40.,210.,-56.,156.
      POSITION=-500.,78.14,65.56
      ROTX=0.,ROTY=-90.,ROTZ=0.
      PROP=0.,0.
      ICS=25
      COM=* +Y OMS END CYLINDER *
S      SURF=86,TYPE=POLY,ACTIVE=BOTTOM,SHADE=BOTH,BSHADE=BOTH
      P1=-710.,140.,40.
      P2=-710.,50.,130.
      P3=-710.,23.75,112.
      P4=-710.,120.,17.5
      PROP=0.,0.
      COM=*TRAP BOTTOM OMS END SEALER *
      ICSN=25
S      SURF=88,TYPE=DISC,ACTIVE=TOP,SHADE=BOTH,BSHADE=BOTH
      P1=-710.,111.88,67.5
      P2=-710.,141.25,95.
      P3=-710.,150.625,58.75
      P4=-710.,140.,40.
      PROP=0.,0.
      COM=*1ST TRIANGLE LT SIDE LOOKING BACK +Y OMS *
      ICSN=25
S      SURF=90,TYPE=DISC,ACTIVE=TOP,BSHADE=BOTH,SHADE=BOTH
      P1=-710.,82.5,71.25
      P2=-710.,13.75,68.75

```

Table II. Orbiter TRASYS Input Listing (cont'd)

```

P3=-710.,50.,131.25
P4=-710.,78.75,138.13
PROP=0.,0.
COM=*LAST TRI RT SIDE +Y OMS *
ICS=25
S SURF=92,TYPE=DISC,ACTIVE=TOP,BSHADE=BOTH,SHADE=BOTH
P1=-710.,96.88,68.75
P2=-710.,135.,27.
P3=-710.,150.,56.88
P4=-710.,137.5,105.
PROP=0.,0.
ICSN=25
COM=*2ND TRI LEFT SIDE +Y OMS *
S SURF=94,TYPE=DISC,ACTIVE=BOTTOM,SHADE=BOTH,BSHADE=BOTH
P1=-710.,81.25,84.38
P2=-710.,43.13,124.375
P3=-710.,76.875,138.75
P4=-710.,120.625,121.875
PROP=0.,0.
ICSN=25
COM=*3RD TRI MIDDLE RT SIDE +Y OMS *
S SURF=96,TYPE=POLY,ACTIVE=BOTTOM,SHADE=BOTH,BSHADE=BOTH
P1=-710.,96.88,68.75
P2=-710.,140.0,105.
P3=-710.,120.625,121.875
P4=-710.,81.25,84.38
PROP=0.,0.
ICSN=25
COM=*TOP INSIDE TRAP *
BCS ENGF
S SURFN=736,TYPE=DISC,ACTIVE=BOTH,SHADE=BOTH,BSHADE=BOTH
P1=467.0,60.5,-46.5
P2=470.0,60.5,-46.5
P3=467.0,62.62,-44.38
P4=467.0,62.62,-44.38
PROP=0.,0.
COM=*... FRONT RCS..LOOKING +/-Y AT 45 DEG. (116) 2/26/76*
S SURFN=738,TYPE=DISC,ACTIVE=BOTH,SHADE=BOTH,BSHADE=BOTH
P1=467.0,-60.5,-46.5
P2=470.0,-60.5,-46.5
P3=467.0,-62.62,-44.38
P4=467.0,-62.62,-44.38
PROP=0.,0.
COM=*...FRONT RCS..LOOKING +/-Y(-YSIDE) 45 DEG. (136)*
S SURFN=740,TYPE=DISC,ACTIVE=BOTH,SHADE=BOTH,BSHADE=BOTH
P1=450.0,0.,12.
P2=450.0,3.,12.
P3=453.0,0.,12.
P4=453.0,0.,12.
PROP=0.,0.
COM=*...FRONT RCS..LOOKING +/-Z ... (125) *
S SURFN=742,TYPE=DISC,ACTIVE=BOTH,SHADE=BOTH,BSHADE=BOTH
P1=468.,0.,6.
P2=468.,0.,3.
P3=468.,3.,6.
P4=468.,3.,6.
PROP=0.,0.
COM=*...FRONT RCS..LOOKING +/-X ... (122) *
S SURFN=744,TYPE=DISC,ACTIVE=BOTH,SHADE=BOTH,BSHADE=BOTH
P1=440.,47.,-20.
P2=437.,47.,-20.
P3=440.,47.,-17.
P4=440.,47.,-17.
PROP=0.,0.
COM=*...FRONT RCS..LOOKING +/-Y .+Y SIDE*

```

Table II. Orbiter TRASYS Input Listing (cont'd)

```

S      SURFN=746,TYPE=DISC,ACTIVE=BOTH,SHADE=BOTH,BSHADE=BOTH
      P1=440.,-47.,-20.
      P2=437.,-47.,-20.
      P3=440.,-47.,-17.
      P4=440.,-47.,-17.
      PROP=0.,0.
      COM=*. . .FRONT RCS..LOOKING +/-Y .-Y SIDE*
BCS   ENGR
S      SURF=710,TYPE=DISC,ACTIVE=BOTH,BSHADE=BOTH,SHADE=BOTH
      DIMENSIONS=0.,0.,3.,0.,360.
      PROP=0.,0.
      ICSN=26
      COM=* -Z 1ST RCS X=1519.75 *
S      SURF=712,TYPE=DISC,ACTIVE=BOTH,BSHADE=BOTH,SHADE=BOTH
      DIMENSIONS=0.,0.,3.,0.,360.
      ICSN=27
      PROP=0.,0.
      COM=* -Z 2ND RCS X=1532.875 *
S      SURF=714,TYPE=DISC,ACTIVE=BOTH,BSHADE=BOTH,SHADE=BOTH
      DIMENSIONS=0.,0.,3.,0.,360.
      ICSN=28
      PROP=0.,0.
      COM=* -Z 3RD RCS X=1545.375 *
S      SURF=720,TYPE=DISC,ACTIVE=BOTH,BSHADE=BOTH,SHADE=BOTH
      P1=-716.,148.75,59.000
      P2=-716.,148.75,62.000
      P3=-719.,148.75,59.000
      P4=-719.,148.75,59.000
      PROP=0.,0.
      COM=* +Y 1ST RCS X=1516. *
S      SURF=722,TYPE=DISC,ACTIVE=BOTH,BSHADE=BOTH,SHADE=BOTH
      P1=-729.,148.75,59.000
      P2=-729.,148.75,62.000
      P3=-732.,148.75,59.000
      P4=-732.,148.75,59.000
      PROP=0.,0.
      COM=* +Y 2ND RCS X=1529. *
S      SURF=724,TYPE=DISC,ACTIVE=BOTH,BSHADE=BOTH,SHADE=BOTH
      P1=-742.,148.75,59.000
      P2=-742.,148.75,62.000
      P3=-745.,148.75,59.000
      P4=-745.,148.75,59.000
      PROP=0.,0.
      COM=* +Y 3RD RCS X=1545. *
S      SURF=726,TYPE=DISC,ACTIVE=BOTH,BSHADE=BOTH,SHADE=BOTH
      P1=-755.,148.75,59.000
      P2=-755.,148.75,62.000
      P3=-758.,148.75,59.000
      P4=-758.,148.75,59.000
      PROP=0.,0.
      COM=* +Y 4TH RC X=1555. *
S      SURF=730,TYPE=DISC,ACTIVE=BOTH,BSHADE=BOTH,SHADE=BOTH
      P1=-716.,132.50,96.5
      P2=-716.,135.50,96.5
      P3=-719.,132.50,96.5
      P4=-719.,132.50,96.5
      PROP=0.,0.
      COM=* +Z 1ST RCS X=1516. *
S      SURF=732,TYPE=DISC,ACTIVE=BOTH,BSHADE=BOTH,SHADE=BOTH
      P1=-729.,132.50,96.5
      P2=-729.,135.50,96.5
      P3=-732.,132.50,96.5
      P4=-732.,132.50,96.5
      PROP=0.,0.
      COM=* +Z 2ND RCS X=1529. *

```

Table II. Orbiter TRASYS Input Listing (cont'd)

```
S      SURFN=902,TYPE=DISC,ACTIVE=BOTH,BSHADE=BOTH,SHADE=BOTH
      DIMENSIONS=0.,0.,22.5,0.,360.
      ICSN=17,PROP=0.,0.
      COM=*.....SUPER ENGINES (OMS LOCATION)..-Y...*
BCS    ENGS
S      SURF=910,TYPE=PARAB,ACTIVE=OUT,SHADE=BOTH,BSHADE=BOTH
      DIMENSIONS=4.4,0.0,100.,0.,360.
      ICSN=13
      PROP=0.,0.
      NNX=2,NNY=2
      COM=* TOP ENGIN *
S      SURF=915,TYPE=PARAB,ACTIVE= OUT,SHADE=BOTH,BSHADE=BOTH
      DIMENSIONS=4.4,0.0,100.,0.,360.
      ICSN=14,TY=+50.
      PROP=0.,0.
      NNX=2,NNY=2
      COM = * + Y ENGIN *
S      SURF=920,TYPE=PARAB,ACTIVE=OUT,SHADE=BOTH,BSHADE=BOTH
      DIMENSIONS=4.4,0.0,100.,0.,360.
      ICSN = 14, TY =-50.
      PROP=0.,0.
      NNX=2,NNY=2
      COM = * -Y ENGIN...*
```

The Orbiter surfaces have been grouped by surface type (i.e., LRSI, HRSI, etc.) and by surface area location (i.e., wings, payload bay, etc.). This was done so that distinct surfaces could be analyzed in their role as far as contributing to the contamination environment.

Figure 14 shows the types of surfaces on the Shuttle Orbiter along with a listing of the surface type data printed out by the contamination model. In a similar manner, Figure 15 shows the location of surface groups (location) used in the model along with a description of the node numbers. This type of information will aid the user in understanding and the evaluation of the contribution of surface types or areas to a specific contamination problem.

3.1.3 Source Characteristics - The characteristics of the Orbiter sources included in the model are presented in this section. Table III summarizes the mass flow rate and properties of the effluents from each surface type source that is pertinent to the modeling. Outgassing, early desorption (offgassing) and leakage are all treated as cosine emitters with respect to the surface normal. For these sources, a viewfactor (or configuration factor, etc) determined from the TRASYS program is required to determine the mass flux at another surface or a point in space. The 100°C column for outgassing and early desorption is the \dot{m}_0 that is input to the model as the rate at 100°C. The associated 25°C column demonstrates how low the rate is at ambient temperatures. For outgassing, the rate at 25°C was calculated using the expression

$$\dot{m}_{25}^{\circ\text{C}} = \dot{m}_0 e^{\frac{25 - 100}{29}}$$

The early desorption rate at 25°C is calculated by assuming an activation energy of 7.5 Kcal/mole for desorption. The rate is then compared to the rate at 100°C and is ratioed such that

$$\frac{\dot{m}_{25}^{\circ\text{C}}}{\dot{m}_0} = \frac{A e^{-E/RT}}{A e^{-E/RT}} = e^{\frac{7500}{R} \left(\frac{1}{373} - \frac{1}{298} \right)},$$

so that

$$\dot{m}_{25}^{\circ\text{C}} = \dot{m}_0 e^{\frac{7500}{R} \left(\frac{1}{373} - \frac{1}{298} \right)}$$

for early desorption. The velocities of the surface source molecules are calculated to be the most probable thermal velocity and

ORIGINAL PAGE IS
OF POOR QUALITY

3-66

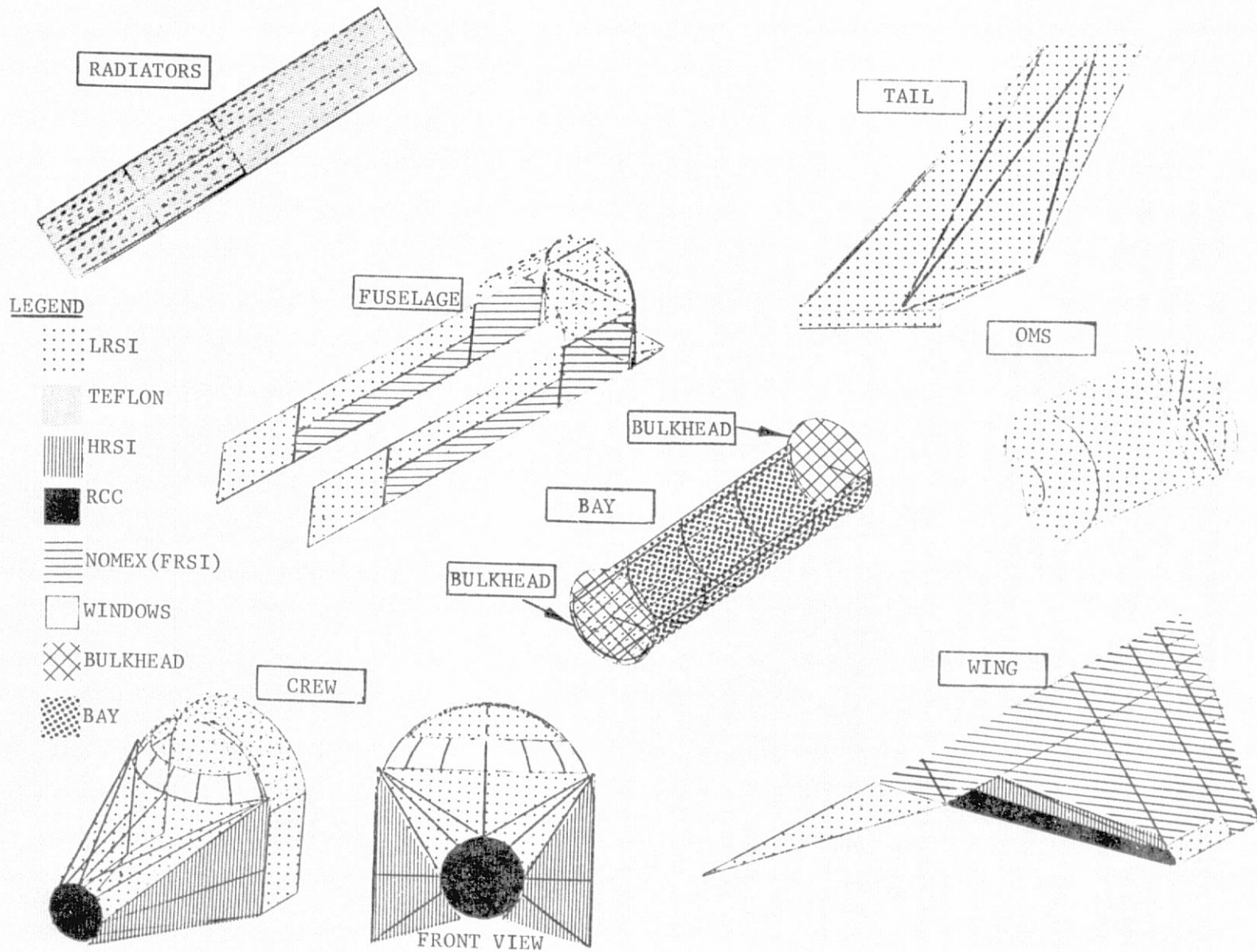


Figure 14. Location of Surface Types Modeled on Shuttle Orbiter

REPORT NO. 3 *** SAMPLE CASE NO. 9 SHUTTLE ORBITER ALL SOURCES (EXCLUDING ENGS)
 CONTENTS: LIST OF SOURCES TO BE EVALUATED

* * * SURFACES * * *

SEQUENCE NO.	IDENT NO.	SECTION	MATERIAL	AREA (SQ IN)
1	20	RADOOR	TEFLON	12200.
2	22	RADOOR	TEFLON	12200.
3	24	RADOOR	TEFLON	12200.
4	26	RADOOR	TEFLON	12200.
5	30	RADOOR	TEFLON	12200.
6	32	RADOOR	TEFLON	12200.
7	34	RADOOR	TEFLON	12200.
8	36	RADOOR	TEFLON	12200.
9	40	RADOOR	TEFLON	25580.
10	42	RADOOR	TEFLON	25560.
11	44	RADOOR	TEFLON	25580.
12	46	RADOOR	TEFLON	25580.
13	50	RADOOR	TEFLON	25580.
14	52	RADOOR	TEFLON	25580.
15	54	RADOOR	TEFLON	25580.
16	56	RADOOR	TEFLON	24990.
17	21	FUSLAG	LRSI	12200.
18	23	FUSLAG	LRSI	12200.
19	25	FUSLAG	LRSI	12200.
20	27	FUSLAG	LRSI	12200.
21	31	FUSLAG	LRSI	12200.
22	33	FUSLAG	LRSI	12200.
23	35	FUSLAG	LRSI	12200.
24	37	FUSLAG	LRSI	12200.
25	41	FUSLAG	LRSI	25580.
26	43	FUSLAG	LRSI	25580.
27	45	FUSLAG	LRSI	25580.
28	47	FUSLAG	LRSI	25580.
29	51	FUSLAG	LRSI	24990.
30	53	FUSLAG	LRSI	24990.
31	55	FUSLAG	LRSI	24990.
32	57	FUSLAG	LRSI	24900.
33	202	FUSLAG	LRSI	32520.
34	203	FUSLAG	LRSI	32520.
35	230	FUSLAG	LRSI	25730.
36	240	FUSLAG	LRSI	16340.
37	241	FUSLAG	LRSI	16340.
38	250	FUSLAG	LRSI	19580.
39	260	FUSLAG	LRSI	20240.
40	301	FUSLAG	LRSI	26600.
41	305	FUSLAG	LRSI	30930.
42	306	FUSLAG	NOMEX	30930.
43	307	FUSLAG	NOMEX	24770.
44	311	FUSLAG	LRSI	26600.
45	315	FUSLAG	LRSI	30930.
46	316	FUSLAG	NOMEX	30930.
47	317	FUSLAG	NOMEX	24770.
48	420	FUSLAG	LRSI	1312.
49	425	FUSLAG	LRSI	1312.
50	60	OMS	LRSI	1145.
51	62	OMS	LRSI	7850.

Figure 14. Location of Surface Types Modeled on Shuttle Orbiter (cont'd)

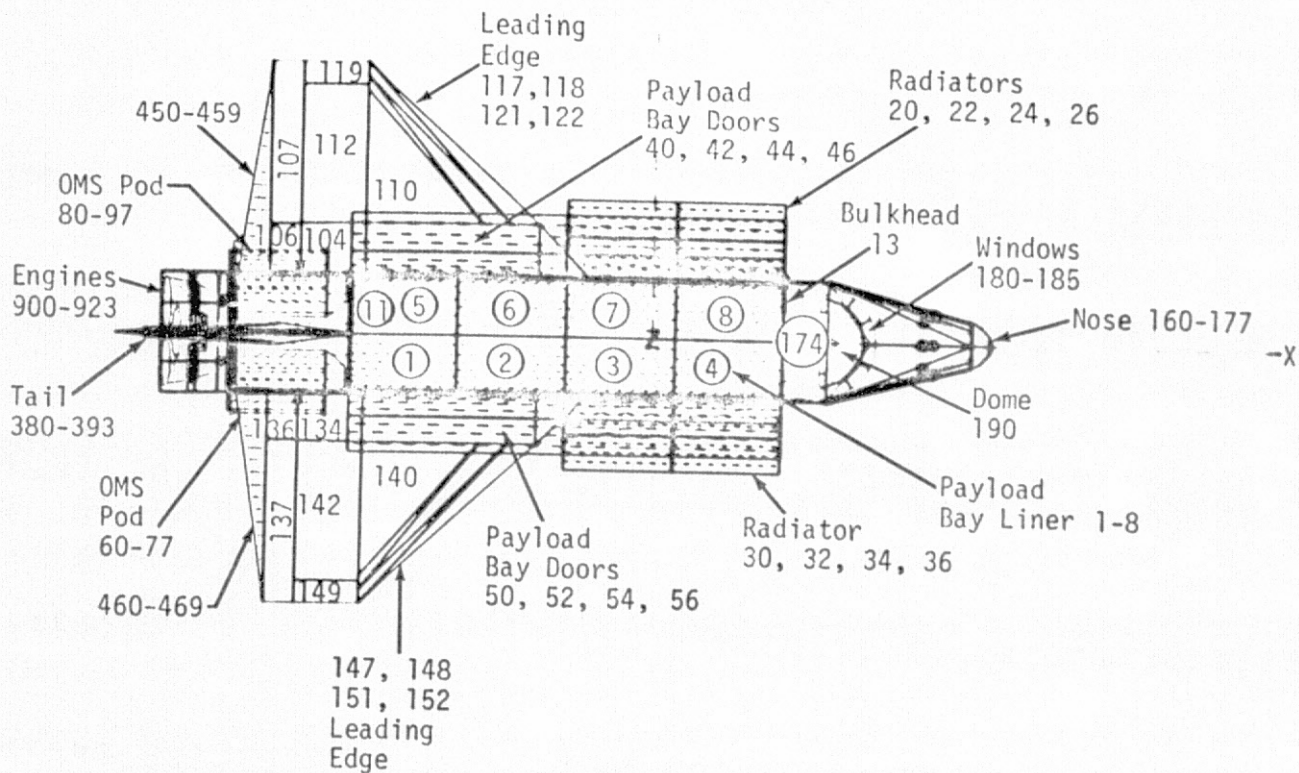
Sequence No.	Ident No.	Section	Material	Area (sq in)
52	64	OMS	LRSI	37920.
53	66	OMS	LRSI	1991.
54	67	OMS	LRSI	2028.
55	68	OMS	LRSI	415.
56	70	OMS	LRSI	895.
57	72	OMS	LRSI	1406.
58	74	OMS	LRSI	1312.
59	76	OMS	LRSI	715.
60	77	OMS	LRSI	600.
61	80	OMS	LRSI	1145.
62	82	OMS	LRSI	7813.
63	84	OMS	LRSI	37740.
64	86	OMS	LRSI	1991.
65	87	OMS	LRSI	2028.
66	88	OMS	LRSI	415.
67	90	OMS	LRSI	895.
68	92	OMS	LRSI	1406.
69	94	OMS	LRSI	1312.
70	96	OMS	LRSI	715.
71	97	OMS	LRSI	601.
72	100	WING	NOMEX	6356.
73	102	WING	NOMEX	29590.
74	104	WING	NOMEX	9125.
75	110	WING	NOMEX	23340.
76	112	WING	NOMEX	19380.
77	115	WING	LRSI	19280.
78	117	WING	HRSI	5650.
79	118	WING	HRSI	2508.
80	119	WING	LRSI	3302.
81	121	WING	RCC	2251.
82	122	WING	RCC	3123.
83	130	WING	NOMEX	6356.
84	132	WING	NOMEX	29590.
85	134	WING	NOMEX	9125.
86	140	WING	NOMEX	23340.
87	142	WING	NOMEX	19380.
88	145	WING	LRSI	19280.
89	147	WING	HRSI	5650.
90	148	WING	HRSI	2508.
91	149	WING	LRSI	3302.
92	151	WING	RCC	2251.
93	152	WING	RCC	3123.
94	106	ELEVON	NOMEX	6499.
95	107	ELEVON	NOMEX	17210.
96	136	ELEVON	NOMEX	6499.
97	137	ELEVON	NOMEX	9125.
98	450	ELEVON	NOMEX	138.
99	451	ELEVON	NOMEX	415.
100	452	ELEVON	NOMEX	692.
101	453	ELEVON	NOMEX	960.
102	454	ELEVON	NOMEX	1246.
103	455	ELEVON	NOMEX	1523.
104	456	ELEVON	NOMEX	1800.
105	457	ELEVON	NOMEX	2076.
106	458	ELEVON	NOMEX	2353.
107	459	ELEVON	NOMEX	2630.
108	460	ELEVON	NOMEX	138.
109	461	ELEVON	NOMEX	415.
110	462	ELEVON	NOMEX	692.
111	463	ELEVON	NOMEX	969.
112	464	ELEVON	NOMEX	1246.
113	465	ELEVON	NOMEX	1523.
114	466	ELEVON	NOMEX	1800.

Figure 14. Location of Surface Types Modeled on Shuttle Orbiter (cont'd)

Sequence No.	Ident No.	Section	Material	Area (sq in)
115	467	ELEVON	NOMEX	2076.
116	468	ELEVON	NOMEX	2353.
117	469	ELEVON	NOMEX	2630.
118	160	CREW	RCC	7191.
119	161	CREW	LRSI	9348.
120	162	CREW	LRSI	9348.
121	163	CREW	LRSI	3380.
122	164	CREW	LRSI	3380.
123	165	CREW	LRSI	4253.
124	166	CREW	LRSI	4253.
125	167	CREW	HRSI	12590.
126	168	CREW	HRSI	12590.
127	169	CREW	HRSI	9600.
128	170	CREW	HRSI	9600.
129	171	CREW	HRSI	3705.
130	172	CREW	HRSI	3705.
131	174	CREW	LRSI	20720.
132	175	CREW	LRSI	10150.
133	177	CREW	LRSI	10150.
134	180	CREW	WINDOW	1424.
135	181	CREW	WINDOW	1424.
136	182	CREW	WINDOW	1424.
137	183	CREW	WINDOW	1424.
138	184	CREW	WINDOW	1424.
139	185	CREW	WINDOW	1424.
140	190	CREW	LRSI	10250.
141	380	TAIL	LRSI	16920.
142	381	TAIL	LRSI	16920.
143	382	TAIL	LRSI	8833.
144	383	TAIL	LRSI	8833.
145	384	TAIL	LRSI	13940.
146	385	TAIL	LRSI	13940.
147	386	TAIL	LRSI	6116.
148	387	TAIL	LRSI	6116.
149	388	TAIL	LRSI	2744.
150	389	TAIL	LRSI	2744.
151	390	TAIL	LRSI	1160.
152	391	TAIL	LRSI	1160.
153	392	TAIL	LRSI	3081.
154	393	TAIL	LRSI	3081.
155	399	TAIL	HRSI	3823.
156	1	BAY	LINER	26620.
157	2	BAY	LINER	26620.
158	3	BAY	LINER	26620.
159	4	BAY	LINER	26620.
160	5	BAY	LINER	26620.
161	6	BAY	LINER	26620.
162	7	BAY	LINER	26620.
163	8	BAY	LINER	26620.
164	11	BAY	BLKHED	32690.
165	13	BAY	BLKHED	32690.
166	440	BAY	LINER	3444.
167	441	BAY	LINER	3444.
168	442	BAY	LINER	3444.
169	443	BAY	LINER	3444.
170	444	BAY	LINER	3444.
171	445	BAY	LINER	3444.
172	447	BAY	LINER	3444.
173	448	BAY	LINER	3444.
174	13	BAYL	CRACKS	32690.

Figure 14. Location of Surface Types Modeled on Shuttle Orbiter (cont'd)

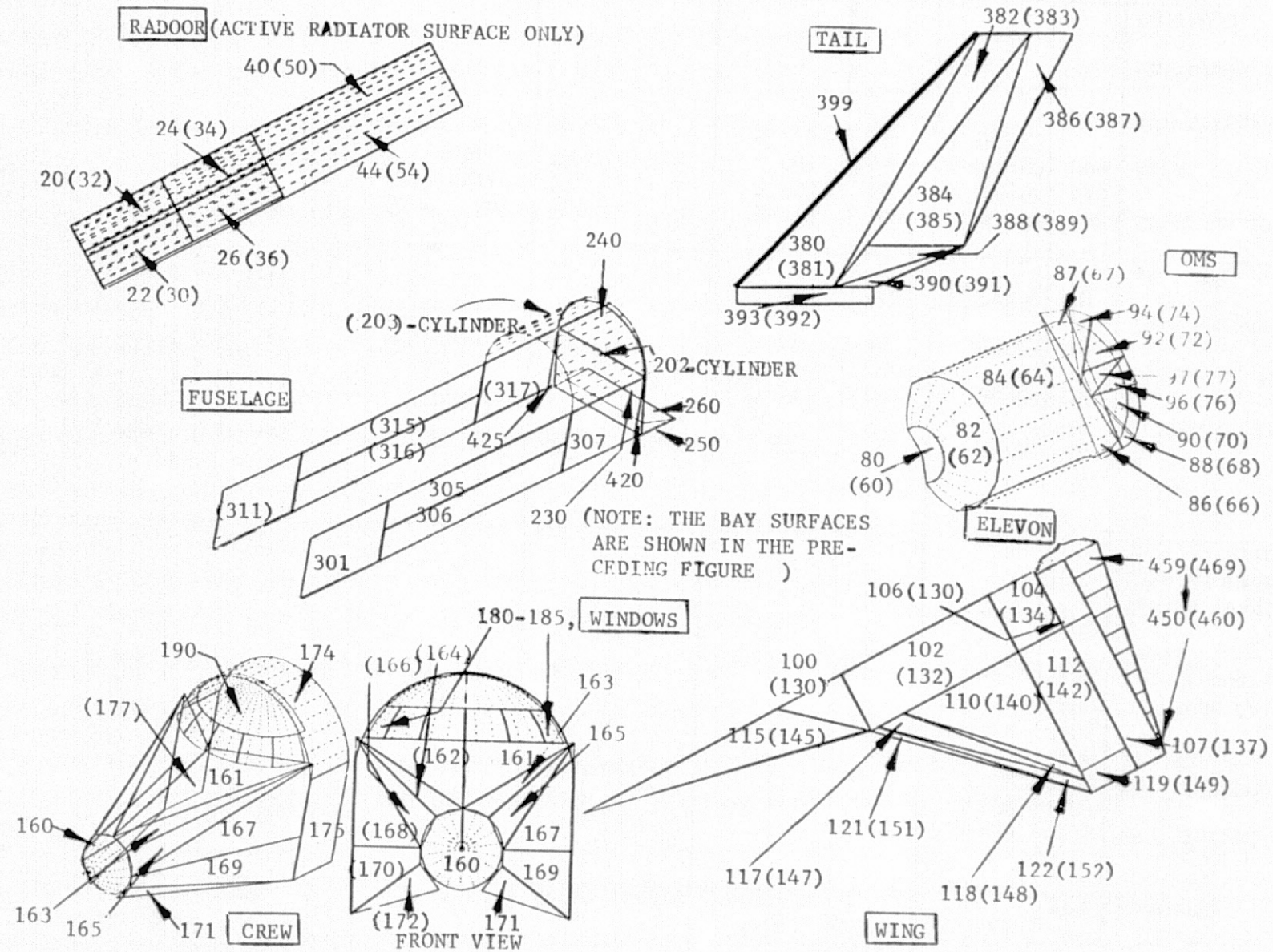
-Y



3-70

ORIGINAL PAGE IS
OF POOR QUALITY

Figure 15. Location of Surface Groups Modeled on Shuttle Orbiter



3-71

Figure 15. Location of Surface Groups Modeled on Shuttle Orbiter (cont'd)

Table III. Major Surface Source Characteristics

Source	Area cm ²	Mass Loss Rate @ 100°C g/cm/s	Mass Loss Rate @ 25°C g/cm/s	Constituents	Mole Fraction	Mole- cular Weight	Mole- cular Diameter cm	τ Hrs	Comments
<u>Outgassing</u>									
Nomex	* 3.0E6	1.24E-09	9.34E-11	Unreacted	1	100	7.8E-08	4100	HRSI Tested at MSEC FRSI (DC92007) Tested at JSC Bulkhead Calculated From Properties of TG-15000 Teflon (Radiators) Es- timated From HRSI Configuration
RCC	3.8E5	1.00E-12	7.53E-14		1	100	7.8E-08	4100	
HRSI	4.8E6	5.20E-10	3.92E-11	Monomers,	1	100	7.8E-08	4100	
LRSI	2.8E6	5.10E-10	3.84E-11		1	100	7.8E-08	4100	
TEFLON	1.3E6	5.00E-10	3.77E-11	Polymer	1	100	7.8E-08	4100	
LINER	1.3E6	7.90E-11	5.95E-12		1	100	7.8E-08	4100	
BULKHEAD	3.3E5	1.00E-09	7.53E-11	Chain Fragments	1	100 100	7.8E-08	4100	
<u>Early Desorption</u>									
Nomex	3.0E6	1.24E-08	9.70E-10	H ₂ O	0.57	18	3.25E-08	18	Estimated to Be Factor of 10 Larger Than Outgassing Rate at 100°C
RCC	3.8E5	1.00E-11	7.82E-13					18	
HRSI	4.8E6	5.20E-09	4.07E-10	N ₂	0.23	28	4.13E-08	18	
LRSI	2.8E6	5.10E-09	3.09E-10					18	
TEFLON	1.3E6	5.00E-09	3.91E-10	CO ₂	0.12	44	4.49E-08	18	
LINER	1.3E6	7.90E-10	6.18E-11					18	
BULKHEAD	3.3E5	1.00E-08	7.82E-10	O ₂	0.08	32	3.85E-08	18	
Cabin At- mosphere Leakage	2.1E5	1.70E-07	Same - Not Influenced By Temper- ature	H ₂ O N ₂ CO ₂ O ₂	0.016 0.758 0.007 0.219	18 28 44 32	3.24E-08 4.13E-08 4.48E-08 3.85E-08	Con- inu- ous	Based on Spec Leak Rates of 3.18 kg/day - All Allowed to Leak Uniformly From Fwd Bulkhead

*3.0E6 = 3 x 10⁶

is expressed as

$$V = 129 \sqrt{\frac{T}{M}}, \text{ m/s,}$$

where ;

T = temperature of surface, °K, and

M = molecular weight.

For the leakage surface source, the temperature used to calculate the velocity is 297°K and corresponds to the crew atmosphere temperature.

Table IV is a table for the point sources used in the model. The plume functions for these sources represent the flux in g/cm²/s at a point a distance r (cm) away and at an angle θ (degrees) off of the plume centerline.

The evaporator flow rates in Table IV represents the flow rate for both nozzles. However, the plume function equations pertain to one nozzle and represent the actual maximum flow rate from the nozzle during operation.

The VCS and RCS engines have been given number descriptors that correlate to the new engine numbering scheme used by Rockwell. For example, the Rockwell scheme uses a 3 digit number. If the number begins with one, it is in the forward nose portion of the vehicle. If it begins with 2, it is in the aft on the left side and a 3 indicates it is aft on the right side. There are a total of 38 RCS, 870 pound engines, shown in Figure 16 and six vernier 25 pound thrust engines. The model numbering scheme uses a seven in front of the Rockwell 3 digit number for the RCS and an 8 for the VCS. Therefore, to access a particular RCS engine in the model a seven should precede the number shown in Figure 16. The VCS engine numbers and location are shown in Table IV.

Table IV. VCS Engine Location Data

<u>Location</u>	<u>Number</u>
Forward Left Side, Down (FLD)	8116
Forward Right Side, Down (FRD)	8136
Aft Left Side, Down (ALD)	8257
Aft Left Side, Side Facing (ALS)	8258
Aft Right Side, Down (ARD)	8357
Aft Right Side, Side Facing (ARS)	8358

Table V. Major Point Source Parameters

Source	Flow Rate	Plume Function g/cm ² /s	Constituents	Mole Fraction	Molecular Weight	Molecular Diameter	Frequency
Evaporator	13.6kg/hr Total Nominal Average - 31.7 kg/hr Total Max. Instantaneous	$\psi_1 = \frac{4.47}{r^2} [\cos (1.01 \theta)]^6$ $0^\circ \leq \theta \leq 36.8^\circ$ $\psi_2 = \frac{1.14}{r^2} e^{-0.0773 (\theta-36.8^\circ)}$ $36.8^\circ < \theta \leq 148^\circ$ $\psi_3 = \frac{1.14}{r^2} e^{-8.6}, 143^\circ < \theta \leq 180^\circ$	H ₂ O	1.0	18	*3.24E-08	Continuous Nominal 100 ms Pulses at 4.3 Hz
Evaporator (Sonic) Baseline Model Plume Function	13.6kg/hr Total Nominal Average - 31.7 kg/hr Total Max. Instantaneous	$\psi_1 = \frac{1.93 \cos^6 (0.608\theta)}{r^2}$ $0^\circ \leq \theta \leq 148^\circ$ $\psi_2 = 0$ $148^\circ < \theta \leq 180^\circ$	H ₂ O	1.0	18	3.24E-08	Continuous Nominal 100 ms Pulses at 4.3 Hz

*3.24E-08 = 3.24 x 10⁻⁸

Table V. Major Point Source Parameters (cont'd)

Source	Flow Rate	Plume Function g/cm ² /s	Constituents	Mole Fraction	Molecular Weight	Molecular Diameter	Frequency
Vernier Control System (VCS) Engines	40.8 g/s per engine	$\psi_1 = \frac{23.2}{r^2} \cos\left(\frac{\pi}{2} \cdot \frac{\theta}{115^\circ}\right)^{8.65}$ $0 \leq \theta < 40^\circ$ $\psi_2 = \frac{5.81}{r^2} e^{-0.0467(\theta-40^\circ)}$ $40^\circ \leq \theta \leq 140^\circ$ $\psi_3 = \frac{5.81}{r^2} e^{-4.67}$ $140^\circ < \theta \leq 180^\circ$	H ₂ O N CO O CO H H NO	0.328 0.306 0.036 0.0004 0.134 0.17 0.015 0.001	18 28 44 32 28 2 1 30	*3.24E-08 4.13E-08 4.49E-08 3.85E-08 4.03E-08 3.33E-08 2.64E-08 3.90E-08	Frequency Depends On Dead-band, Altitude and Attitude
Reaction Control System (RCS) Engines	1420 g/s per engine	$\psi_1 = \frac{1353.3}{r^2} \cos\left(\frac{\pi}{2} \cdot \frac{\theta}{125^\circ}\right)^{10}$ $0 \leq \theta \leq 64^\circ$ $\psi_2 = \frac{35.0}{r^2} e^{-0.035(\theta-64^\circ)}$ $64^\circ \leq \theta \leq 180^\circ$	Same as VCS	Same as VCS	Same as VCS	Same as VCS	As Required

*3.24E-08 = 3.24 x 10⁻⁸

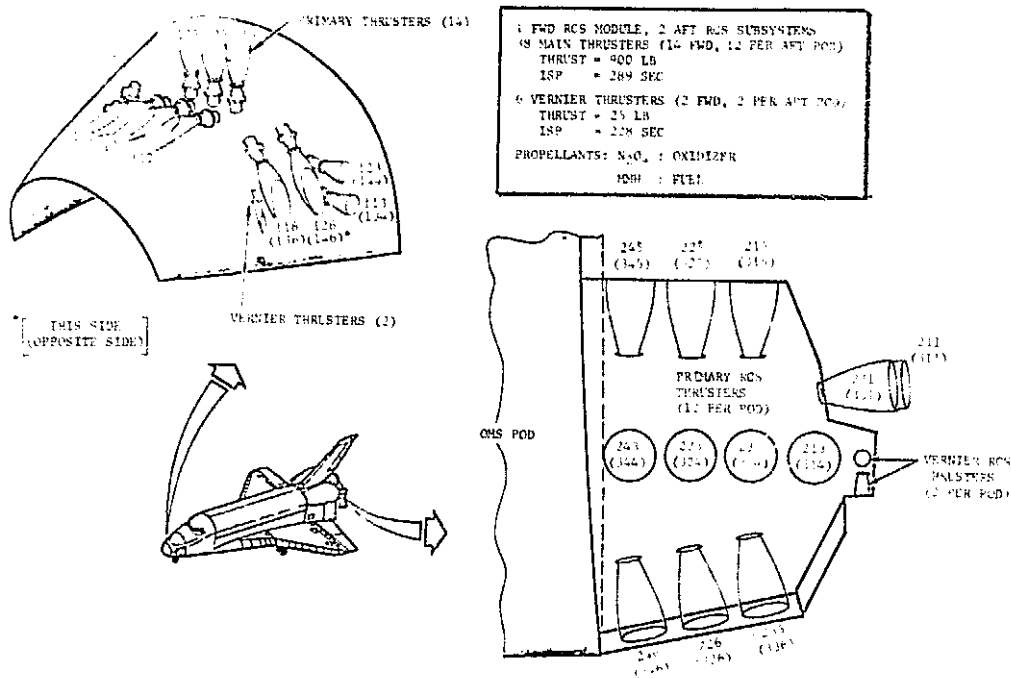


Figure 16. RCS Engine Location Using the Rockwell Numbering System (Adapted from "Shuttle Documentation Data Base", RI, August 1975)

The location of the evaporator in the model presently is $X_0 = 1505.6$, $Y_0 = \pm 127.1$ (mold line) and $Z_0 = 305$. The evaporator vent plume centerlines are parallel to the Y axis.

Of the sources presented above, several will require updating in the near future. The evaporator test for the new evaporator design should yield a new plume function and information on particulates. Presently, particles have not been addressed by the model. Programs do exist to model the trajectory of emitted particles but the program requires knowledge of emission directions, velocities and particle sizes.

The outgassing source characteristics should be updated as test data becomes available. It is recommended the form of the mathematical expressions be similar to those discussed in subsection 3.1.1.1 of this report.

Engine plume distributions and particle content of the effluent should be updated when or if data becomes available through testing. Testing planned at AEDC on scaled down bipropellant engines are

planned to be correlated to the CONTAM Program. If this data can be extrapolated to 25 pound and 870 pound bipropellant engines, it should be included in the model.

3.1.4 Lines-of-Sight - The upper hemisphere region of the Shuttle Orbiter is the volume through which the largest majority of all payloads will view. Because of light scatter from Shuttle Orbiter surfaces, the actual viewing is restricted to near 60 degrees off of the Z axis. In order to accommodate the volume of this 120 degree cone centered about the Z axis, 17 lines-of-sight have been predetermined to establish the baseline density profile. These lines-of-sight originated at $X_0 = 1107$, $Y_0 = 0$ and $Z_0 = 507$.

There is a total of 16 points along each line-of-sight at which densities are calculated. They are spaced at increments of 5 meters up to 50 meters and then at 75, 100, 150, 200 and 300 meters. The 17 lines-of-sight are:

- 0 degrees, along the Z axis,
- 30 degrees off Z towards \pm Y,
- 30 degrees off Z towards \pm X,
- 60 degrees off Z towards \pm Y,
- 60 degrees off Z towards \pm X,
- 30 degrees off Z towards \pm Y and 45 degrees towards +X,
- 60 degrees off Z towards \pm Y and 45 degrees towards +X,
- 30 degrees off Z towards \pm Y and 45 degrees towards -X and
- 60 degrees off Z towards \pm Y and 45 degrees towards -X.

Even though there are precalculated viewfactors from the Shuttle Orbiter to all points in the above lines-of-sight, an option exists to use a $1/r^2$ variation wherever the user desires anywhere along the 300 meter extent of the line-of-sight. This option was created since it was observed that in many cases the viewfactors decrease simply as $1/r^2$ beyond 150 meters,

This option decreases the computer run time required to calculate the contributions from all sources to a point. For example, if the density has been calculated at points out to 100 meters the program can be instructed to calculate the density at the remaining points by considering a $1/r^2$ dependence before integrating the mass column density.

The option also exists that any other origin and direction can be requested for a line-of-sight. The program automatically interpolates from all points of the 17 baseline lines-of-sight that are near a point on the requested line-of-sight. This option will

allow trade studies to be performed for payload susceptibilities as a function of position in the payload bay and viewing direction.

As mentioned previously, the density at each point along a line-of-sight from each source is calculated in units of grams or molecules per cm^3 . By integrating this density as a function of the distance from the origin to the 300 meter point, the mass or molecular column density is calculated. The column density is the area under the curve of a plot of density versus distance from the vehicle. It corresponds to the mass per unit area that is within the field-of-view of a sensor or instrument.

3.1.5 Sample Output Format - The model has been developed with a multitude of options available to the user. The options allow increased fidelity where desired and parameters to be changed that cover a range of potential inputs. In this way, the model becomes an effective tool in evaluating missions and performing trade studies.

There is a baseline output that the program "defaults" to. If no options are exercised, the program will automatically print out the early desorption and outgassing maximums for the zero line-of-sight. The output includes the mass and number column density of the surface types contribution and surface area contribution and the corresponding return flux due to ambient atmosphere scattering at 400 km. Figures 17 and 18 illustrates the output format. Figure 17 shows the contribution from outgassing molecules and the contribution by species for early desorption. A summary section on the far right of the figure includes the percent that each area or surface type is of the total contribution. Figure 18 is an identical output for return flux to a 0.19 steradian surface.

The output options are summarized in Table VI. The term "report number" is used to indicate the option that is chosen. For example, Figure 17 is report number 35, while Figure 18 is report number 43. These report numbers allow printout of selective sets of data that can be used for detailed analysis, trade studies, record keeping or an understanding of portions of the program.

3.1.6 Model Delivery and Checkout - At the end of the first 12 month period of this total 15 month contract, two contamination model subroutines were delivered to JSC. These were the surface source routine and the point source routine. The surface source routine included outgassing, early desorption (offgassing) and cabin leakage. The point source routine included the flash evaporator and the VCS and RCS engines. These programs were checked out

CONTENTS: SUMMARY *** MASS/NUMBER COLUMN DENSITIES ***

LINE-OF-SIGHT NO. = 7
 THETA (DEG) = 60.0
 PHI (DEG) = 90.0

*** LISTED BY MATERIALS *** (CONT)

SECTION SUMMARY	SPECIES NUMBER COLUMN DENSITY (MOLECULES/CM**2)					EARLY DESORPTION (GM/CM**2) (MOLECULES/CM**2)	OUT GASSING	TOTAL	% OF TOTAL
	OUTG1 O2	OUTG2 CO	H2O H2	N2 H	CO2 MMHNO3				
LINER	.32E+10	0.	.18E+11	.91E+10	.59E+10	.16E-11	.54E-12	.21E-11	
TEFLON	.33E+10	0.	0.	0.	0.	.37E+11	.32E+10	.40E+11	11.9
NOMEX	.40E+10	0.	.23E+11	.11E+11	.73E+10	.19E-11	.66E-12	.26E-11	
LRSI	.14E+11	0.	.79E+11	.40E+11	.26E+11	.45E+11	.40E+10	.49E+11	14.7
HRSI	.14E+11	0.	0.	0.	0.	.68E-11	.23E+11	.81E-11	
RCC	.15E+10	0.	.86E+10	.43E+10	.28E+10	.16E+12	.14E+11	.17E+12	51.6
BLKHED	.15E+10	0.	0.	0.	0.	.74E-12	.25E-12	.99E-12	
CRACKS	.69E+09	0.	.39E+10	.20E+10	.13E+10	.17E+11	.15E+10	.19E+11	5.6
TOTAL	.71E+09	0.	0.	0.	0.	.34E-12	.11E-12	.45E-12	
	.86E+06	0.	.49E+07	.24E+07	.16E+07	.79E+10	.69E+09	.86E+10	2.6
	.87E+06	0.	0.	0.	0.	.42E-15	.14E-15	.56E-15	
	.31E+10	0.	.18E+11	.90E+10	.58E+10	.98E+07	.86E+06	.11E+08	.0
	.32E+10	0.	0.	0.	0.	.15E-11	.52E-12	.21E-11	
	0.	0.	.47E+08	.28E+10	.30E+10	.36E+11	.31E+10	.39E+11	11.7
	.81E+09	0.	0.	0.	0.	.39E-12	0.	.39E-12	
	.25E+11	0.	.15E+12	.78E+11	.52E+11	.67E+10	0.	.67E+10	2.0
	.28E+11	0.	0.	0.	0.	.13E-10	.44E-11	.18E-10	
						.31E+12	.26E+11	.33E+12	100.0

3-79

ORIGINAL PAGE IS
 OF POOR QUALITY

Figure 17. Baseline Column Density Output of Contamination Model

CONTENTS: SUMMARY RETURN FLUX AT 400.0 KM ALTITUDE

CRITICAL SURFACE NO. = 8
FIELD-CF-VIEW = .190

*** LISTED BY MATERIAL TYPE *** (CONT)

SECTION SUMMARY	SPECIES RETURN FLUX (MOLECULES/CM**2)					EARLY DESORPTION (GM/CM**2) (MOLECULES/CM**2)	OUT GASSING (MOLECULES/CM**2)	TOTAL	% OF TOTAL
	OUTG1	OUTG2	H2O	N2	CO2				
	O2	CO	H2	H	MMHNO3				
LINER	.90E+09	0.	.12E+10	.76E+09	.54E+09	.12E-12	.15E-12	.27E-12	
TEFLON	.25E+09	0.	0.	0.	0.	.27E+10	.90E+09	.36E+10	5.2
NOMEX	.48E+10	0.	.54E+10	.42E+10	.30E+10	.67E-12	.80E-12	.15E-11	28.5
LRSI	.14E+10	0.	0.	0.	0.	.15E+11	.48E+10	.20E+11	
HRSI	.73E+10	0.	.97E+10	.63E+10	.45E+10	.10E-11	.12E-11	.22E-11	43.2
RCC	.21E+10	0.	0.	0.	0.	.23E+11	.73E+10	.30E+11	
BLKHED	.20E+10	0.	.27E+10	.17E+10	.12E+10	.28E-12	.33E-12	.61E-12	11.9
CRACKS	.57E+09	0.	0.	0.	0.	.62E+10	.20E+10	.82E+10	
TOTAL	.79E+09	0.	.10E+10	.68E+09	.48E+09	.11E-12	.13E-12	.24E-12	4.6
	.22E+09	0.	0.	0.	0.	.24E+10	.79E+09	.32E+10	
	.43E+06	0.	.57E+06	.37E+06	.26E+06	.60E-16	.71E-16	.13E-15	.0
	.12E+06	0.	0.	0.	0.	.13E+07	.43E+06	.18E+07	
	.90E+09	0.	.12E+10	.78E+09	.55E+09	.13E-12	.15E-12	.27E-12	5.3
	.26E+09	0.	0.	0.	0.	.28E+10	.90E+09	.37E+10	
	0.	0.	.49E+07	.38E+09	.45E+09	.56E-13	0.	.56E-13	1.3
	.10E+09	0.	0.	0.	0.	.93E+09	0.	.93E+09	
TOTAL	.17E+11	0.	.22E+11	.15E+11	.11E+11	.24E-11	.28E-11	.52E-11	100.0
	.49E+10	0.	0.	0.	0.	.53E+11	.17E+11	.69E+11	

3-80

Figure 18. Baseline Return Flux Output of Contamination Model

Table VI. User Output Options

<u>Report No.</u>	<u>Contents</u>
01	Listing of Input Control Parameters
02	Preset List of Surfaces, Engines and Vents
03	List of Sources to Be Evaluated
04	List of Changes to Preset Contaminant Sources
05	List of Mass Loss Rate Coefficients to Be Used
06	Modified List of Mass Loss Rate Coefficients
07	List of Surface Temperatures That Will Be Used
08	List of Mission Data That Will Be used
09	List of Mass Transport Factor Data - Surface to Points
10	List of Mass Transport Factor Data - Surface to Surface
11	Physical Characteristics of Surface Sources
12	Surface Characteristics Including Second Sources
13-30	(Currently Inoperative)
31	Output From Line-of-Sight Point Selector
32	Summary Output From Line-of-Sight Point Selector
33	Number Column Densities - Enumerated by Source - Highest to Lowest Contributor
34	Mass/Number Column Densities - Sorted by Materials, Leakage Components, or Engines/Vents
35	Summary: Mass/Number Column Densities - Listed by Materials or Leakage Components
36	Mass/Number Column Densities - Sorted by Locations
37	Summary: Mass/Number Column Densities - Listed by Location
38	(Currently Inoperative)
39	Plot of Density Along Line-of-Sight
40	(Currently Inoperative)
41	Return Flux Enumerated by Source - Highest to Lowest Contributor
42	Return Flux Enumerated by Source - Sorted by Materials, Leakage Components or Engines/Vents
43	Summary: Return Flux - Listed by Materials or Leakage Components
44	Return Flux Enumerated by Source - Sorted by Location
45	Summary: Return Flux - Listed by Location
46	Return Flux Due to Self-Scattering
47	Return Flux Deposition
48-49	(Currently Inoperative)
50	Final Prediction Summary
• DBUGA = .T./ .F. (FALSE)	In addition to the nominal output reports, debug options exist for each of the primary overlays or segments. This
• DBUGB = .T./ .F. (FALSE)	allows the user to obtain additional printout on TAPE 8 for
• DBUGC = .T./ .F. (FALSE)	intermediate computational steps or to monitor complex data
• DBUGD = .T./ .F. (FALSE)	manipulations. Only the debug flag for the segment being
• DBUGE = .T./ .F. (FALSE)	examined should be activated to avoid excessive output.

and successfully run on the JSC UNIVAC computer system. Direct correlation was achieved with the same program run at MMA Denver.

During the extended three months of the contract, the routines were integrated into the present form of the model as described herein and was delivered to JSC at the end of the contract period. Table VII illustrates the differences and similarities between the integrated program and the previously delivered subroutines. The total core requirements of the integrated model has been held relatively constant while significantly increasing its capability. The independent subroutines previously delivered to JSC are still operational and can be used in a limited sense to calculate column densities and return flux for the +Z line-of-sight.

The original intent of the independent surface and point source routines delivered to JSC was to reduce core requirements so that the routines could be run interactively on remote terminals. This was completed for the point source routine and was underway for the surface source routine when the decision was made to integrate the point and surface routines into the beginnings of a mission profile model. The mission profile model contains a great deal more flexibility than the independent routines and will eventually simulate an entire mission as will be required for mission analysis and correlation to sensors. The independent surface source routine could be trimmed to meet interactive remote terminal core requirements but in the future the use of it would require modifying 2 programs and doesn't warrant the effort because of its limited capability when compared to the integrated model.

Even though the new integrated form of the model has necessarily increased core requirements, an attempt to minimize the core requirements was continued during the integration process. In particular, an internal program segmented interactive capability has been reviewed in depth during the design phase of the present Shuttle/Payload Contamination Environment model (SPACE). The present integrated model in an unsegmented internal format would require approximately 45,000 ($\approx 130,000_8$) words of central memory. This amount of core is within storage limitations for batch processing at JSC. However, an effort was put forth to segment the model, such that core requirements could be optimized with absolutely no compromising of the resolution of the analysis.

The present segmentation of the model dropped core requirements to 35,000₁₀ (115,000₈), a savings of 10,000₁₀ words. The method of segmentation used, overwrites Fortran instructions, (after those instructions have been exercised and their resulting data stored) with the next set of instructions necessary for the analysis.

Table VII. Integrated Contamination Model Similarities and Differences to Previous Independent Subroutines

FUNCTIONS	INTEGRATED PROGRAM (Segmented)	INDEPENDENT SUB-ROUTINES (Linear)																						
<p>Nodes</p> <p>Total Core Requirements</p> <p>Run Time Orbiter Zero LOS Out/Off</p>	<p>300 Surfaces 50 Engines ~ 35,000₁₀ ~ 115,000₈</p> <p>Baseline Default Mode ~ 15 sec User Options Up to Hundreds of Seconds</p>	<p>300 Surfaces 50 Engines</p> <p>Out/Off/Leakage } 36,864₁₀ And Eng/Vent } 110,000₈</p> <p>100 sec (including compilation orbiter zero LOS, out/off)</p>																						
<p>Contaminant Cloud</p>	<ul style="list-style-type: none"> • Generalized Line-of-Sight Input θ, \emptyset Origin • Monitors 10 Species Simultaneously <table style="margin-left: 40px;"> <tr> <td></td> <td style="text-align: right;">MW</td> </tr> <tr> <td>2 Outgassing Species</td> <td style="text-align: right;">100</td> </tr> <tr> <td></td> <td style="text-align: right;">85 (?)</td> </tr> <tr> <td>H₂O</td> <td style="text-align: right;">18</td> </tr> <tr> <td>CO₂</td> <td style="text-align: right;">44</td> </tr> <tr> <td>CO</td> <td style="text-align: right;">32</td> </tr> <tr> <td>N₂</td> <td style="text-align: right;">28</td> </tr> <tr> <td>O₂</td> <td style="text-align: right;">32</td> </tr> <tr> <td>H₂</td> <td style="text-align: right;">2</td> </tr> <tr> <td>H</td> <td style="text-align: right;">1</td> </tr> <tr> <td>NO</td> <td style="text-align: right;">30</td> </tr> </table> <ul style="list-style-type: none"> • Mean Free Path Attenuation Option 		MW	2 Outgassing Species	100		85 (?)	H ₂ O	18	CO ₂	44	CO	32	N ₂	28	O ₂	32	H ₂	2	H	1	NO	30	<ul style="list-style-type: none"> • Zero Line-of-Sight (or fixed line-of-sight) • Outgassing MW = 100 Offgassing MW = 18 • No Attenuation Option
	MW																							
2 Outgassing Species	100																							
	85 (?)																							
H ₂ O	18																							
CO ₂	44																							
CO	32																							
N ₂	28																							
O ₂	32																							
H ₂	2																							
H	1																							
NO	30																							
<p>Return Flux</p>	<ul style="list-style-type: none"> • Ambient Scattering Cross Section Varies With Species • Self Scattering • Variable Orbiter Attitude 	<ul style="list-style-type: none"> • Ambient Scattering Fixed Collision Cross Section • No Self Scattering • Fixed Attitude 																						

Table VII. Integrated Contamination Model Similarities and Differences to Previous Independent Subroutines

FUNCTIONS	INTEGRATED PRO-GRAM (Segmented)	INDEPENDENT SUB-ROUTINES (Linear)
Return Flux (cont'd)	<ul style="list-style-type: none"> • Variable Altitude (205 → 2000 km) • Variable Field of View (0 → 2π) 	<ul style="list-style-type: none"> • Altitudes 250, 400, 700 km • $\Omega = 0.19$ and 2π
Sources	<ul style="list-style-type: none"> • Simultaneous Sources Out Off or Early Desorption (ED) Eng Evap • Time Dependent Mass Loss Rates 	<ul style="list-style-type: none"> • Out/Off Eng/Evap } Separate Runs • Fixed Time
Surface Temperatures	<ul style="list-style-type: none"> • Min/Max Plus 5 Other Orbiter Attitudes 	<ul style="list-style-type: none"> • Min/Max One Attitude
Input	<ul style="list-style-type: none"> • Control Flags • Override Options • Permanent Files 	<ul style="list-style-type: none"> • Permanent Files

COMPUTER PROGRAM SIMILARITIES

- Block Data
- Same Answers
- Same Temperatures
- Same Rates
- Same Node Numbers
- Same View Factor Files
- Same Plume Functions
- Same Output Scheme

All future work on the model will be incorporated in a segmented fashion to allow the model to execute in a minimum of core, while maximizing prediction integrity.

3.2 Induced Environment Predictions

This section presents some of the updated induced environment predictions using the new Orbiter geometry, surface temperature profile and source characteristics. The temperature profile corresponds to a $\beta = 90^\circ$, solar inertial, and X IOP attitude and does represent the maximum hot case in the model.

The data presented is for seven lines-of-sight and they are:

LOS	Direction
1	- along +Z
2	- 30° aft
3	- 60° aft
4	- 30° \pm Y
5	- 60° \pm Y
6	- 30° FWD
7	- 60° FWD

These lines-of-sight were selected for comparison to report MCR-75-13, June 1975, so that the updated model could be evaluated. A detailed summary printout for the sources is presented in this section and includes mass column density, number column density and return flux. The contributions to the column densities are subdivided by species, area contribution and material contribution.

Table VIII presents the total values and is included for ease of comparison to the previous predictions in report MCR-75-13. Several observations are apparent when compared to previous predictions. First of all, the mass and number column densities are lower for outgassing and early desorption (offgassing). This results from source rate changes and surface temperature changes. Secondly, the return flux is also reduced for outgassing but has increased for early desorption (offgassing). The reason for the increase is that the collision cross section has increased almost an order of magnitude from previous predictions. Since the total column density has decreased by a factor of 3, the net increase in return flux from previous predictions is near a factor of 3.

The detailed printout includes contributions by species, location and surface material type. Table IX includes this data for the 7 lines-of-sight presented in this section. It is shown that nomex surfaces account for more than 50% for lines-of-sight 1 through 5 and for lines-of-sight 6 and 7 (forward 30 degrees and 60 degrees respectively), the nomex contribution falls to lower contributions (43% for LOS 6 and 28% for LOS 7).

Table VIII. Outgassing, Early Desorption Predictions*

Line-of-Sight	Outgassing		Return Flux mol/cm ²
	MCD g/cm ²	NCD mol/cm ²	
1	4.5-12 ^{***}	2.7+10	3.1+10
2	4.8-12	2.9+10	2.8+10
3	5.1-12	3.0+10	1.7+10
4	4.6-12	2.8+10	2.7+10
5	4.4-12	2.6+10	1.5+10
6	4.1-12	2.5+10	2.4+10
7	3.7-12	2.2+10	1.2+10
<u>Early Desorption</u>			
1	1.3-11	3.2+11	9.7+10
2	1.4-11	3.3+11	8.9+10
3	1.5-11	3.5+11	5.4+10
4	1.4-11	3.3+11	8.6+10
5	1.3-11	3.0+11	4.7+10
6	1.2-11	2.8+11	7.6+10
7	1.1-11	2.6+11	4.0+10

*Return flux values should be divided by cosine the LOS makes with the Z-axis
^{***}4.5-12 = 4.5 x 10⁻¹²

The major contributing area is the wing which represents 30-39% of the contribution for lines-of-sight 1 through 6 and 21% for LOS 7.

Table X shows the updated predictions for the aft downward facing (-Z) VCS and RCS engines. The predicted values are lower than previously predicted due to refinements in the wing geometry.

Table XI shows the updated predictions for the evaporator contribution to the 7 lines-of-sight investigated. The table shows that the contribution to many of the lines-of-sight could be reduced if the wing reflected components were eliminated. This could be performed by raising the elevon thus blocking the wing surfaces from the evaporator. The evaporator average flow is 13.6 kg/hr (30lb/hr) and the instantaneous flow (during actual operation) is 31.7kg/hr (70lb/hr). The instantaneous flow rate is used in the model, whereas previously, the average rate was used.

Table IX. Detailed Outgassing, Early Desorption Prediction in Computer Format

REPORT NO. 35 *** SAMPLE CASE NO. 9 SHUTTLE ORBITER ALL SOURCES (EXCLUDING ENGS)

05/03/77 13.47.23. PAGE 229

CONTENTS: SUMMARY *** MASS/NUMBER COLUMN DENSITIES ***

LINE-OF-SIGHT NO = 1
 THETA (DEG) = 0.0
 PHI (DEG) = 0.0

*** LISTED BY MATERIALS *** (CONT)

SECTION SUMMARY	SPECIES NUMBER COLUMN DENSITY (MOLECULES/CM**2)						EARLY DESORPTION (GM/CM**2) (MOLECULES/CM**2)	OUT GASSING (GM/CM**2)	TOTAL	% OF TOTAL
	OUTG1	OUTG2	H2O	N2	CO2					
	O2	CO	H2	H	MMHNO3					
LINER	.43E+10	0.	.24E+11	.12E+11	.70E+10	.21E-11	.71E-12	.26E-11		
TEFLON	.44E+10	0.	0.	0.	0.	.49E+11	.43E+10	.53E+11	15.4	
NOMEX	.33E+10	0.	.19E+11	.94E+10	.80E+10	.10E-11	.54E-12	.22E-11		
LRSI	.14E+11	0.	.82E+11	.41E+11	.26E+11	.37E+11	.33E+10	.41E+11	11.9	
HRSI	.15E+11	0.	0.	0.	0.	.71E-11	.24E-11	.94E-11		
RCC	.19E+10	0.	.10E+11	.51E+10	.33E+10	.16E+12	.14E+11	.18E+12	51.8	
SLKHED	.18E+10	0.	0.	0.	0.	.88E-12	.30E-12	.12E-11		
CRACKS	.57E+09	0.	.33E+10	.18E+10	.10E+10	.21E+11	.18E+10	.22E+11	6.5	
	.53E+09	0.	0.	0.	0.	.28E-12	.05E-13	.38E-12		
	.69E+06	0.	.40E+07	.20E+07	.13E+07	.65E+10	.57E+09	.71E+10	2.1	
	.71E+06	0.	0.	0.	0.	.34E-15	.12E-15	.46E-15		
	.23E+10	0.	.16E+11	.82E+10	.53E+10	.79E+07	.69E+06	.86E+07	.0	
	.28E+10	0.	0.	0.	0.	.14E-11	.48E-12	.19E-11		
	0.	0.	.48E+06	.29E+10	.31E+10	.33E+11	.29E+10	.36E+11	10.4	
	.84E+09	0.	0.	0.	0.	.41E-12	0.	.41E-12		
TOTAL	.27E+11	0.	.15E+12	.80E+11	.50E+11	.14E-10	.15E-11	.18E-10		
	.29E+11	0.	0.	0	0.	.32E+12	.27E+11	.34E+12	100.0	

3-88

ORIGINAL PAGE IS
 OF POOR QUALITY

Table IX. Detailed Outgassing, Early Desorption Prediction in Computer Format (cont'd)

REPORT NO. 37 *** SAMPLE CASE NO. 9 SHUTTLE ORBITER ALL SOURCES (EXCLUDING ENGS)

05/03/77 13.47.24. PAGE 238

CONTENTS: SUMMARY *** MASS/NUMBER COLUMN DENSITIES ***

LINE-OF-SIGHT NO. = 1
 THETA (DEG) = 0.0
 PHI (DEG) = 0.0

*** LISTED BY LOCATION *** (CONT)

SECTION SUMMARY	SPECIES NUMBER COLUMN DENSITY (MOLECULES/CM ²)						EARLY DESCRIPTION (GM/CM ²) (MOLECULES/CM ²)	OUT GASSING (MOLECULES/CM ²)	TOTAL	% OF TOTAL
	OUTG1		H2O	N2	CO2					
	O2	CO								
BAY	.72E+10	0.	.41E+11	.20E+11	.13E+11	.35E-11	.12E-11	.47E-11		
CREW	.73E+10	0.	0.	0.	0.	.81E+11	.72E+10	.89E+11	25.8	
FUSLAG	.56E+09	0.	.32E+10	.16E+10	.10E+10	.27E-12	.93E-13	.37E-12		
OMS	.57E+09	0.	0.	0.	0.	.64E+10	.96E+09	.69E+10	2.0	
RADOOR	.95E+08	0.	.54E+09	.27E+09	.17E+09	.47E-13	.16E-13	.63E-13		
TAIL	.97E+08	0.	0.	0.	0.	.11E+10	.95E+08	.12E+10	.3	
WING	.85E+09	0.	.49E+10	.25E+10	.16E+10	.42E-12	.14E-12	.57E-12		
ELEVON	.88E+09	0.	0.	0.	0.	.99E+10	.86E+09	.11E+11	3.1	
TOTAL	.33E+10	0.	.19E+11	.94E+10	.60E+10	.16E-11	.54E-12	.22E-11		
	.33E+10	0.	0.	0.	0.	.37E+11	.33E+10	.41E+11	11.9	
	.56E+08	0.	.32E+09	.16E+09	.10E+09	.28E-13	.93E-14	.37E-13		
	.57E+09	0.	0.	0.	0.	.64E+09	.96E+08	.70E+09	.2	
	.10E+11	0.	.59E+11	.29E+11	.19E+11	.51E-11	.17E-11	.66E-11		
	.10E+11	0.	0.	0.	0.	.12E+12	.10E+11	.13E+12	37.2	
	.48E+10	0.	.28E+11	.14E+11	.89E+10	.24E-11	.80E-12	.32E-11		
	.49E+10	0.	0.	0.	0.	.55E+11	.46E+10	.60E+11	17.5	
TOTAL	.27E+11	0.	.15E+12	.77E+11	.50E+11	.13E-10	.45E-11	.18E-10		
	.28E+11	0.	0.	0.	0.	.31E+12	.27E+11	.34E+12	100.0	

3-89

ORIGINAL PAGE IS OF POOR QUALITY

Table IX. Detailed Outgassing, Early Desorption, Prediction in Computer Format (cont'd)

REPORT NO. 43 *** SAMPLE CASE NO. 9 SHUTTLE ORBITER ALL SOURCES (EXCLUDING ENGS)

05/03/77 13.47.26. PAGE 247

CONTENTS: SUMMARY RETURN FLUX AT 400.0 KM ALTITUDE

CRITICAL SURFACE NO. = 1
FIELD-OF-VIEW (SR) = .190

*** LISTED BY MATERIAL TYPE *** (CONT)

SECTION SUMMARY	SPECIES RETURN FLUX (MOLECULES/CM**2)					EARLY DESORPTION (GM/CM**2) (MOLECULES/CM**2)	OUT GASSING (MOLECULES/CM**2)	TOTAL	% OF TOTAL
	OUTG1	OUTG2	H2O	N2	CO2				
	O2	CO	H2	H	MMHNO3				
LINER	.49E+10	0.	.63E+10	.41E+10	.30E+10	.67E-12	.81E-12	.15E-11	
TEFLON	.14E+10	0.	0.	0.	0.	.15E+11	.49E+10	.20E+11	15.4
NOMEX	.37E+10	0.	.49E+10	.32E+10	.23E+10	.52E-12	.61E-12	.11E-11	
LRSI	.11E+10	0.	0.	0.	0.	.11E+11	.37E+10	.15E+11	11.9
HRSI	.16E+11	0.	.21E+11	.14E+11	.99E+10	.23E-11	.27E-11	.49E-11	
RCC	.46E+10	0.	0.	0.	0.	.50E+11	.16E+11	.66E+11	51.8
BLKHED	.20E+10	0.	.27E+10	.18E+10	.12E+10	.28E-12	.34E-12	.62E-12	
CRACKS	.58E+09	0.	0.	0.	0.	.63E+10	.20E+10	.83E+10	6.5
	.64E+09	0.	.85E+09	.56E+09	.39E+09	.90E-13	.11E-12	.20E-12	
	.18E+09	0.	0.	0.	0.	.20E+10	.64E+09	.26E+10	2.1
	.78E+06	0.	.10E+07	.68E+06	.48E+06	.11E-15	.13E-15	.24E-15	
	.22E+06	0.	0.	0.	0.	.24E+07	.78E+06	.32E+07	.0
	.32E+10	0.	.43E+10	.28E+10	.20E+10	.45E-12	.54E-12	.99E-12	
	.93E+09	0.	0.	0.	0.	.10E+11	.32E+10	.13E+11	10.4
	0.	0.	.13E+08	.99E+09	.12E+10	.15E-12	0.	.15E-12	
	.26E+09	0.	0.	0.	0.	.24E+10	0.	.24E+10	1.9
TOTAL	.31E+11	0.	.41E+11	.27E+11	.20E+11	.44E-11	.51E-11	.95E-11	
	.90E+10	0.	0.	0.	0.	.97E+11	.31E+11	.13E+12	100.0

3-90

ORIGINAL PAGE IS
OF POOR QUALITY

Table IX. Detailed Outgassing, Early Desorption, Prediction in Computer Format (cont'd)

REPORT NO. 35 *** SAMPLE CASE NO. 9 SHUTTLE ORBITER ALL SOURCES (EXCLUDING ENGS)

05/03/77 13.47.51. PAGE 272

CONTENTS: SUMMARY *** MASS/NUMBER COLUMN DENSITIES ***

LINE-OF-SIGHT NO. = 2
 THETA (DEG) = 0.0
 PHI (DEG) = 0.0

*** LISTED BY MATERIALS *** (CONT)

SECTION SUMMARY	SPECIES NUMBER COLUMN DENSITY (MOLECULES/CM**2)					EARLY DESCRIPTION (GM/CM**2)	OUT GASSING (MOLECULES/CM**2)	TOTAL	% OF TOTAL
	OUTG1 O2	OUTG2 CO	H2O H2	N2 H	CO2 MMHNO3				
LINER	.37E+10	0.	.21E+11	.11E+11	.08E+10	.16E-11	.62E-12	.24E-11	
TEFLON	.38E+10	0.	0.	0.	0.	.42E+11	.37E+10	.46E+11	12.5
NOMEX	.31E+10	0.	0.	0.	0.	.15E-11	.51E-12	.20E-11	
LRSI	.17E+11	0.	.97E+11	.48E+11	.31E+11	.35E+11	.31E+10	.39E+11	10.4
HRSI	.22E+10	0.	.12E+11	.62E+10	.40E+10	.83E-11	.28E-11	.11E-10	
RCC	.22E+10	0.	0.	0.	0.	.19E+12	.17E+11	.21E+12	57.6
BLKHED	.59E+09	0.	.34E+10	.17E+10	.11E+10	.11E-11	.36E-12	.14E-11	
CRACKS	.60E+09	0.	0.	0.	0.	.25E+11	.22E+10	.27E+11	7.4
	.60E+06	0.	.34E+07	.17E+07	.11E+07	.29E-12	.98E-13	.39E-12	
	.61E+06	0.	0.	0.	0.	.68E+10	.59E+09	.74E+10	2.0
	.24E+10	0.	.14E+11	.68E+10	.44E+10	.29E-15	.99E-16	.39E-15	
	.24E+10	0.	0.	0.	0.	.68E+07	.60E+06	.74E+07	.0
	0.	0.	.52E+08	.31E+10	.33E+10	.12E-11	.40E-12	.16E-11	
	.90E+09	0.	0.	0.	0.	.27E+11	.24E+10	.30E+11	8.1
TOTAL	.29E+11	0.	.16E+12	.86E+11	.56E+11	.44E-12	0.	.44E-12	
	.30E+11	0.	0.	0.	0.	.74E+10	0.	.74E+10	2.0
						.15E-10	.48E-11	.19E-10	
						.34E+12	.29E+11	.37E+12	100.0

3-91

ORIGINAL PAGE IS OF POOR QUALITY

Table IX. Detailed Outgassing, Early Desorption, Prediction in Computer Format (cont'd)

REPORT NO. 37 *** SAMPLE CASE NO. 9 SHUTTLE ORBITER ALL SOURCES (EXCLUDING ENGS)

05/03/77 13.47.53. PAGE 282

CONTENTS: SUMMARY *** MASS/NUMBER COLUMN DENSITIES ***

LINE-OF-SIGHT NO. = 2
 THETA (DEG) = 0.0
 PHI (DEG) = 0.0

*** LISTED BY LOCATION *** (CONT)

SECTION SUMMARY	SPECIES NUMBER COLUMN DENSITY (MOLECULES/CM**2)						EARLY DESORPTION (GM/CM**2)	OUT GASSING (MOLECULES/CM**2)	TOTAL	% OF TOTAL
	OUTG1 O2	OUTG2 CO	H2O H2	N2 H	CO2 MMHNO3					
BAY	.61E+10	0.	.35E+11	.17E+11	.11E+11	.30E-11	.10E-11	.40E-11		
CREW	.62E+10	0.	0.	0.	0.	.69E+11	.61E+10	.75E+11	20.6	
FUFLAG	.25E+09	0.	.14E+10	.71E+09	.46E+09	.12E-12	.41E-13	.16E-12		
OMS	.94E+08	0.	.54E+09	.27E+09	.17E+09	.28E+10	.25E+09	.31E+10	.8	
RADOOR	.96E+08	0.	0.	0.	0.	.46E-13	.15E-13	.62E-13		
TAIL	.15E+10	0.	.84E+10	.42E+10	.27E+10	.11E+10	.94E+08	.12E+10	.3	
WING	.15E+10	0.	0.	0.	0.	.72E-12	.24E-12	.97E-12		
ELEVON	.31E+10	0.	.18E+11	.88E+10	.57E+10	.17E+11	.15E+10	.18E+11	5.0	
	.31E+10	0.	0.	0.	0.	.15E-11	.51E-12	.20E-11		
	.95E+08	0.	.54E+09	.27E+09	.18E+09	.35E+11	.31E+10	.38E+11	10.4	
	.97E+08	0.	0.	0.	0.	.47E-13	.16E-13	.63E-13		
	.12E+11	0.	.67E+11	.34E+11	.22E+11	.11E+10	.95E+08	.12E+10	.3	
	.12E+11	0.	0.	0.	0.	.58E-11	.20E-11	.77E-11		
	.60E+10	0.	.35E+11	.17E+11	.11E+11	.13E+12	.12E+11	.15E+12	39.9	
	.62E+10	0.	0.	0.	0.	.30E-11	.10E-11	.40E-11		
TOTAL	.29E+11	0.	.16E+12	.82E+11	.53E+11	.69E+11	.60E+10	.75E+11	20.5	
	.29E+11	0.	0.	0.	0.	.14E-10	.48E-11	.19E-10		
						.33E+12	.29E+11	.36E+12	100.0	

3-92

Table IX. Detailed Outgassing, Early Desorption, Prediction in Computer Format (cont'd)

REPORT NO. 43 *** SAMPLE CASE NO. 9 SHUTTLE ORBITER ALL SOURCES (EXCLUDING ENGS)

05/03/77 13.47.55. PAGE 292

CONTENTS: SUMMARY RETURN FLUX AT 400.0 KM ALTITUDE

CRITICAL SURFACE NO. = 2
FIELD-OF-VIEW (SR) = .190

*** LISTED BY MATERIAL TYPE *** (CONT)

SECTION SUMMARY	SPECIES RETURN FLUX (MOLECULES/CM**2)					EARLY DESORPTION (GM/CM**2) (MOLECULES/CM**2)	OUT GASSING (GM/CM**2)	TOTAL	% OF TOTAL
	OUTG1	OUTG2	H2O	N2	CO2				
	O2	CO	H2	H	MMHNO3				
LINER	.36E+10	0.	.47E+10	.31E+10	.22E+10	.50E-12	.61E-12	.11E-11	
	.10E+10	0.	0.	0.	0.	.11E+11	.36E+10	.15E+11	12.5
TEFLON	.30E+10	0.	.40E+10	.26E+10	.18E+10	.42E-12	.50E-12	.92E-12	
	.86E+09	0.	0.	0.	0.	.93E+10	.30E+10	.12E+11	10.4
NOMEX	.17E+11	0.	.22E+11	.14E+11	.10E+11	.23E-11	.28E-11	.51E-11	
	.47E+10	0.	0.	0.	0.	.51E+11	.17E+11	.68E+11	57.6
LRSI	.21E+10	0.	.28E+10	.18E+10	.13E+10	.30E-12	.35E-12	.65E-12	
	.60E+09	0.	0.	0.	0.	.66E+10	.21E+10	.87E+10	7.4
HRSI	.53E+09	0.	.77E+09	.50E+09	.36E+09	.81E-13	.96E-13	.18E-12	
	.16E+09	0.	0.	0.	0.	.18E+10	.58E+09	.24E+10	2.0
RCC	.58E+06	0.	.77E+06	.51E+06	.36E+06	.82E-16	.97E-16	.18E-15	
	.17E+06	0.	0.	0.	0.	.18E+07	.58E+06	.24E+07	.0
BLKHED	.23E+10	0.	.31E+10	.20E+10	.14E+10	.33E-12	.39E-12	.71E-12	
	.66E+09	0.	0.	0.	0.	.72E+10	.23E+10	.95E+10	8.1
CRACKS	0.	0.	.12E+08	.92E+09	.11E+10	.14E-12	0.	.14E-12	
	.25E+09	0.	0.	0.	0.	.23E+10	0.	.23E+10	1.9
TOTAL	.28E+11	0.	.37E+11	.25E+11	.18E+11	.41E-11	.47E-11	.88E-11	
	.83E+10	0.	0.	0.	0.	.89E+11	.28E+11	.12E+12	100.0

3-93

Table IX. Detailed Outgassing, Early Desorption, Prediction in Computer Format (cont'd)

REPORT NO. 35 *** SAMPLE CASE NO. 9 SHUTTLE ORBITER ALL SOURCES (EXCLUDING ENGS)

05/03/77 13.48.17. PAGE 318

CONTENTS: SUMMARY *** MASS/NUMBER COLUMN DENSITIES ***

LINE-OF-SIGHT NO. = 3
 THETA (DEG) = 0.0
 PHI (DEG) = 0.0

*** LISTED BY MATERIALS *** (CONT)

SECTION SUMMARY	SPECIES NUMBER COLUMN DENSITY (MOLECULES/CM*2)					EARLY DESORPTION (GM/CM*2)	OUT GASSING (MOLECULES/CM*2)	TOTAL	% OF TOTAL
	OUTG1 O2	OUTG2 CO	H2O H2	N2 H	CO2 MMHND3				
LINER	.37E+10	0.	.21E+11	.11E+11	.68E+10	.18E-11	.62E-12	.24E-11	
TEFLON	.38E+10	0.	0.	0.	0.	.42E+11	.37E+10	.46E+11	11.9
NOMEX	.23E+10	0.	.13E+11	.65E+10	.42E+10	.11E-11	.38E-12	.15E-11	
LRSI	.17E+11	0.	.97E+11	.49E+11	.31E+11	.26E+11	.23E+10	.28E+11	7.4
HRSI	.43E+10	0.	.24E+11	.12E+11	.79E+10	.84E-11	.28E-11	.11E-10	
RCC	.44E+10	0.	0.	0.	0.	.19E+12	.17E+11	.21E+12	55.0
BLKHED	.74E+09	0.	.42E+10	.21E+10	.14E+10	.21E-11	.71E-12	.28E-11	
CRACKS	.75E+09	0.	0.	0.	0.	.49E+11	.43E+10	.53E+11	13.8
TOTAL	.59E+06	0.	.34E+07	.17E+07	.11E+07	.36E-12	.12E-12	.48E-12	
	.60E+06	0.	0.	0.	0.	.84E+10	.74E+09	.91E+10	2.4
	.23E+10	0.	.13E+11	.66E+10	.43E+10	.29E-15	.98E-16	.39E-15	
	.24E+10	0.	0.	0.	0.	.67E+07	.59E+06	.73E+07	.0
	0.	0.	.57E+08	.34E+10	.36E+10	.11E-11	.39E-12	.15E-11	
	.98E+09	0.	0.	0.	0.	.27E+11	.23E+10	.29E+11	7.5
						.48E-12	0.	.48E-12	
						.81E+10	0.	.81E+10	2.1
TOTAL	.30E+11	0.	.17E+12	.90E+11	.60E+11	.15E-10	.51E-11	.20E-10	
	.32E+11	0.	0.	0.	0.	.36E+12	.30E+11	.39E+12	100.0

3-94

ORIGINAL PAGE IS
 OF POOR QUALITY

Table IX. Detailed Outgassing, Early Desorption, Prediction in Computer Format (cont'd)

REPORT NO. 37 *** SAMPLE CASE NO. 9 SHUTTLE ORBITER ALL SOURCES (EXCLUDING ENGS)

05/03/77 13.48.19. PAGE 329

CONTENTS: SUMMARY *** MASS/NUMBER COLUMN DENSITIES ***

LINE-OF-SIGHT NO. = 3
 THETA (DEG) = 0.0
 PHI (DEG) = 0.0

*** LISTED BY LOCATION *** (CONT)

SECTION SUMMARY	SPECIES NUMBER COLUMN DENSITY (MOLECULES/CM ²)					EARLY DESORPTION (GM/CM ²) (MOLECULES/CM ²)	CUT GASSING	TOTAL	% OF TOTAL
	OUTG1	OUTG2	H2O	N2	CO2				
	O2	CO	H2	H	MMHNO3				
BAY	.60E+10	0.	.34E+11	.17E+11	.11E+11	.30E-11	.10E-11	.40E-11	
	.62E+10	0.	0.	0.	0.	.69E+11	.60E+10	.75E+11	19.3
CREW	.65E+08	0.	.37E+09	.19E+09	.12E+09	.32E-13	.11E-13	.43E-13	
	.65E+08	0.	0.	0.	0.	.74E+09	.65E+08	.81E+09	.2
FUSLAG	.24E+09	0.	.14E+10	.69E+09	.44E+09	.12E-12	.40E-13	.16E-12	
	.24E+09	0.	0.	0.	0.	.27E+10	.24E+09	.30E+10	.8
OMS	.35E+10	0.	.20E+11	.10E+11	.65E+10	.17E-11	.59E-12	.23E-11	
	.36E+10	0.	0.	0.	0.	.40E+11	.35E+10	.44E+11	11.4
RADOOR	.23E+10	0.	.13E+11	.65E+10	.42E+10	.11E-11	.36E-12	.15E-11	
	.23E+10	0.	0.	0.	0.	.26E+11	.23E+10	.28E+11	7.4
TAIL	.39E+09	0.	.22E+10	.11E+10	.71E+09	.19E-12	.64E-13	.25E-12	
	.39E+09	0.	0.	0.	0.	.44E+10	.39E+09	.43E+10	1.2
WING	.12E+11	0.	.67E+11	.34E+11	.22E+11	.58E-11	.20E-11	.77E-11	
	.12E+11	0.	0.	0.	0.	.13E+12	.12E+11	.15E+12	37.9
ELEVON	.61E+10	0.	.35E+11	.17E+11	.11E+11	.30E-11	.10E-11	.40E-11	
	.62E+10	0.	0.	0.	0.	.70E+11	.61E+10	.76E+11	19.7
TOTAL	.30E+11	0.	.17E+12	.87E+11	.56E+11	.15E-10	.51E-11	.20E-10	
	.31E+11	0.	0.	0.	0.	.35E+12	.30E+11	.38E+12	100.0

3-95

ORIGINAL PAGE IN
 OF FOUR QUANT.

Table IX. Detailed Outgassing, Early Desorption, Prediction in Computer Format (cont'd)

REPORT NO. 43 *** SAMPLE CASE NO. 9 SHUTTLE ORBITER ALL SOURCES (EXCLUDING ENGS)

05/03/77 13.48.21. PAGE 340

COMMENTS: SUMMARY RETURN FLUX AT 400.0 KM ALTITUDE

CRITICAL SURFACE NO. = 3
FIELD-OF-VIEW (SR) = .190

*** LISTED BY MATERIAL TYPE *** (CONT)

SECTION SUMMARY	SPECIES RETURN FLUX (MOLECULES/CM**2)					EARLY DESORPTION (GM/CM**2) (MOLECULES/CM**2)	OUT GASSING	TOTAL	% OF TOTAL
	OUTG1	OUTG2	H2O	N2	CO2				
	O2	CO	H2	H	MMHNO3				
LINER	.21E+10	0.	.27E+10	.18E+10	.13E+10	.29E-12	.35E-12	.64E-12	
TEFLON	.60E+09	0.	0.	0.	0.	.64E+10	.21E+10	.85E+10	11.9
NOMEX	.13E+10	0.	.17E+10	.11E+10	.79E+09	.18E-12	.21E-12	.39E-12	
LRSI	.37E+09	0.	0.	0.	0.	.40E+10	.13E+10	.53E+10	7.4
HRSI	.96E+10	0.	.13E+11	.83E+10	.59E+10	.13E-11	.16E-11	.29E-11	
RCC	.27E+10	0.	0.	0.	0.	.30E+11	.96E+10	.39E+11	55.0
BLKHED	.24E+10	0.	.32E+10	.21E+10	.15E+10	.34E-12	.40E-12	.74E-12	
CRACKS	.69E+09	0.	0.	0.	0.	.75E+10	.24E+10	.99E+10	13.9
TOTAL	.42E+09	0.	.55E+09	.36E+09	.25E+09	.58E-13	.69E-13	.13E-12	
	.12E+09	0.	0.	0.	0.	.13E+10	.42E+09	.17E+10	2.4
	.33E+06	0.	.44E+06	.29E+06	.20E+06	.46E-16	.55E-16	.10E-15	
	.94E+05	0.	0.	0.	0.	.10E+07	.33E+06	.14E+07	.0
	.13E+10	0.	.17E+10	.11E+10	.80E+09	.18E-12	.22E-12	.40E-12	
	.37E+09	0.	0.	0.	0.	.40E+10	.13E+10	.54E+10	7.5
	0.	0.	.74E+07	.58E+09	.68E+09	.86E-13	0.	.86E-13	
	.15E+09	0.	0.	0.	0.	.14E+10	0.	.14E+10	2.0
TOTAL	.17E+11	0.	.23E+11	.15E+11	.11E+11	.25E-11	.29E-11	.53E-11	
	.50E+10	0.	0.	0.	0.	.54E+11	.17E+11	.72E+11	100.0

3-96

Table IX. Detailed Outgassing, Early Desorption, Prediction in Computer Format (cont'd)

REPORT NO. 35 *** SAMPLE CASE NO. 9 SHUTTLE ORBITER ALL SOURCES (EXCLUDING ENGS)

05/03/77 13.49.10. PAGE 364

CONTENTS: SUMMARY *** MASS/NUMBER COLUMN DENSITIES ***

LINE-OF-SIGHT NO. = 4
 THETA (DEG) = 0.0
 PHI (DEG) = 0.0

*** LISTED BY MATERIALS *** (CONT)

SECTION SUMMARY	SPECIES NUMBER COLUMN DENSITY (MOLECULES/CM**2)						EARLY DESORPTION (GM/CM**2)	OUT GASSING (MOLECULES/CM**2)	TOTAL	% OF TOTAL
	OUTG1	OUTG2	H2O	N2	CO2					
	O2	CO	H2	H	MMHNO3					
LINER	.39E+10	0.	.22E+11	.11E+11	.71E+10	.19E-11	.65E-12	.25E-11		
	.40E+10	0.	0.	0.	0.	.44E+11	.39E+10	.48E+11	13.5	
TEFLON	.35E+10	0.	.20E+11	.99E+10	.64E+10	.17E-11	.58E-12	.23E-11		
	.35E+10	0.	0.	0.	0.	.40E+11	.35E+10	.43E+11	12.2	
NOMEX	.15E+11	0.	.88E+11	.44E+11	.28E+11	.75E-11	.25E-11	.10E-10		
	.16E+11	0.	0.	0.	0.	.13E+12	.15E+11	.19E+12	53.8	
LRSI	.18E+10	0.	.10E+11	.50E+10	.32E+10	.87E-12	.29E-12	.12E-11		
	.18E+10	0.	0.	0.	0.	.20E+11	.18E+10	.22E+11	6.2	
HRSI	.54E+09	0.	.31E+10	.15E+10	.99E+09	.26E-12	.89E-13	.35E-12		
	.55E+09	0.	0.	0.	0.	.61E+10	.54E+09	.67E+10	1.9	
RCC	.68E+06	0.	.39E+07	.19E+07	.12E+07	.33E-15	.11E-15	.45E-15		
	.69E+06	0.	0.	0.	0.	.77E+07	.68E+06	.84E+07	.0	
BLKHED	.30E+10	0.	.17E+11	.85E+10	.55E+10	.15E-11	.49E-12	.20E-11		
	.30E+10	0.	0.	0.	0.	.34E+11	.30E+10	.37E+11	10.4	
CRACKS	0.	0.	.49E+08	.30E+10	.32E+10	.42E-12	0.	.42E-12		
	.85E+09	0.	0.	0.	0.	.70E+10	0.	.70E+10	2.0	
TOTAL	.28E+11	0.	.16E+12	.83E+11	.55E+11	.14E-10	.46E-11	.19E-10		
	.29E+11	0.	0.	0.	0.	.33E+12	.26E+11	.35E+12	100.0	

3-97

Table IX. Detailed Outgassing, Early Desorption, Prediction in Computer Format (cont'd)

REPORT NO. 37 *** SAMPLE CASE NO. 9. SHUTTLE ORBITER ALL SOURCES (EXCLUDING ENGS)

05/03/77 13.49.12. PAGE 373

CONTENTS: SUMMARY *** MASS/NUMBER COLUMN DENSITIES ***

LINE-OF-SIGHT NO. = 4
 THETA (DEG) = 0.0
 PHI (DEG) = 0.0

*** LISTED BY LOCATION *** (CONT)

SECTION SUMMARY	SPECIES NUMBER COLUMN DENSITY (MOLECULES/CM ²)					EARLY DESORPTION (GM/CM ²) (MOLECULES/CM ²)	OUT GASSING (MOLECULES/CM ²)	TOTAL	% OF TOTAL
	OUTG1 O2	OUTG2 CO	H2O H2	N2 H	CO2 MMHND3				
BAY	.69E+10	0.	.39E+11	.19E+11	.13E+11	.34E-11	.11E-11	.45E-11	
	.70E+10	0.	0.	0.	0.	.78E+11	.69E+10	.85E+11	24.0
CREW	.53E+09	0.	.30E+10	.15E+10	.97E+09	.26E-12	.89E-13	.35E-12	
	.54E+09	0.	0.	0.	0.	.60E+10	.53E+09	.60E+10	1.9
FUSLAG	.29E+09	0.	.16E+10	.83E+09	.53E+09	.14E-12	.48E-13	.19E-12	
	.29E+09	0.	0.	0.	0.	.33E+10	.29E+09	.36E+10	1.0
OMS	.70E+09	0.	.40E+10	.20E+10	.13E+10	.34E-12	.12E-12	.46E-12	
	.71E+09	0.	0.	0.	0.	.80E+10	.70E+09	.87E+10	2.4
RADOOR	.35E+10	0.	.20E+11	.99E+10	.64E+10	.17E-11	.58E-12	.23E-11	
	.35E+10	0.	0.	0.	0.	.40E+11	.35E+10	.43E+11	12.2
TAIL	.11E+09	0.	.64E+09	.32E+09	.21E+09	.55E-13	.18E-13	.73E-13	
	.11E+09	0.	0.	0.	0.	.13E+10	.11E+09	.14E+10	.4
WING	.11E+11	0.	.65E+11	.32E+11	.21E+11	.56E-11	.19E-11	.74E-11	
	.12E+11	0.	0.	0.	0.	.13E+12	.11E+11	.14E+12	39.7
ELEVON	.47E+10	0.	.27E+11	.13E+11	.86E+10	.23E-11	.78E-12	.31E-11	
	.48E+10	0.	0.	0.	0.	.54E+11	.47E+10	.58E+11	16.5
TOTAL	.28E+11	0.	.16E+12	.80E+11	.51E+11	.14E-10	.46E-11	.78E-10	
	.29E+11	0.	0.	0.	0.	.32E+12	.28E+11	.35E+12	100.0

3-98

Table IX. Detailed Outgassing, Early Desorption, Prediction in Computer Format (ccnt'd)

REPORT NO. 43 *** SAMPLE CASE NO. 9 SHUTTLE ORBITER ALL SOURCES (EXCLUDING ENGS)

05/03/77 13.49.14. PAGE 383

CONTENTS: SUMMARY RETURN FLUX AT 400.0 KM ALTITUDE

CRITICAL SURFACE NO. = 4
FIELD-OF-VIEW (SR) = .190

*** LISTED BY MATERIAL TYPE *** (CONT)

SECTION SUMMARY	SPECIES RETURN FLUX (MOLECULES/CM ²)					EARLY DESORPTION (GM/CM ²) (MOLECULES/CM ²)	OUT GASSING	TOTAL	% OF TOTAL
	OUTG1 O2	OUTG2 CO	H2O H2	N2 H	CO2 MMHNO3				
LINER	.38E+10	0.	.50E+10	.33E+10	.23E+10	.53E-12	.63E-12	.12E-11	
TEFLON	.11E+10	0.	0.	0.	0.	.12E+11	.36E+10	.15E+11	13.6
NOMEX	.34E+10	0.	.45E+10	.29E+10	.21E+10	.47E-12	.66E-12	.10E-11	
LRSI	.96E+09	0.	0.	0.	0.	.10E+11	.34E+10	.14E+11	12.2
LRSI	.15E+11	0.	.20E+11	.13E+11	.92E+10	.21E-11	.25E-11	.46E-11	
HRSI	.43E+10	0.	0.	0.	0.	.46E+11	.15E+11	.61E+11	53.9
HRSI	.17E+10	0.	.23E+10	.15E+10	.11E+10	.24E-12	.29E-12	.53E-12	
RCC	.49E+09	0.	0.	0.	0.	.53E+10	.17E+10	.70E+10	6.2
RCC	.15E+09	0.	.70E+09	.45E+09	.32E+09	.73E-13	.87E-13	.16E-12	
BLKHED	.66E+06	0.	.88E+06	.57E+06	.41E+06	.16E+10	.53E+09	.21E+10	1.9
CRACKS	.19E+06	0.	0.	0.	0.	.93E-16	.11E-15	.20E-15	
CRACKS	.29E+10	0.	.38E+10	.25E+10	.18E+10	.20E+07	.66E+06	.27E+07	.0
CRACKS	.83E+09	0.	0.	0.	0.	.41E-12	.48E-12	.89E-12	
CRACKS	0.	0.	.11E+09	.88E+09	.10E+10	.90E+10	.29E+10	.12E+11	10.4
CRACKS	.23E+09	0.	0.	0.	0.	.13E-12	0.	.13E-12	
TOTAL	.27E+11	0.	.36E+11	.24E+11	.18E+11	.22E+10	0.	.22E+10	1.9
TOTAL	.80E+10	0.	0.	0.	0.	.39E-11	.45E-11	.85E-11	
TOTAL						.86E+11	.27E+11	.11E+12	100.0

3-99

ORIGINAL PAGE IS OF POOR QUALITY

Table IX. Detailed Outgassing, Early Desorption, Prediction in Computer Format (cont'd)

REPORT NO. 35 *** SAMPLE CASE NO. 9 SHUTTLE ORBITER ALL SOURCES (EXCLUDING ENGS)

05/03/77 13.49.45. PAGE 406

CONTENTS: SUMMARY *** MASS/NUMBER COLUMN DENSITIES ***

LINE-OF-SIGHT NO. = 5
 THETA (DEG) = 0.0
 PHI (DEG) = 0.0

*** LISTED BY MATERIALS *** (CONT)

SECTION SUMMARY	SPECIES NUMBER COLUMN DENSITY (MOLECULES/CM ²)					EARLY DESORPTION (GM/CM ²) (MOLECULES/CM ²)	OUT GASSING (GM/CM ²)	TOTAL	% OF TOTAL
	OUTG1 O2	OUTG2 CO	H2O H2	N2 H	CO2 MMHNO3				
LINER	.32E+10	0.	.18E+11	.91E+10	.59E+10	.16E-11	.54E-12	.21E-11	
TEFLON	.33E+10	0.	0.	0.	0.	.37E+11	.32E+10	.40E+11	11.9
NOMEX	.40E+10	0.	.23E+11	.11E+11	.73E+10	.19E-11	.66E-12	.26E-11	
LRSI	.40E+10	0.	0.	0.	0.	.45E+11	.40E+10	.49E+11	14.7
HRSI	.14E+11	0.	.79E+11	.40E+11	.26E+11	.68E-11	.23E-11	.91E-11	
RCC	.14E+11	0.	0.	0.	0.	.16E+12	.16E+11	.17E+12	51.6
BLKHED	.15E+10	0.	.85E+10	.43E+10	.28E+10	.74E-12	.25E-12	.99E-12	
CRACKS	.15E+10	0.	0.	0.	0.	.17E+11	.15E+10	.19E+11	5.6
TOTAL	.69E+09	0.	.39E+10	.20E+10	.13E+10	.34E-12	.11E-12	.45E-12	
	.71E+09	0.	0.	0.	0.	.79E+10	.69E+09	.86E+10	2.6
	.85E+06	0.	.49E+07	.24E+07	.16E+07	.42E-15	.14E-15	.56E-15	
	.87E+06	0.	0.	0.	0.	.97E+07	.85E+06	.11E+08	.0
	.31E+10	0.	.18E+11	.90E+10	.58E+10	.15E-11	.52E-12	.21E-11	
	.32E+10	0.	0.	0.	0.	.36E+11	.31E+10	.39E+11	11.7
	0.	0.	.47E+08	.28E+10	.30E+10	.40E-12	0.	.40E-12	
	.81E+09	0.	0.	0.	0.	.67E+10	0.	.67E+10	2.0
TOTAL	.26E+11	0.	.15E+12	.78E+11	.52E+11	.13E-10	.44E-11	.18E-10	
	.28E+11	0.	0.	0.	0.	.31E+12	.26E+11	.33E+12	100.0

3-100

Table IX. Detailed Outgassing, Early Desorption, Prediction in Computer Format (cont'd)

REPORT NO. 37 *** SAMPLE CASE NO. 9 SHUTTLE ORBITER ALL SOURCES (EXCLUDING ENGS)

05/03/77 13.49.47. PAGE 415

CONTENTS: SUMMARY *** MASS/NUMBER COLUMN DENSITIES ***

LINE-OF-SIGHT NO. = 5
 THETA (DEG) = 0.0
 PHI (DEG) = 0.0

*** LISTED BY LOCATION *** (CONT)

SECTION SUMMARY	SPECIES NUMBER COLUMN DENSITY (MOLECULES/CM**2)					EARLY DESCRIPTION GASSING (GM/CM**2) (MOLECULES/CM**2)	GUT	TOTAL	% OF TOTAL
	OUTG1	OUTG2	H2O	N2	CO2				
	O2	CO	H2	H	MMHND3				
BAY	.64E+10	0.	.36E+11	.18E+11	.12E+11	.31E-11	.11E-11	.42E-11	
	.65E+10	0.	0.	0.	0.	.72E+11	.64E+10	.79E+11	23.5
CREW	.43E+09	0.	.25E+10	.12E+10	.80E+09	.21E-12	.72E-13	.29E-12	
	.44E+09	0.	0.	0.	0.	.50E+10	.42E+09	.54E+10	1.6
FUSLAG	.49E+09	0.	.28E+10	.14E+10	.90E+09	.24E-12	.81E-13	.32E-12	
	.50E+09	0.	0.	0.	0.	.56E+10	.49E+09	.61E+10	1.8
OMS	.51E+09	0.	.29E+10	.15E+10	.95E+09	.25E-12	.65E-13	.34E-12	
	.52E+09	0.	0.	0.	0.	.59E+10	.51E+09	.64E+10	1.9
RADOOR	.40E+10	0.	.23E+11	.11E+11	.73E+10	.19E-11	.66E-12	.26E-11	
	.40E+10	0.	0.	0.	0.	.45E+11	.40E+10	.49E+11	14.7
TAIL	.15E+09	0.	.86E+09	.43E+09	.26E+09	.75E-13	.25E-13	.10E-12	
	.15E+09	0.	0.	0.	0.	.17E+10	.15E+09	.19E+10	.6
WING	.10E+11	0.	.59E+11	.30E+11	.19E+11	.51E-11	.17E-11	.63E-11	
	.11E+11	0.	0.	0.	0.	.12E+12	.10E+11	.13E+12	38.6
ELEVON	.41E+10	0.	.23E+11	.12E+11	.75E+10	.20E-11	.66E-12	.27E-11	
	.42E+10	0.	0.	0.	0.	.47E+11	.41E+10	.51E+11	15.2
TOTAL	.26E+11	0.	.15E+12	.75E+11	.49E+11	.13E-10	.44E-11	.17E-10	
	.27E+11	0.	0.	0.	0.	.30E+12	.26E+11	.33E+12	100.0

3-101

Table IX. Detailed Outgassing, Early Desorption, Prediction in Computer Format (cont'd)

REPORT NO. 43 *** SAMPLE CASE NO. 9 SHUTTLE ORBITER ALL SOURCES (EXCLUDING ENGS)

05/03/77 13.49.49. PAGE 424

CONTENTS: SUMMARY RETURN FLUX AT 400.0 KM ALTITUDE

CRITICAL SURFACE NO. = 5
FIELD-OF-VIEW (SR) = .190

*** LISTED BY MATERIAL TYPE *** (CONT)

SECTION SUMMARY	SPECIES RETURN FLUX (MOLECULES/CM**2)					EARLY DESCRIPTION (CM/CM**2) (MOLECULES/CM**2)	OUT CASING	TOTAL	% OF TOTAL
	OUTG1	OUTG2	H2O	N2	CO2				
	G2	CO	H2	H	MMHNO3				
LINER	.18E+10	0.	.24E+10	.16E+10	.11E+10	.25E-12	.30E-12	.56E-12	
TEFLON	.52E+09	0.	0.	0.	0.	.56E+10	.18E+10	.74E+10	11.9
NOMEX	.22E+10	0.	.30E+10	.19E+10	.14E+10	.31E-12	.37E-12	.68E-12	
LRSI	.64E+09	0.	0.	0.	0.	.69E+10	.22E+10	.91E+10	14.7
HRSI	.78E+10	0.	.10E+11	.68E+10	.48E+10	.11E-11	.13E-11	.24E-11	
RCC	.22E+10	0.	0.	0.	0.	.24E+11	.76E+10	.32E+11	51.7
BLKHED	.85E+09	0.	.11E+10	.73E+09	.52E+09	.12E-12	.14E-12	.26E-12	
CRACKS	.24E+09	0.	0.	0.	0.	.26E+10	.85E+09	.35E+10	5.6
TOTAL	.39E+09	0.	.52E+09	.34E+09	.24E+09	.54E-13	.65E-13	.12E-12	
	.11E+09	0.	0.	0.	0.	.12E+10	.39E+09	.16E+10	2.6
	.48E+06	0.	.64E+06	.42E+06	.30E+06	.67E-16	.80E-16	.15E-15	
	.14E+06	0.	0.	0.	0.	.15E+07	.48E+06	.20E+07	.0
	.18E+10	0.	.23E+10	.15E+10	.11E+10	.25E-12	.29E-12	.54E-12	
	.50E+09	0.	0.	0.	0.	.55E+10	.16E+10	.72E-10	11.7
	0.	0.	.62E+07	.48E+09	.57E+09	.71E-13	0.	.71E-13	
	.13E+09	0.	0.	0.	0.	.12E+10	0.	.12E+10	1.9
TOTAL	.15E+11	0.	.20E+11	.13E+11	.97E+10	.22E-11	.25E-11	.46E-11	
	.44E+10	0.	0.	0.	0.	.47E+11	.15E+11	.62E+11	100.0

ORIGINAL PAGE IS
OF POOR QUALITY

Table IX. Detailed Outgassing, Early Desorption, Prediction in Computer Format (cont'd)

REPORT NO. 35 *** SAMPLE CASE NO. 9 SHUTTLE ORBITER ALL SOURCES (EXCLUDING ENGS)

05/03/77 13.50.12. PAGE 448

CONTENTS: SUMMARY *** MASS/NUMBER COLUMN DENSITIES ***

LINE-OF-SIGHT NO. = 6
 THETA (DEG) = 0.0
 PHI (DEG) = 0.0

*** LISTED BY MATERIALS *** (CONT)

SECTION SUMMARY	SPECIES NUMBER COLUMN DENSITY (MOLECULES/CM ²)					EARLY DESORPTION (GM/CM ²) (MOLECULES/CM ²)	OUT GASSING (GM/CM ²) (MOLECULES/CM ²)	TOTAL	% OF TOTAL
	OUTG1	OUTG2	H2O	N2	CO2				
	O2	CO	H2	H	MMHNO3				
LINER	.45E+10	0.	.25E+11	.13E+11	.82E+10	.22E-11	.75E-12	.29E-11	
	.46E+10	0.	0.	0.	0.	.51E+11	.45E+10	.55E+11	17.7
TEFLON	.33E+10	0.	.19E+11	.95E+10	.61E+10	.16E-11	.55E-12	.22E-11	
	.34E+10	0.	0.	0.	0.	.38E+11	.33E+10	.41E+11	13.2
NOMEX	.11E+11	0.	.62E+11	.31E+11	.20E+11	.53E-11	.18E-11	.71E-11	
	.11E+11	0.	0.	0.	0.	.12E-12	.11E+11	.13E+12	43.1
LRSI	.19E+10	0.	.11E+11	.55E+10	.36E+10	.95E-12	.32E-12	.13E-11	
	.20E+10	0.	0.	0.	0.	.22E+11	.19E+10	.24E+11	7.7
HRSI	.50E+09	0.	.29E+10	.14E+10	.93E+09	.25E-12	.84E-13	.33E-12	
	.51E+09	0.	0.	0.	0.	.58E+10	.50E+09	.63E+10	2.0
RCC	.87E+06	0.	.50E+07	.25E+07	.16E+07	.43E-15	.14E-15	.57E-15	
	.89E+06	0.	0.	0.	0.	.99E+07	.57E+06	.11E+08	.0
BLKHED	.35E+10	0.	.20E+11	.10E+11	.65E+10	.17E-11	.59E-12	.23E-11	
	.36E+10	0.	0.	0.	0.	.40E+11	.35E+10	.44E+11	14.1
CRACKS	0.	0.	.49E+08	.30E+10	.32E+10	.42E-12	0.	.42E-12	
	.85E+09	0.	0.	0.	0.	.70E+10	0.	.70E+10	2.3
TOTAL	.25E+11	0.	.14E+12	.73E+11	.48E+11	.13E-10	.41E-11	.17E-10	
	.26E+11	0.	0.	0.	0.	.29E+12	.25E+11	.31E+12	100.0

3-103

ORIGINAL PAGE IS
 OF POOR QUALITY

Table IX. Detailed Outgassing, Early Description, Prediction in Computer Format (cont'd)

REPORT NO. 37 *** SAMPLE CASE NO. 9 SHUTTLE ORBITER ALL SOURCES (EXCLUDING ENGS)

05/03/77 13.50.14. PAGE 457

CONTENTS: SUMMARY *** MASS/NUMBER COLUMN DENSITIES ***

LINE-OF-SIGHT NO. = 6
 THETA (DEG) = 0.0
 PHI (DEG) = 0.0

*** LISTED BY LOCATION *** (CONT)

SECTION SUMMARY	SPECIES NUMBER COLUMN DENSITY (MOLECULES/CM ²)					EARLY DESCRIPTION (GM/CM ²) (MOLECULES/CM ²)	CUT CASSING (MOLECULES/CM ²)	TOTAL	% OF TOTAL
	OUTG1	OUTG2	H2O	N2	CO2				
	O2	CO	H2	H	MMHND3				
BAY	.80E+10	0.	.45E+11	.23E+11	.15E+11	.39E-11	.13E-11	.53E-11	
CREW	.82E+10	0.	0.	0.	0.	.91E+11	.80E+10	.99E+11	31.7
FUSLAG	.11E+10	0.	.63E+10	.32E+10	.20E+10	.54E-12	.18E-12	.73E-12	4.4
OMS	.94E+08	0.	0.	0.	0.	.13E+11	.11E+10	.14E+11	.4
RADOOR	.49E+09	0.	.28E+10	.14E+10	.90E+09	.45E-13	.15E-13	.61E-13	
TAIL	.50E+09	0.	0.	0.	0.	.11E+10	.92E+08	.11E+10	
WING	.33E+10	0.	.19E+11	.95E+10	.61E+10	.24E-12	.82E-13	.32E-12	2.0
ELEVON	.34E+10	0.	0.	0.	0.	.56E+10	.49E+09	.61E+10	
TOTAL	.33E+08	0.	.22E+09	.11E+09	.71E+08	.16E-11	.55E-12	.22E-11	13.2
	.39E+08	0.	0.	0.	0.	.38E+11	.33E+10	.41E+11	
	.77E+10	0.	.44E+11	.22E+11	.14E+11	.19E-13	.64E-14	.25E-13	.2
	.78E+10	0.	0.	0.	0.	.44E+09	.38E+08	.48E+09	
	.39E+10	0.	.22E+11	.11E+11	.71E+10	.38E-11	.13E-11	.51E-11	30.6
	.39E+10	0.	0.	0.	0.	.88E+11	.77E+10	.95E+11	
						.19E-11	.64E-12	.25E-11	15.4
						.44E+11	.39E+10	.48E+11	
TOTAL	.25E+11	0.	.14E+12	.70E+11	.45E+11	.12E-10	.41E-11	.16E-10	
	.25E+11	0.	0.	0.	0.	.28E+12	.25E+11	.31E+12	100.0

3-104

Table IX. Detailed Outgassing, Early Desorption, Prediction in Computer Format (cont'd)

REPORT NO. 43 *** SAMPLE CASE NO. 9 SHUTTLE ORBITER ALL SOURCES (EXCLUDING ENGS)

05/03/77 13.50.16. PAGE 467

CONTENTS: SUMMARY RETURN FLUX AT 400.0 KM ALTITUDE

CRITICAL SURFACE NO. = 6
FIELD-OF-VIEW (SR) = .190

*** LISTED BY MATERIAL TYPE *** (CONT)

SECTION SUMMARY	SPECIES RETURN FLUX (MOLECULES/CM ²)					EARLY DESORPTION (GM/CM ²) (MOLECULES/CM ²)	OUT GASSING (GM/CM ²)	TOTAL	% OF TOTAL
	OUTG1	OUTG2	H2O	N2	CO2				
	O2	CO	H2	H	MMHNO3				
LINER	.44E+10	0.	.57E+10	.38E+10	.27E+10	.61E-12	.72E-12	.13E-11	
TEFLON	.13E+10	0.	0.	0.	0.	.13E+11	.44E+10	.18E+11	17.7
	.32E+10	0.	.43E+10	.28E+10	.20E+10	.45E-12	.54E-12	.99E-12	
NOMEX	.92E+09	0.	0.	0.	0.	.10E+11	.32E+10	.13E+11	13.2
	.11E+11	0.	.14E+11	.92E+10	.65E+10	.15E-11	.18E-11	.32E-11	
LRSI	.30E+10	0.	0.	0.	0.	.33E+11	.11E+11	.43E+11	43.1
	.19E+10	0.	.25E+10	.16E+10	.12E+10	.28E-12	.31E-12	.59E-12	
HRSI	.54E+09	0.	0.	0.	0.	.58E+10	.19E+10	.77E+10	7.7
	.49E+09	0.	0.	0.	0.	.69E-13	.82E-13	.15E-12	
RCC	.14E+09	0.	0.	0.	0.	.15E+10	.49E+09	.20E+10	2.0
	.85E+06	0.	.11E+07	.73E+06	.52E+06	.12E-15	.14E-15	.26E-15	
BLKHED	.24E+06	0.	0.	0.	0.	.25E+07	.85E+06	.35E+07	.0
	.35E+10	0.	.46E+10	.30E+10	.21E+10	.48E-12	.57E-12	.11E-11	
CRACKS	.98E+09	0.	0.	0.	0.	.11E+11	.35E+10	.14E+11	14.1
	0.	0.	.11E+08	.83E+09	.10E+10	.13E-12	0.	.13E-12	
	.23E+09	0.	0.	0.	0.	.22E+10	0.	.22E+10	2.1
TOTAL	.24E+11	0.	.32E+11	.22E+11	.16E+11	.35E-11	.40E-11	.75E-11	
	.71E+10	0.	0.	0.	0.	.76E+11	.24E+11	.10E+12	100.0

3-105

Table IX. Detailed Outgassing, Early Desorption, Prediction in Computer Format (cont'd)

REPORT NO. 43 *** SAMPLE CASE NO. 9 SHUTTLE ORBITER ALL SOURCES (EXCLUDING ENGS)

05/03/77 13.50.32. PAGE 511

CONTENTS: SUMMARY RETURN FLUX AT 400.0 KM ALTITUDE

CRITICAL SURFACE NO. = 7
FIELD-OF-VIEW (SR) = .190

*** LISTED BY MATERIAL TYPE *** (CONT)

SECTION SUMMARY	SPECIES RETURN FLUX (MOLECULES/CM**2)					EARLY DESORPTION (GM/CM**2) (MOLECULES/CM**2)	OUT GASSING	TOTAL	% OF TOTAL
	OUTG1 O2	OUTG2 CO	H2O H2	N2 H	CO2 MMHNO3				
LINER	.30E+10	0.	.40E+10	.26E+10	.19E+10	.42E-12	.51E-12	.93E-12	
TEFLON	.87E+09	0.	0.	0.	0.	.93E+10	.30E+10	.12E+11	23.5
NOMEX	.17E+10	0.	.22E+10	.14E+10	.10E+10	.23E-12	.27E-12	.50E-12	
LRSI	.47E+09	0.	0.	0.	0.	.51E+10	.17E+10	.67E+10	12.9
HRSI	.36E+10	0.	.47E+10	.31E+10	.22E+10	.50E-12	.59E-12	.11E-11	
RCC	.10E+10	0.	0.	0.	0.	.11E+11	.36E+10	.15E+11	27.8
BLKHED	.17E+10	0.	.23E+10	.15E+10	.11E+10	.24E-12	.29E-12	.53E-12	
CRACKS	.49E+09	0.	0.	0.	0.	.53E+10	.17E+10	.70E+10	13.4
TOTAL	.17E+09	0.	.22E+09	.15E+09	.10E+09	.24E-13	.28E-13	.52E-13	
	.48E+08	0.	0.	0.	0.	.52E+09	.17E+09	.69E+09	1.3
	.88E+06	0.	.12E+07	.76E+06	.54E+06	.12E-15	.15E-15	.27E-15	
	.25E+06	0.	0.	0.	0.	.27E+07	.88E+06	.36E+07	.0
	.23E+10	0.	.30E+10	.20E+10	.14E+10	.32E-12	.38E-12	.69E-12	
	.65E+09	0.	0.	0.	0.	.70E+10	.23E+10	.93E+10	17.7
	0.	0.	.92E+07	.72E+09	.85E+09	.11E-12	0.	.11E-12	
	.19E+09	0.	0.	0.	0.	.18E+10	0.	.18E+10	3.4
TOTAL	.12E+11	0.	.16E+11	.11E+11	.85E+10	.18E-11	.21E-11	.39E-11	
	.37E+10	0.	0.	0.	0.	.40E+11	.12E+11	.52E+11	100.0

3-106

Table IX. Detailed Outgassing, Early Desorption, Prediction in Computer Format (cont'd)

REPORT NO. 37 *** SAMPLE CASE NO. 9 SHUTTLE ORBITER ALL SOURCES (EXCLUDING ENGS)

05/03/77 13.50.30. PAGE 50:

CONTENTS: SUMMARY *** MASS/NUMBER COLUMN DENSITIES ***

LINE-OF-SIGHT NO. = 7
 THETA (DEG) = 0.0
 PHI (DEG) = 0.0

*** LISTED BY LOCATION *** (CONT)

SECTION SUMMARY	SPECIES NUMBER COLUMN DENSITY (MOLECULES/CM ²)					EARLY DESORPTION (GM/CM ²) (MOLECULES/CM ²)	OUT GASSING	TOTAL	% OF TOTAL
	OUTG1 O2	OUTG2 CO	H2O H2	N2 H	CO2 MMHNO3				
BAY	.94E+10	0.	.53E+11	.27E+11	.17E+11	.46E-11	.16E-11	.62E-11	
CREW	.96E+10	0.	0.	0.	0.	.11E+12	.94E+10	.12E+12	41.1
FUSLAG	.24E+10	0.	.14E+11	.69E+10	.44E+10	.12E-11	.40E-12	.16E-11	
	.25E+10	0.	0.	0.	0.	.28E+11	.24E-12	.30E+11	10.6
OMS	.36E+08	0.	.20E+09	.10E+09	.66E+08	.18E-13	.89E-14	.24E-13	
	.37E+08	0.	0.	0.	0.	.41E-09	.20E+08	.45E+09	.2
RADOOR	.23E+09	0.	.13E+10	.65E+09	.42E+09	.11E-12	.36E-13	.15E-12	
	.29E+10	0.	0.	0.	0.	.26E+10	.23E+09	.28E+10	1.0
TAIL	.30E+10	0.	.17E+11	.83E+10	.54E+10	.14E-11	.49E-12	.19E-11	
	.27E+08	0.	0.	0.	0.	.33E+11	.29E+10	.36E+11	12.8
WING	.28E+08	0.	.16E+09	.79E+08	.51E+08	.14E-13	.46E-14	.18E-13	
	.48E+10	0.	0.	0.	0.	.31E+09	.27E+08	.34E+09	.1
ELEVON	.49E+10	0.	.27E+11	.14E+11	.88E+10	.24E-11	.80E-12	.32E-11	
	.22E+10	0.	0.	0.	0.	.55E+11	.48E+10	.60E+11	21.1
	.22E+10	0.	.12E+11	.62E+10	.40E+10	.11E-11	.36E-12	.14E-11	
TOTAL	.22E+11	0.	.13E+12	.63E+11	.40E+11	.25E+11	.22E+10	.27E+11	9.6
	.22E+11	0.	0.	0.	0.	.11E-10	.37E-11	.14E-10	
						.25E+12	.22E+11	.27E+12	100.0

3-107

Table IX. Detailed Outgassing, Early Desorption, Prediction in Computer Format (cont'd)

REPORT NO. 35 *** SAMPLE CASE NO. 9 SHUTTLE ORBITER ALL SOURCES (EXCLUDING ENGS)

05/03/77 13.50.28. PAGE 491

CONTENTS: SUMMARY *** MASS/NUMBER COLUMN DENSITIES ***

LINE-OF-SIGHT NO. = 7
 THETA (DEG) = 0.0
 PHI (DEG) = 0.0

*** LISTED BY MATERIALS *** (CONT)

SECTION SUMMARY	SPECIES NUMBER COLUMN DENSITY (MOLECULES/CM**2)						EARLY DESORPTION (CM/CM**2) (MOLECULES/CM**2)	OUT GASSING (CM/CM**2)	TOTAL	% OF TOTAL
	OUTG1		H2O	N2	CO2	MMHNO3				
	O2	CO								
LINER	.54E+10	0.	.30E+11	.15E+11	.98E+10	.26E-11	.90E-12	.35E-11		
TEFLON	.55E+10	0.	0.	0.	0.	.61E+11	.54E+10	.66E+11	23.4	
NOMEX	.29E+10	0.	.17E+11	.82E+10	.54E+10	.14E-11	.49E-12	.19E-11		
LRSI	.30E+10	0.	0.	0.	0.	.33E+11	.29E+10	.36E+11	12.8	
HRSI	.63E+10	0.	.36E+11	.18E+11	.12E+11	.31E-11	.11E-11	.42E-11		
RCC	.65E+10	0.	0.	0.	0.	.72E+11	.63E+10	.79E+11	27.8	
BLKHED	.31E+10	0.	.17E+11	.87E+10	.56E+10	.15E-11	.51E-12	.20E-11		
CRACKS	.31E+10	0.	0.	0.	0.	.35E+11	.31E+10	.38E+11	13.4	
TOTAL	.30E+09	0.	.17E+10	.86E+09	.55E+09	.15E-12	.50E-13	.20E-12		
	.16E+07	0.	.89E+07	.44E+07	.29E+07	.34E+10	.30E+09	.37E+10	1.3	
	.16E+07	0.	0.	0.	0.	.77E-15	.26E-15	.10E-14		
	.40E+10	0.	.23E+11	.11E+11	.74E+10	.18E+08	.16E+07	.19E+08	.0	
	.41E+10	0.	0.	0.	0.	.20E-11	.67E-12	.26E-11		
	0.	0.	.70E+08	.42E+10	.45E+10	.46E+11	.40E+10	.50E+11	17.7	
	.12E+10	0.	0.	0.	0.	.59E-12	0.	.59E-12		
						.10E+11	0.	.10E+11	3.5	
TOTAL	.22E+11	0.	.13E+12	.67E+11	.45E+11	.11E-10	.37E-11	.15E-10		
	.24E+11	0.	0.	0.	0.	.26E+12	.22E+11	.28E+12	100.0	

3-108

ORIGINAL PAGE IS
 OF POOR QUALITY

Table X. VCS/RCS Induced Environment Predictions*

VCS Aft -Z					
LOS	MCD (g/cm ²)		NCD (mol/cm ²)		RF (mol/cm ²)
	Direct	Wing Reflect	Direct	Wing Reflect	
1	6.9-11	8.4-9	2.1+12	2.1+14	6.5+13
2	9.7-11	9.8-9	2.9+12	2.5+14	6.6+13
3	4.6-10	9.8-9	1.4+13	2.5+14	3.8+13
4	7.5-11	1.3-8	2.2+12	3.3+14	8.8+13
5	2.5-10	1.3-8	7.6+12	3.3+14	5.2+13
6	1.2-11	6.9-9	3.5+11	1.7+14	4.7+13
7	-	3.7-9	-	9.2+14	1.4+13
RCS Aft -Z					
1	2.9-10	3.9-7	8.5+13	9.7+15	3.0+15
2	2.4-9	5.1-7	7.2+13	1.3+16	3.4+15
3	5.2-9	5.7-7	1.5+14	1.4+16	2.2+15
4	1.2-9	8.1-7	3.5+13	2.0+16	5.5+15
5	8.0-9	8.0-7	2.4+14	2.0+16	3.1+15
6	-	3.5-7	-	8.7+15	2.3+15
7	-	2.1-7	-	5.2+15	8.1+14

**The Return Flux values should be divided by the cosine of the angle the LOS makes with the Z-axis.

** 6.9-11 = 6.9 x 10⁻¹¹

ORIGINAL PAGE IS
OF POOR QUALITY

Table XI. Evaporator Predictions*

Line-of-Sight	MCD (g/cm ²)		NCD (mol/cm ²)		RF (mol/cm ²)
	Direct	Wing Reflect	Direct	Wing Reflect	
1	-	1.2-9**	-	4.1+13	1.1+13
2	-	1.8-9	-	6.1+13	1.4+13
3	-	2.4-9	-	8.0+13	1.0+13
4	1.8-9	3.1-9	6.0+13	1.0+14	3.8+13
5	7.2-9	3.0-9	2.4+14	1.0+14	4.5+13
6	-	1.2-9	-	4.0+13	9.0+12
7	-	7.4-10	-	2.5+13	3.2+12

*The Return Flux values should be divided by the cosine of the angle the LOS makes with the Z-axis.

**1.2-9 = 1.2×10^{-9}

3.3 Trade Studies

This section summarizes the trade studies performed during the contract period. Primarily these studies involved evaluating various evaporator locations and orientation plus the impact of surface resolution on model predictions.

3.3.1 Evaporator Location Influence - The evaporator contamination contribution was analyzed for new locations to minimize its impact upon the induced environment. The evaporator was moved up 14 and 24 inches along the Z axis from the previously analyzed position of X = 1504, Z = 291. The location coordinates analyzed were X = 1504, Z = 305 and X = 1504, Z = 315. The resulting contribution to the zero degree (along +Z) line-of-sight is 2.1×10^{13} mol/cm² for Z = 305 and 3.3×10^{13} mol/cm² for Z = 315. These values correspond to both evaporators operating at a nominal flowrate of 15 lb/hr per nozzle. Figure 19 shows the variation in molecular number column density for the zero degree line-of-sight as the evaporator is moved along +Z with the X location held fixed at X = 1504.

With the evaporator at Z = 291, the trailing edge of the wing was the major contributor and represented 98% of the total molecular column density. At Z = 305, it reduces to 89% of the wing reflection contribution and at Z = 315 it is 90%. By moving the evaporator up along +Z, the rest of the wing is now seen by the evaporator and contributes a significant amount to the zero degree line-of-sight.

The following table shows the total mass reflected for each evaporator location analyzed, the mass reflected by the trailing edge, and the percent of evaporator flow that is reflected by the total wing surface area.

<u>Evaporator Location</u>	<u>Mass Reflected Per Evaporator g/s</u>	<u>Mass Reflected by Trailing Edge g/s</u>	<u>Percent Evaporator Flow</u>
X = 1504, Z = 291	0.129	0.126	7.0
X = 1504, Z = 305	0.199	0.177	10.5
X = 1504, Z = 315	0.29	0.26	15.3

The supersonic nozzle was evaluated at the location of Z = 315 and was found to be 75% of the sonic nozzle. This is the opposite of the Z = 291 location in which the supersonic nozzle was 1.64 times higher than the sonic.

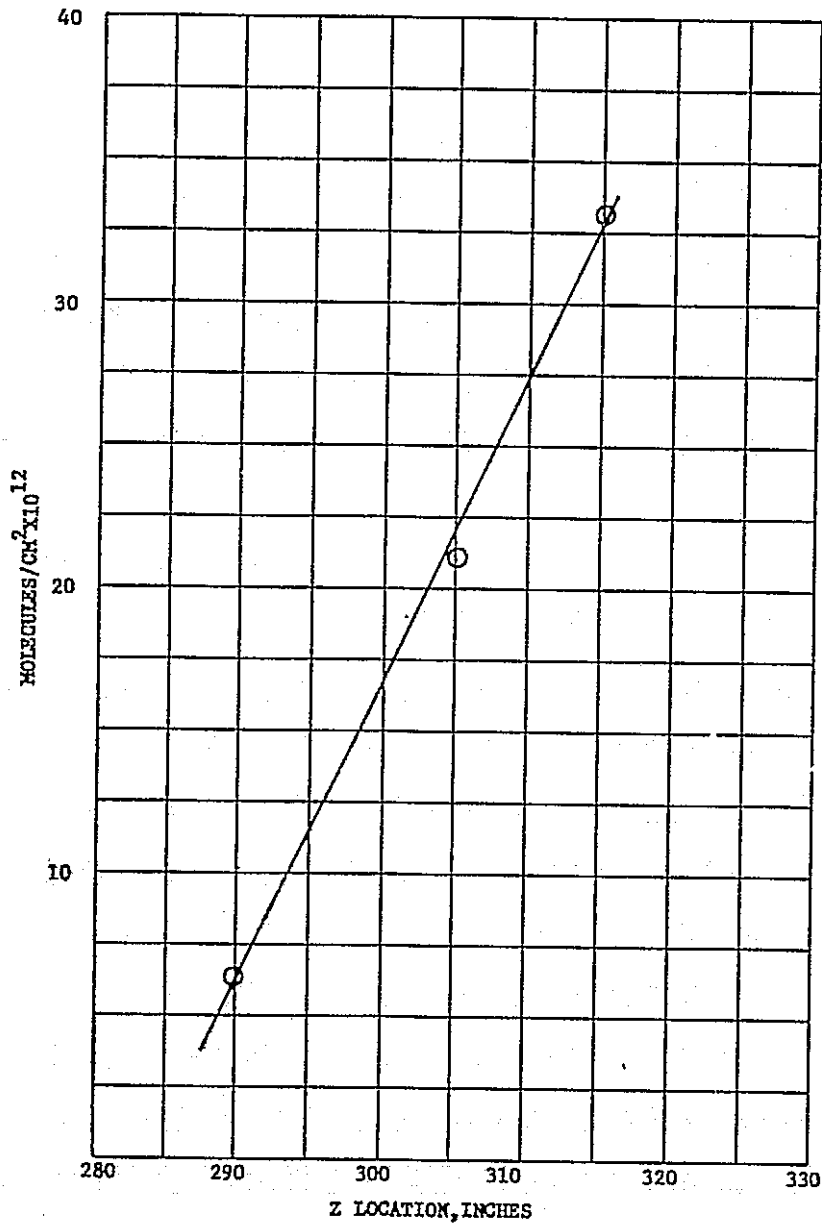


Figure 19. Molecular Number Column Density From Evaporator Effluents for the Zero Degree Line-of-Sight as a Function of Z Location With X Location Constant and Equal to 1504

At some locations on the Orbiter, the reflected evaporator effluents can create unwanted forces. The magnitude of these forces will strongly influence the VCS engine duty cycle required to compensate for these forces. These forces were calculated at several locations and are summarized in the following table.

<u>Location</u>	<u>Force</u>
X = 985, Z = 355, Y = 104	0.16 lb _f in +Z direction
X = 1390, Z = 326, Y = 113	0.42 lb _f in -Z direction
X = 1519, Z = 287, Y = 126	0.0486 lb _f in -X direction and 0.01 lb _f in +Z direction

The location near X = 1504 and Z = 305 was arrived at as the baseline case and is presently the position in the model. This location was decided upon after considering acceptable penetration areas on the vehicle, plumbing considerations (heaters, freezing, condensation), contamination levels, forces generated and weight restrictions. All of these parameters had to be considered. The choice of this location was therefore, not based on contamination levels alone.

3.3.2 Surface Resolution Influence - When the evaporator is near a long narrow surface the reflected effluents off of this surface can be in error if the surface resolution and exhaust plume function are not properly considered. For example, with the evaporator at X = 1504 and Z = 291, the trailing edge of the wing (represented by a long narrow triangle) has its center (centroid) only 32 inches from the Orbiter fuselage while the overall length of the triangle is 366 inches. This situation is shown in Figure 20 where a top and side view of the wing are shown. The net result is that the flux levels on the triangle from the evaporator are calculated to the center of the triangle and are then assigned to the entire triangle surface area as a reflected source. This results in a wing reflected rate that is too high and leads to erroneous results. For this case, the molecular number column density for a +Z line-of-sight, positioned at X = 1107 was 3.3×10^{13} mol/cm² per evaporator or a total of 6.6×10^{13} mol/cm² for both evaporators.

As a result of this, a trade study was undertaken to determine the degrees of resolution required to minimize the error for reflection to a point source from a large narrow surface. The triangular trailing edge was subdivided sequentially into 4, 10 and 20 nodes as shown in Figure 21. For each of these configurations, the evaporator flux on each subsurface was calculated and then allowed to reflect diffusely to the +Z line-of-sight. The results are summarized in Figure 22. Also included in Figure 22 is the percent of

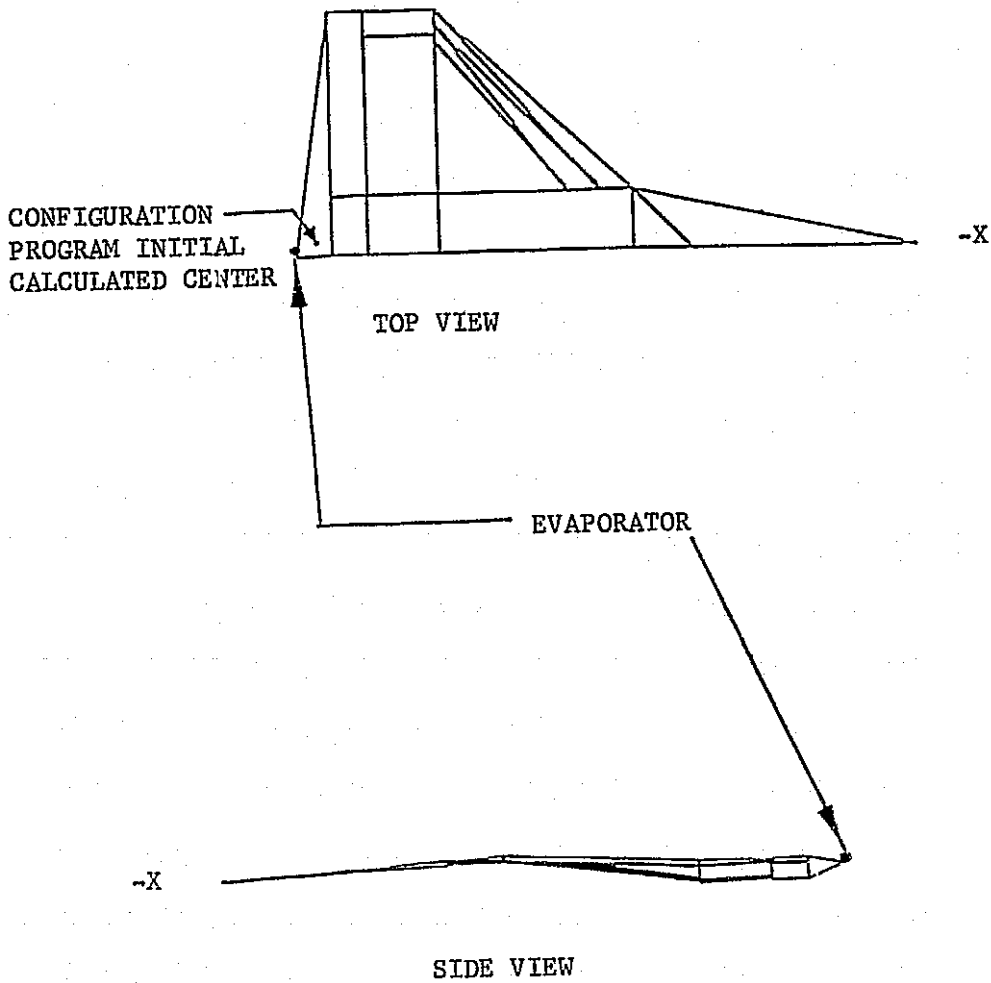
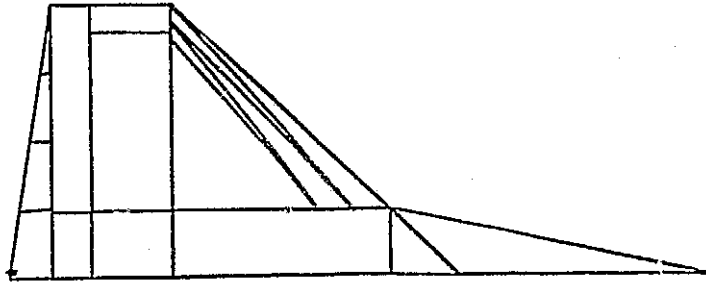
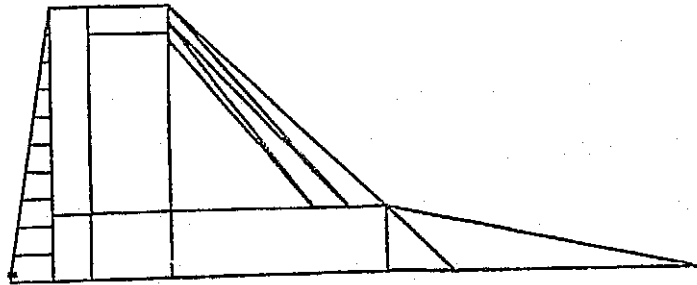


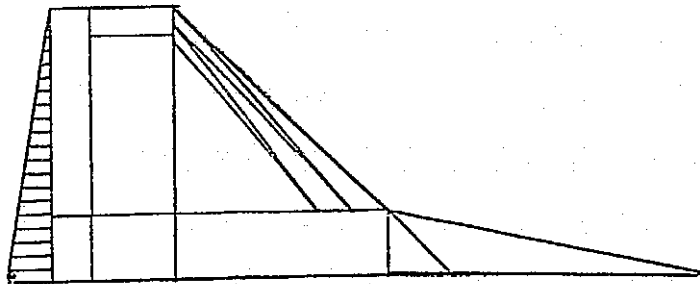
Figure 20. Top and Side View of Original Orbiter Wing Configuration and Splash Evaporator at $X = 1504$ and $Z = 291$



4 NODE TRAILING EDGE



10 NODE TRAILING EDGE



20 NODE TRAILING EDGE

Figure 21. Further Subdivisions of Wing Trailing Edge for Investigation of Surface Resolution Requirements

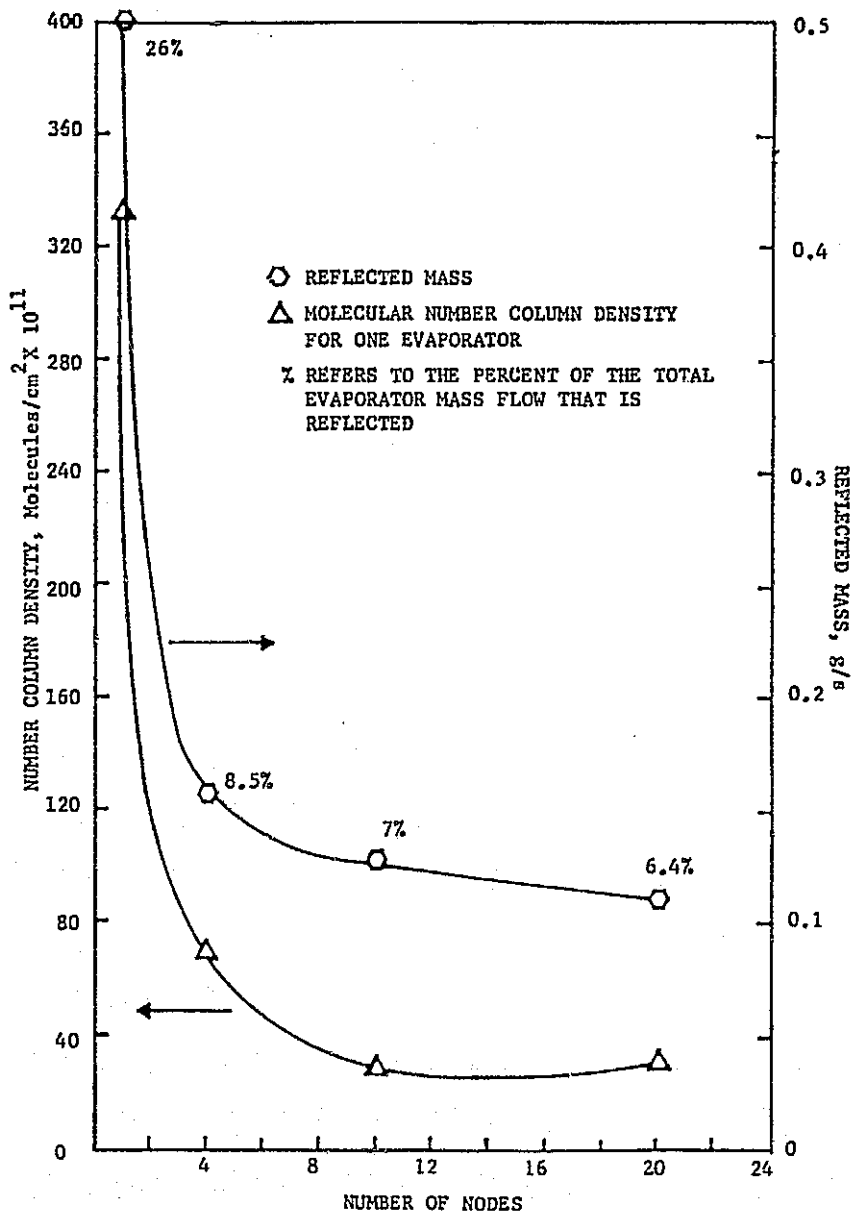


Figure 22. Variation of Molecular Number Column Density and Reflected Mass as a Function of Surface Resolution

total evaporator flow that is reflected. The results clearly show that long and narrow one node triangular surfaces such as that representing the trailing edge leads to results that predict values that are too high for point sources. The 10 node trailing edge configuration has been chosen for this evaporator situation for resolution and acceptable computer run time for viewfactor determinations for the new evaporator position. The contribution to the +Z line-of-sight for the 10 node case is 2.8×10^{12} for both evaporators operating at 15 lb/hr. The contribution to a line-of-sight 50 degrees off of Z towards -X (FWD) still yields a value of 2.8×10^{12} mol/cm² for one evaporator.

The supersonic nozzle plume distribution was analyzed at this position for a 10 node trailing edge and was found to produce a +Z line-of-sight column density of 4.8×10^{12} mol/cm² for one nozzle which is 1.6 times the sonic evaporator nozzle.

Because the elevon trailing edge subdivision to 10 nodes significantly influenced the evaporator reflected effluents, the impact on the VCS and RCS engines was also analyzed. In particular, the change in predicted mass column densities and total reflected mass to the +Z line-of-sight from the -Z RCS, -Z VCS and Y VCS aft engines have been analyzed. The total number of nodes representing the wing is now 23. The previous wing node structure used for wing reflection predictions utilized 6 nodes (Final Report NAS9-14212 MCR 75-13 dated June 1975).

The results are presented in Table VIII. The -Z VCS aft engine shows a reduction in column density by a factor of 3.2 and a total reflected mass by a factor of 1.5. The Y facing aft VCS shows a reduction in column density by a factor of 1.3 while the reflected mass increased by a factor of 1.1 unlike the -Z VCS or the new evaporator location which decreased. This is readily explained by considering the angle/distance relationships and the plume function of the VCS engines.

The previous aft RCS data was based on the distance/angle relationships of the -Z VCS to the old wing. The case of the RCS impinging on the wing and subsequently reflecting was not previously analyzed in detail for the old wing since the RCS is not timed to operate while experiments are operating. However, it was decided to include it in the present analysis for completeness. Limited data for the previous wing shape does indicate that the RCS contributions to the line-of-sight will be reduced for the current wing configuration.

It is important to note that for all of the engine cases analyzed in Table VIII that the mass reflected by the remainder of the wing

excluding the 10 node triangular trailing edge) did not change appreciably even though this portion of the wing increased from 5 nodes to 13 nodes. This again shows that the long narrow triangular trailing edge, closest to the aft engines and evaporator, is the major contributor to the discovered inaccuracy.

Table XII. Variation in Column Density and Reflected Mass for VCS and RCS Engines

Engine	+Z LOS Column Density Mol/cm ²	Trailing Edge Contribution g/s	Remainder of Wing Contribution g/s	Total Percent of Engine Flow Reflected
Previous Predictions (6 node wing)				
-Z VCS	4.4x10 ¹⁴	3.2	1.01	10.3%
Y VCS	1.5x10 ¹⁴	0.13	0.82	2.4%
-Z RCS	-	282.0	30.0	17.6%
Current Predictions (23 node wing)				
-Z VCS	1.4x10 ¹⁴	1.74	1.02	6.8%
Y VCS	1.4x10 ¹⁴	0.27	0.78	2.6%
-Z RCS	1.9x10 ¹⁵	109.0	25.0	7.6%

It should be noted that the viewfactors between surfaces do not inherently have the problem discussed above for a point source (e.g., engines and evaporators) to a surface. The viewfactors between surfaces are calculated by subdividing each surface into many sub-nodes internally in the TRASYS Program so that an integrated view-factor results. The point sources to a surface requires determination of a separation distance from the point source to the surface center and the angle relationships with respect to the normal of the point source exit plane and the surface. Then, this data is input to the point source plume distribution function to determine the flux per unit area on the surface which then becomes a source for surface reflection.

The conclusion is that the triangular shaped trailing edge of the wing has a greater impact on the evaporator predictions than it does on the aft engines. Also, it has more impact on predictions when subdivided than the rest of the wing when it is subdivided. By using a 10 node trailing edge versus a one node, the evaporator column density contribution to the +Z line-of-sight is reduced by a factor of 12 while the engine contributions (aft Y and -Z) are reduced by a factor of 1.3 and 3 respectively.

3.3.3 Canted Elevon Influence on Evaporator Effluents - The elevon has a total upward motion of 35 degrees and a downward motion of 20 degrees from its nominal position. The capability exists that the elevon can be moved during evaporator operations (on-orbit) so that it could effectively shield portions of the major lines-of-sight from the evaporator effluents.

The evaporator location at $Z = 305$ and $X = 1507$ has been evaluated for contributions to payload lines-of-sight with the elevon in its normal baseline position and with the elevon canted upward (+Z) 35 degrees from its baseline position. The lines-of-sight evaluated with the elevon up were:

- a) $60^{\circ}Z$ towards Y,
- b) $45^{\circ}Z$ towards Y,
- c) $40^{\circ}Z$ towards Y,
- d) $35^{\circ}Z$ towards Y,
- e) $30^{\circ}Z$ towards Y,
- f) $60^{\circ}Z$ towards Y and $45^{\circ}Y$ towards +X (aft),
- g) $30^{\circ}Z$ towards Y and $45^{\circ}Y$ towards +X (aft) and
- h) $60^{\circ}Z$ towards Y and $45^{\circ}Y$ towards -X (fwd).

The effect of the elevon raised is to eliminate wing reflections of evaporator exhausts. In this configuration, the evaporator is shielded from the wings topside. Therefore, the only contribution the evaporator has to lines-of-sight is direct flow, Table IX shows the predictions for the number column density with the elevon up and the elevon down. More cases were run with the elevon up since additional resolution was required to determine when shadowing by the elevon hides the line-of-sight from the evaporator. Several baseline cases with the elevon down were run for comparison. These included direct flow from the evaporator and wing reflections as shown in Table IX. The elevon up values do not include the evaporator effluents that can reach the lines-of-sight by passing between the elevon and the fuselage through the 6 inch spacing that exists.

Table XIII. *NCD for Evaporator at X = 1507, Z = 305

Elevon Up, mol/cm ²		Elevon Down, mol/cm ²		
Line-of-Sight	Direct	Direct	Reflect	Total
60°Z → Y	1.6 x 10 ¹³	1.0 x 10 ¹⁴	5 x 10 ¹³	1.5 x 10 ¹⁴
45°Z → Y	5.7 x 10 ¹²			
40°Z → Y	4.9 x 10 ¹²			
35°Z → Y	1.6 x 10 ¹²			
30°Z → Y	0	2.5 x 10 ¹³	5 x 10 ¹³	7.5 x 10 ¹³
0° along Z	0	0	1.47 x 10 ¹³	1.47 x 10 ¹³
{ 60°Z → Y + 45°Y-x (aft)	6.4 x 10 ¹³			
{ 30°Z → Y + 45°Y → x (aft)	1.2 x 10 ¹³			
{ 60°Z → Y+ 45°Y → x (fwd)	0			

*Does not include evaporator exhaust that can escape through the elevon/fuselage gap.

The contribution of the evaporator flow between the elevon and fuselage wall, with the elevon up 35 degrees, was assessed. Figure 23 schematically shows the geometry used for the analysis.

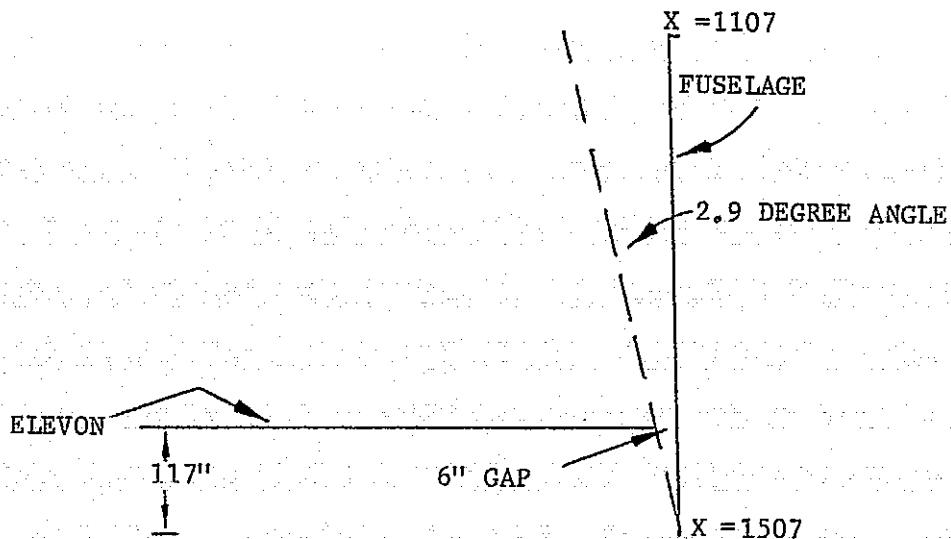


Figure 23. Elevon/Fuselage-Evaporator Geometry

Table X shows the results of the analysis for various lines-of-sight originating at $X_e = 1107$. The density at the line-of-sight is $1.5 \times 10^{13} \text{ g/cm}^3 = 9 \times 10^9 \text{ mol/cm}^3$. This value corresponds to an angle 88.33 degrees off of the evaporator axis and is 1532 cm away.

Table XIV. Number Column Density Due to Evaporator Flow Between Elevon and Fuselage

Line-of-Sight	Distance Along LOS for Integration, cm	NCD mol/cm ²
90°Z → Y	52	2.6×10^{11}
60°Z → Y	60	3.0×10^{11}
30°Z → Y	104	5.2×10^{11}
{ 45°Y → X and 90°Z → Y	23.5	3.7×10^{11}
{ 60°Z → Y and 45°Y → Z	85	4.2×10^{11}
{ 30°Z → Y and 45°Y → X	147	7.4×10^{11}

When combined with the direct flow that the evaporator has to the portions of the lines-of-sight in excess of 30 degrees off of Z towards Y, the resulting number column density is shown in Figure 24. These results show that the NCD falls below 10^{12} mol/cm^2 near 30 degrees off Z towards Y.

The mass past 90 degrees off of the evaporator also has the capability of flowing through the elevon/fuselage gap. If this were true, the result would be to increase the NCD below 30 degrees. Because of the uncertainties in the analytical treatment, it is recommended that the flow through a simulated elevon/fuselage geometry be tested for the evaporator. The flux at the opening would be near $5 \times 10^{-7} \text{ g/cm}^2/\text{s}$. If a cryogenically cooled QCM at LN₂ temperatures were used to detect this flow, a net buildup should exist because of the low vapor pressure of water at LN₂ (less than 10^{-21} torr). However, if the QCM is at -100°C (173.2°K), then the sublimation rate of water from the QCM is

$$\begin{aligned} \dot{m} &= 5.83 \times 10^{-2} P_v \left(\frac{M}{T} \right)^{1/2} \\ &= (5.83 \times 10^{-2}) (1.1 \times 10^{-5}) \left(\frac{18}{173.2} \right)^{1/2} \\ &= 2.1 \times 10^{-7} \text{ g/cm}^2/\text{s}. \end{aligned}$$

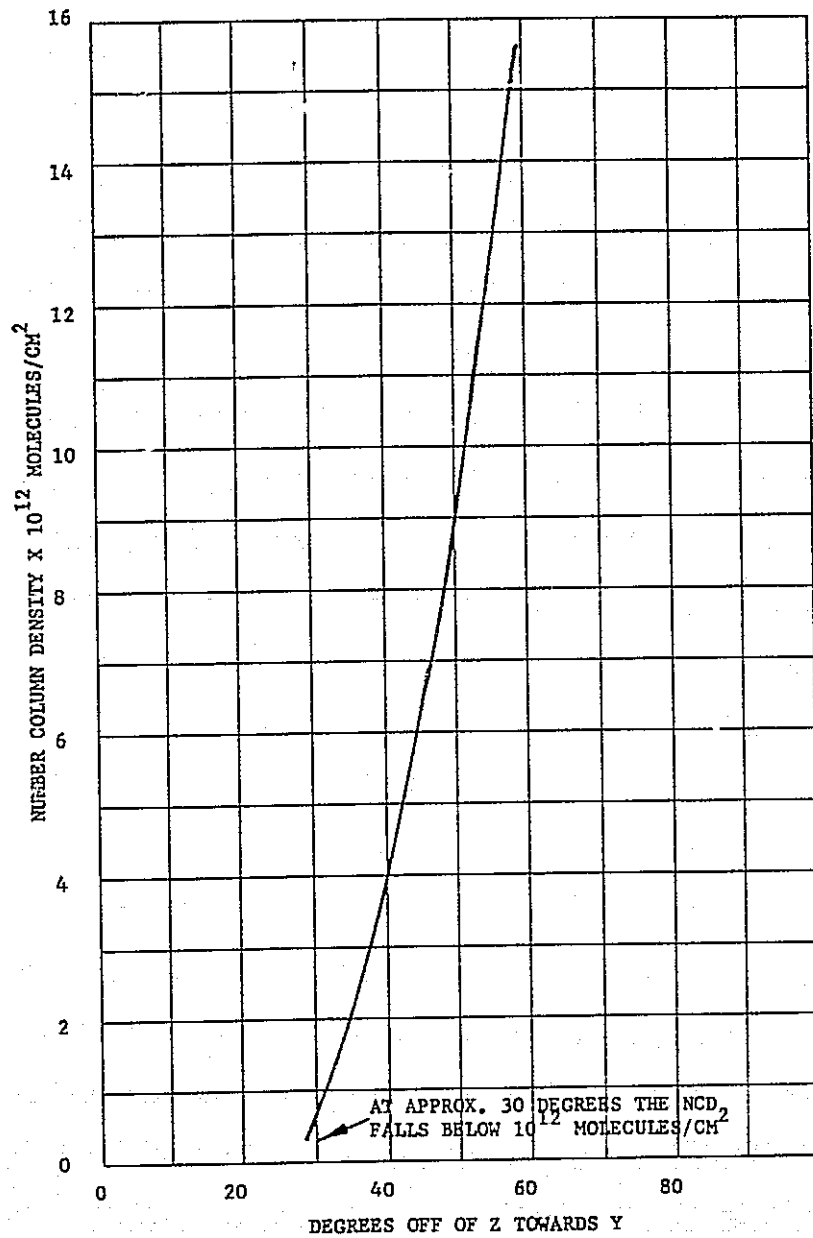


Figure 24. Evaporator Induced Molecular Number Column Density for Elevon Canted up 35 Degrees

and is thus near the calculated flux rate of the evaporator exhausts. Therefore, any detector should be at temperatures much less than -100°C (173°K) to insure trapping of the H_2O .

Thus, it appears rotating the elevon to the up position eliminates the wing reflection for the payload lines-of-sight. The only mass that enters the lines-of-sight is that from direct flow and occurs for angles near thirty degrees off of Z towards + Y.

4.0 CONCLUSIONS AND RECOMMENDATIONS

4.1 Conclusions

The model delivered to JSC at the end of the total contract period exceeded the expectations and intent of the original model to be delivered. This resulted because of company supported modeling activities and a similar effort being conducted for MSFC, Huntsville concurrent with this study. The model's versatility and structure is such that it can form the basis and be extended to become a true simulation of a mission profile. The time dependence of sources and the temperature variations during an orbit are structured such that a mission timeline can be easily incorporated. This present form of the model supercedes all previous models.

The model predictions for the sources and selected lines-of-sight show that the NCD varies between 2.2×10^{10} and 3.0×10^{10} mol/cm² for the outgassing and from 2.6×10^{11} and 3.5×10^{11} mol/cm² for early desorption. The major contributing surface types are nomex for the majority of lines-of-sight and the wing area is the largest contributing location.

The column densities are lower than previously predicted in report MCR-75-13 for outgassing and early desorption. This results from temperature changes and source rate differences. The return flux for the outgassing is also reduced but is increased for early desorption because of an increase in collision cross section.

Surface resolution for a point source near a surface can lead to erroneous flux rates on the surface for unique situations. This was discovered for the evaporator at $X = 1504$ and $Z = 305$ in relation to the trailing edge of the elevon. By evaluating and correcting the surface area/point source relation, the NCD contribution to lines-of-sight along +Z were reduced by an order of magnitude. It became apparent the surface resolution must be thoroughly understood. This type of analysis cannot be accurately done with a wing consisting of one or two nodes. The result of this wing node modification to reduce the column densities due to wing reflection for the VCS and RCS engines and the evaporator.

The location of the evaporator at $X = 1505.6$ and $Z = 305$ was a final result of a great many trade studies. This location is acceptable from plumbing and surface penetration requirements, force considerations and in some cases contamination consideration. The whole approach was to locate the nozzle as far down toward the wing as possible and still be behind it. This would then reduce the surface reflections of the evaporator off of the wings and would reduce the

forces generated by impinging on the wing topside surfaces. It has been shown the contamination levels for this location be further reduced by moving the elevon to an upward location on orbit thus eliminating wing reflections off of the topside that can reflect to payload lines-of-sight.

4.2 Recommendations

There are several parameters in the model that will require updating in the future to increase the fidelity of the model. The following subsections describe those areas considered important during future development of the contamination model.

4.2.1 Source Updates - The results of the evaporator test program currently planned at JSC for the end of 1977 should be input to the model plume functions for the evaporator as an update. The particulate content that is measured during the test should be evaluated separately to assess the potential of the particles intersecting payload lines-of-sight.

The mass loss behavior of outgassing and early desorption species of nonmetallic materials should be updated based on test data that yields the necessary function of relationships and parameters that can predict mass loss rates as a function of temperature and time. These parameters will be unique for each material type.

4.2.2 Source Transport Updates - Associated with mass transport of contaminant species are several parameters vital to the accuracy of the model and the resulting predictions. The parameters that should be updated wherever possible are the collision cross section of ambient and vehicle induced species for the interaction velocities anticipated, the ultraviolet degradation of surfaces that are contaminated, the condensation coefficient of outgassing sources and the reevaporation of deposited materials with and without ultraviolet irradiation. These parameters will require specific testing so that they are applicable to the model. Additional source such as the payload bay liner vent areas and the bulkhead TG 15000 vent areas should be included for payload assessment and overall bay pressure profiles.

4.2.3 Mission Model Updates - For simulation of flight profiles, it is recommended that a temperature conversion program be integrated into or used in conjunction with the SPACE Program. This program has been developed at NMA for in-house activities. Essentially, its' function is to take the JSC thermal node structure and predicted temperatures and convert them to the contamination model node structure and calculate the temperatures that

correspond to the math model by weighting the corresponding nodal areas. The conversion program would require some modification such that its output would be compatible with the SPACE Program data input format. Also, the method of inputting temperatures of the JSC thermal predictions to the conversion program would be enhanced if punched cards could be used as input.

The model should be used to predict the levels of the Induced Environment Contamination Monitor (IECM) that will be flown on the early Shuttle flights. This would require positioning of the IECM sensor package in its proper location relative to the Orbiter and timelining the mission parameters. The next logical step in the SPACE model development would be to incorporate software capability to operate the model in such a manner as to simulate an actual mission profile. This would be a select logic program for all sources, temperature profiles and attitude changes.

4.2.4 User's Manual Update - As updates are performed on the SPACE model at JSC, the User's Manual should be continually updated. The loose leaf form of the User's Manual delivered during this contract should allow this to be done without a great deal of effort.

5.0 NOTES

5.1 Abbreviations

A_o	Nonmetallic materials outgassing rate constant.
a_o	Initial amount of active outgassing mass available.
C_L	Centerline.
cm^2	Square centimeters.
dA	Elemental unit of area.
D_i	Deposition on surface i .
\dot{D}_i	Deposition rate on surface i .
E	Activation energy.
FOV	Field-of-view.
FRSI	Flexible reusable surface insulation (same as Nomex).
g	Grams.
hr	Hours.
HRSI	High temperature reusable surface insulation tile.
Hz	Frequency.
i	Subscript denoting receiving surface or location of interest.
in	Inches.
j	Subscript denoting source.
JSC	Lyndon B. Johnson Space Center.
kg	Kilograms.
km	Kilometers.
$k(T)$	Rate constant as a function of temperature.
LOS	Line-of-sight.
LRSI	Low temperature reusable surface insulation tile.
M	Molecular weight; or integrated mass lost over time and temperature (Appendix A).
m	Meters; or active mass remaining in an outgassing source.
max	Maximum.

\dot{m}_{ej}	Reevaporation rate of deposit j.
min	Minimum.
\dot{m}_j	Emission rate from j.
$\dot{m}(t,T)$	Mass loss rate as a function of time and temperature.
MCD	Mass column density in g/cm ² .
MMA	Martin Marietta Aerospace.
MSFC	George C. Marshall Space Flight Center.
n	Order of reaction.
N_A	Ambient density in molecules/cm ³ .
N_C	Contaminant density in molecules/cm ³ .
NASA	National Aeronautics and Space Administration.
NCD	Molecular number column density in molecules/cm ² .
Nomex	Coated felt insulation (FRSI).
OGR	Outgassing rate.
OMS	Orbital maneuvering system.
P	Point in the modeled hemispherical volume.
P_v	Vapor pressure.
R	Distance from source to point (mean free path determination); or molar gas constant.
r	Distance.
RCC	Reinforced carbon-carbon insulation.
RCS	Reaction control system 870 lb. thrusters.
RF	Return flux.
s	Seconds.
S	Sticking coefficient.
S_{A-B}	Sticking coefficient between source A and surface B.
SPACE	Shuttle/Payload Contamination Evaluation computer program.
STS	Space Transportation System.
t	Time.
T	Temperature.
TGA	Thermogravimetric analysis.

TRASYS Thermal Radiation Analysis System.
 IV Ultraviolet radiation.
 V_A Velocity of ambient atmosphere (approximately equal to orbital velocity).
 VCS Vernier Control System 25 lb. thrusters.
 VF Viewfactor.
 VF_{i-j} Viewfactor between source j and receiver i .
 V_{oo} Velocity of contaminant species,
 A Angstroms,
 α Angle between ambient flux and line-of-sight,
 β Angle between orbital plane and earth-sun line,
 θ Volume element midpoint angle off +Z axis; or field-of-view definition angle off surface normal,
 λ_j Mean free path of specie j ,
 μ Molecular diameter velocity factor,
 σ_A Scattering or collision cross-section.
 τ Mass loss decay constant; time to reach 1/e of original value.
 ψ_j Source function of j .
 Ω Surface geometric acceptance angle in steradians.